

Protection of Electrical Power Systems with Full Penetration of Converter-Interface Generation

by

Luis Santiago Azuara Grande

A dissertation submitted by in partial fulfillment of the requirements
for the degree of Doctor of Philosophy in

Electrical Engineering, Electronics and Automation

Universidad Carlos III de Madrid

Advisors:

Dr. Santiago Arnaltes Gómez

Dr. Ricardo Granizo Arrabé

Tutor:

Dr. Santiago Arnaltes Gómez

May 2023

This thesis is distributed under license “Creative Commons **Attribution – Non Commercial – Non Derivatives**”.



Acknowledgements

First, I would like to thank Dr. Santiago Arnaltes for giving me the opportunity to do this thesis 5 years ago, as well as for his important supervision and extensive knowledge. Thanks also to Dr. Ricardo Granizo Arrabé for his brief but essential contribution to this thesis.

I would like to thank the Universidad Carlos III de Madrid for their financial support to complete my thesis and to carry out a research internship at the University of South-Eastern Norway. Thanks also to the Porsgrunn laboratory colleagues (Gioacchino, Raju, Aleksandra, Ashish, Le and Sudan) for their outstanding collaboration.

Thank you to the professors and staff of the Electrical Engineering Department of the Universidad Carlos III de Madrid for your kindness and support, in special to the Dr. Francisco Arredondo. Also, to my colleagues Marcial González, Jesús Castro, Pedro Camuñas, Juan Dolado, Carolina Martin, David Rebollal and Ángel Manuel Gómez.

I express my gratitude to my family and friends, who make my life happy and support me along the way. I would like to thank my parents and brother for their love, constant encouragement, and remarkable patience. Without them, this achievement would not have been within my reach.

Thank you!

Published and submitted content

Journal papers (2)

Title: Wavelet Analysis to Detect Ground Faults in Electrical Power Systems with Full Penetration of Converter Interface Generation

Authors: Luis Santiago Azuara-Grande, Ricardo Granizo Arrabé, Santiago Arnaltes

Publication date: February 2023

Journal: Electronics

Publisher: MDPI

DOI: <https://doi.org/10.3390/electronics12051085>

This material is wholly included in the thesis in Chapter 2 and 3.

The material from this source included in this thesis is not singled out with typographic means and references.

Title: Comparison of Two Energy Management System Strategies for Real-Time Operation of Isolated Hybrid Microgrids

Authors: Luis Santiago Azuara-Grande, Santiago Arnaltes, Jaime Alonso-Martínez and José Luis Rodríguez-Amenedo

Publication date: October 2021

Journal: Energies

Publisher: MDPI

DOI: <https://doi.org/10.3390/en14206770>

International conference papers (4)

Title: Influence of Negative-Sequence Control under Converter-Interface-based Generation in Distance Protection Relays

Authors: Luis Santiago Azuara-Grande, Ricardo Granizo Arrabé, Santiago Arnaltes

Publication date: Submitted March 2023

Conference: 2023 IEEE International Conference on Environment and Electrical Engineering and 2023 IEEE Industrial and Commercial Power Systems Europe (EEEIC / I&CPS Europe)

Publisher: IEEE

DOI:

This material is wholly included in the thesis in Chapter 2, 3 and 5.

The material from this source included in this thesis is not singled out with typographic means and references.

Title: Real-Time Implementation of Two Grid-Forming Power Converter Controls to Emulate Synchronous Generators

Authors: Luis Santiago Azuara-Grande, Francisco Gonzalez-Longatt, Gioacchino Tricarico, Raju Wagle, Santiago Arnaltes, Ricardo Granizo Arrabé

Publication date: November 2022

Conference: 2022 IEEE Biennial Congress of Argentina (ARGENCON)

Publisher: IEEE

DOI: [10.1109/ARGENCON55245.2022.9940076](https://doi.org/10.1109/ARGENCON55245.2022.9940076)

This material is wholly included in the thesis in Chapter 2.

The material from this source included in this thesis is not singled out with typographic means and references.

Title: **EMS for fuel saving in an isolated hybrid system (solar/diesel/battery)**

Authors: Luis Santiago Azuara-Grande, Santiago Arnaltes, Jaime Alonso-Martínez, José Luis Rodríguez-Amenedo

Publication date: August 2020

Conference: 2020 IEEE International Conference on Environment and Electrical Engineering and 2020 IEEE Industrial and Commercial Power Systems Europe (EEEIC / I&CPS Europe)

Publisher: IEEE

DOI: [10.1109/EEEIC/ICPSEurope49358.2020.9160853](https://doi.org/10.1109/EEEIC/ICPSEurope49358.2020.9160853)

Title: **Distributed Control Strategy for Isolated Electrical Hybrid Power Systems**

Authors: Luis Santiago Azuara-Grande, Santiago Arnaltes, Jaime Alonso-Martínez, José Luis Rodríguez-Amenedo

Publication date: September 2020

Conference: 18th International Conference on Renewable Energies and Power Quality - ICREPQ'20

Publisher: European Association for the Development of Renewable Energy, Environment and Power Quality (EA4EPQ)

DOI: <https://www.icrepq.com/icrepq20/365-20-azuara.pdf>

Other research merits

International conference papers (2)

Title: Security Constrained Unit Commitment and Economic Dispatch by AC Sensitivity Factors

Authors: Gioacchino Tricarico, Raju Wagle, Luis Santiago Azuara-Grande, Francisco Gonzalez-Longatt, Maria Dicorato, Giuseppe Forte, José Luis Rueda

Publication date: November 2022

Conference: 2022 IEEE Biennial Congress of Argentina (ARGENCON)

Publisher: IEEE

DOI: [10.1109/ARGENCON55245.2022.9939863](https://doi.org/10.1109/ARGENCON55245.2022.9939863)

Title: Security Constrained Unit Commitment and Economic Dispatch applied to the Modified IEEE 39-bus system Case

Authors: Gioacchino Tricarico, Luis Santiago Azuara-Grande, Raju Wagle, Francisco Gonzalez-Longatt, Maria Dicorato, Giuseppe Forte, José Luis Rueda

Publication date: December 2022

Conference: IECON 2022 – 48th Annual Conference of the IEEE Industrial Electronics Society

Publisher: IEEE

DOI: [10.1109/IECON49645.2022.9968474](https://doi.org/10.1109/IECON49645.2022.9968474)

International conference (1)

Title: International Student Energy Summit 2019

Institution: Imperial College of London

Location: London (United Kingdom)

Period: 17-20 July 2019

Mobility (1)

Institution: **University South-Eastern of Norway**

Location: Porsgrunn (Norway)

Responsible researcher: Prof. Dr. Francisco Gonzalez-Longatt

Period: May 2022-July 2022

Grants (2)

PhD. Scholarship: “Personal Investigador Pre-Doctoral en Formación”

Period: 2018-2023

Funded by: Universidad Carlos III de Madrid

Grant for researcher mobility in a foreign research centre: “Ayudas para la Movilidad del Programa Propio de Investigación”

Period: May 2022-July 2022

Funded by: Universidad Carlos III de Madrid

Abstract

Since the advent of generation with converter-interface, mainly wind and solar photovoltaic (PV), power system operators have deal with some problems to maintain system stability and security. However, due to its low penetration in the system, it had barely any consequences and its study lack of interest. But over the years the generation scheme has changed, and converter-interface generators have been increasing their presence due to their low energy costs and policies against climate change.

When the penetration rate is 100 %, protection systems have detection problems in the overcurrent scheme and pick-up problems in the distance scheme, jeopardising the safety of the electrical power system. This thesis proposes to use the Wavelet transform analysis method to solve these problems in full penetration scenarios of converter-interface generation. It can detect high and low frequency variations in voltage and current signals, and classify them in time and magnitude when they occur.

In order to be able to propose a satisfactory solution, this thesis has carried out a study of the main key factors to be considered for fault detection. Analysing the differences between synchronous generators and generators with converter-interface, and the consequences of each of them for the protection systems. Describing the main converter control architectures and defining the equivalent model of converter short-circuit. Introducing the different types of faults in power systems. And describing the fundamental criteria for protection, and the most common protection schemes.

The model used to obtain the results and check the feasibility of the proposal is the IEEE nine-bus system in a ring layout. It has been modelled including all power system elements (transmission lines, transformers, and loads) and both generation technologies (synchronous generators and converter-interface generators). In addition, the converter control strategy and its current limiting have also been considered. The results show a correct and immediate fault detection.

Resumen

Desde la aparición de los sistemas de generación de energía eléctrica con interfaz de convertidor electrónico, mayoritariamente eólica y solar fotovoltaica, los operadores de red han tenido que lidiar con los diferentes problemas que estos provocan para mantener la estabilidad y la seguridad del sistema. Aunque debido a su baja penetración en el sistema apenas tenía consecuencias y su estudio carecía de interés. Pero con el paso de los años ha ido cambiando el esquema de generación y los generadores con interfaz de convertidor electrónico han ido incrementando su presencia debido a sus bajos costes de la energía y a las políticas de lucha contra el cambio climático.

Cuando se alcanzan niveles de penetración del 100 %, los sistemas de protección tienen problemas de detección en el esquema de sobrecorriente y de arranque en el esquema de distancia, poniendo en riesgo la seguridad del sistema eléctrico. Esta tesis propone utilizar el método de análisis de la transformada de Wavelet para solventar estos problemas en escenarios con máxima penetración de generación con interfaz de convertidor. El cual permite detectar variaciones de alta y baja frecuencia en las señales de tensión y de corriente, y clasificarlas tanto en tiempo como en tamaño cuando se producen.

Para poder presentar una solución con garantías de ser satisfactoria, en esta tesis se ha realizado un estudio de los principales factores clave para tener en cuenta para la detección de faltas. Analizando las diferencias entre generadores síncronos y generadores con interfaz de convertidor electrónico, y qué consecuencias tiene cada uno de ellos para los sistemas de protección. Describiendo las principales arquitecturas de control de convertidores y definiendo los modelos equivalentes de cortocircuito del convertidor. Presentando los diferentes tipos de faltas en los sistemas eléctricos. Y describiendo los criterios fundamentales de las protecciones y los esquemas de protección más comunes.

El modelo utilizado para la obtención de los resultados y comprobar la viabilidad de la propuesta es el sistema de nueve nudos del IEEE dispuesto en anillo. El cual ha sido modelado incluyendo todos los elementos del sistema (líneas de transmisión, transformadores y cargas) y ambas tecnologías de generación (generadores síncronos y generadores con interfaz de convertidor electrónico). Además, también se ha tenido en cuenta la estrategia de control del convertidor y su limitación de corriente. Los resultados muestran una correcta e inmediata detección de la falta.

Contents

Acknowledgements.....	5
Published and submitted content.....	7
Journal papers (2).....	7
International conference papers (4)	7
Other research merits	9
International conference papers (2)	9
International conference (1)	9
Mobility (1).....	9
Grants (2).....	9
Abstract	11
Resumen.....	13
Contents	15
List of Figures	17
List of Tables.....	21
1 Introduction	23
1.1 Context and motivation	23
1.2 State-of-the-art	26
1.3 Background.....	27
1.4 Objectives.....	27
1.5 Thesis outline	28
2 Literature review	29
2.1 Power converter control architectures	29
2.2 Impact on fault current	31
2.3 Converter Short-Circuit Analysis	34
2.3.1 Zero-Sequence Model	34
2.3.2 Positive-Sequence Model.....	34
2.3.3 Negative-Sequence Model	35
2.4 Faults	36
2.5 Protections	37
2.5.1 Overcurrent protection	39
2.5.2 Directional overcurrent protection	39
2.5.3 Distance protection	39
2.5.4 Differential protection.....	39
2.5.5 Adaptive protection	39

2.5.6	Voltage-based protection.....	40
2.6	New protection system proposal: Wavelet transform	40
2.7	Simulation and Real-Time Tools.....	42
2.7.1	MATLAB/Simulink.....	42
2.7.2	PowerWorld	42
2.7.3	Typhoon HIL	42
3	Modelling	43
3.1	Grid Model and Characteristics.....	43
3.1.1	IEEE nine-bus System	43
3.1.2	Synchronous generators	45
3.1.3	Voltage Source Converters.....	45
3.1.4	Arc Model	50
4	HIL testing platform implementation.....	53
4.1	Emulated	53
4.2	Real.....	53
4.2.1	SEL-751 Configuration	54
4.3	Wavelet Implementation	57
5	Results	59
5.1	Short-circuits Analysis 100 % SG Scheme.....	59
5.2	Short-circuits Analysis 100 % VSC Scheme.....	61
5.3	Comparison between 100 % SG and 100 % VSC Scheme.....	62
5.3.1	Generation bus: overcurrent protection relays	62
5.3.2	Transmission line: distance protection relays.....	67
5.4	Wavelet Protection System Proposal.....	73
5.4.1	Generation bus: overcurrent protection relays	73
5.4.2	Transmission line: distance protection relays.....	84
6	Conclusions	89
	References.....	91

List of Figures

Figure 1. New solar PV installations in EU-27 in 2021 [5]	24
Figure 2. New onshore and offshore wind installations in EU-27 in 2021 [6]	24
Figure 3. Share of energy from renewable sources in EU-27 in 2020 [7]	25
Figure 4. Comparison of control strategy of grid-following (a) and grid-forming (b) [35].....	29
Figure 5. Evolution of the short-circuit current in a synchronous machine, without considering the DC component [41]	32
Figure 6. Terminal voltage and output current of SG (A) & IIDG (B) with a 3-phase fault [43] ..	33
Figure 7. Equivalent model of grid-forming converters in the positive-sequence circuit when the converter currents are (a) below the threshold on all phases (b) limited at the threshold at least on one phase [48]	34
Figure 8. Grid-forming converter in the negative-sequence circuit (a) when all three phase currents are below the threshold (b) when the current is limited at least on one phase [48] ..	35
Figure 9. Equivalent model of the grid-forming in each sequence circuit when the fault pushes converter current to exceed the threshold on at least one phase [49]	36
Figure 10. Fault types scheme: a) LLL, b) LL, c) LLG and d) SLG [51]	37
Figure 11. Frequency bands of the discrete Wavelet transform related to decomposition steps [72]	41
Figure 12. IEEE nine-bus test system scheme	43
Figure 13. Dimensions of tower used in medium voltage power distribution network [34]	44
Figure 14. The power stage of a grid-forming (GFM) VSC [35]	46
Figure 15. Cascaded control scheme of grid-forming VSC in dq [79].....	46
Figure 16. Cascaded control scheme of grid-forming VSC in dq by sequences [79]	47
Figure 17. Sequence extraction algorithm [81].....	48
Figure 18. Calculation of sequence components of voltages and currents [81].....	48
Figure 19. Simulation of the operation of the grid-forming control converter	49
Figure 20. Vector amplitude saturation implementation [82]	50
Figure 21. Implementation of the <i>Cassie</i> arc model [86].....	51
Figure 22. Implementation of the IEEE nine-bus test system in Typhoon HIL real-time simulation framework	53
Figure 23. HIL testing platform scheme	54
Figure 24. Protection Laboratory of the University South-Eastern of Norway	56
Figure 25. Protection relay SEL-751	57
Figure 26. Flowchart of Wavelet implementation in Typhoon HIL	58

Figure 27. IEEE nine-bus test system implemented in PowerWorld.....	59
Figure 28. Fault currents & tripping thresholds during a SLG fault in Bus 7 for 100 % VSC.....	63
Figure 29. Fault currents & tripping thresholds during a SLG fault in Bus 7 for 100 % SG	63
Figure 30. Fault currents & tripping thresholds during a SLG fault in Line 7-5 for 100 % VSC ...	64
Figure 31. Fault currents & tripping thresholds during a SLG fault in Line 7-5 for 100 % SG	64
Figure 32. Fault currents & tripping thresholds during a SLG fault in Bus 9 for 100 % VSC.....	65
Figure 33. Fault currents & tripping thresholds during a SLG fault in Bus 9 for 100 % SG	65
Figure 34. Fault currents & tripping thresholds during a SLG fault in Line 8-9 for 100 % VSC ...	66
Figure 35. Fault currents & tripping thresholds during a SLG fault in Line 8-9 for 100 % SG	66
Figure 36. Example of a R–X diagram of distance relaying [89].....	68
Figure 37. Flowchart of fault classification [13]	68
Figure 38. Angular relationship between the negative current (I_2) and the positive-sequence current (I_1): (a) Single-phase and two-phase-to-ground fault diagram; (b) two-phase fault diagram [46]	69
Figure 39. Sequence voltages and currents during an unbalance and a SLG fault in relay 71 for 100 % SG.....	70
Figure 40. Sequence voltages and currents during an unbalance and a SLG fault in relay 71 for 100 % VSC.....	71
Figure 41. Currents and voltages in relay 73 during a SLG fault in Bus 7 for 100 % VSC	73
Figure 42. Currents and voltages in relay 73 during a SLG fault in Line 7-5 for 100 % VSC	74
Figure 43. Currents and voltages in relay 73 during a SLG fault in Line 8-9 for 100 % VSC	75
Figure 44. Currents and voltages in relay 73 during a SLG fault in Load A for 100 % VSC	76
Figure 45. Wavelet coefficients $Cd8 - dB1$ in relay 73 at different fault locations, phase A.....	77
Figure 46. Wavelet coefficients $Cd8 - dB1$ in relay 73 at different fault locations, phase B.....	78
Figure 47. Wavelet coefficients $Cd8 - dB1$ in relay 73 at different fault locations, phase C.....	79
Figure 48. Wavelet coefficients $Cd7 - dB3$ in relay 73 at different fault locations, phase A.....	80
Figure 49. Wavelet coefficients $Cd7 - dB3$ in relay 73 at different fault locations, phase B.....	81
Figure 50. Wavelet coefficients $Cd7 - dB3$ in relay 73 at different fault locations, phase C.....	82
Figure 51. Flowchart of the operational sequence of the generation bus overcurrent protection relays	83
Figure 52. Sequence voltages and currents during an unbalance and a SLG fault in relay 71 for 100 % VSC.....	84
Figure 53. Sequence voltages and currents during an unbalance and a SLG fault in relay 52 for 100 % VSC.....	85
Figure 54. Wavelet coefficients $Cd11 - dB4$ in relays 52 & 71.....	86

Figure 55. Flowchart of the pick-up sequence of the transmission line distance protection
relays 87

List of Tables

Table 1. Typical synchronous generator reactance values	32
Table 2. Fault statistics based on fault type [52]	37
Table 3. Fault statistics based on power systems elements [52]	37
Table 4. Grid model specifications	44
Table 5. Main features of conductor LA-56 [34]	44
Table 6. Overhead-line features [34]	45
Table 7. Overhead-line RL features [34]	45
Table 8. Grid-forming VSC parameters (in p.u.)	47
Table 9. Inputs and outputs of Universal HIL Connect.....	54
Table 10. SEL-751 protection functions [87]	55
Table 11. Variables of SEL-751 configuration.....	55
Table 12. Nominal and contingency currents in 100 % SG scheme	60
Table 13. Fault currents in 100 % SG scheme	60
Table 14. Relays trip threshold values in 100 % SG scheme	60
Table 15. Fault currents in 100 % VSC scheme	61
Table 16. Relays trip threshold values in 100 % VSC scheme	62
Table 17. Distance relay operating measurement and faulted loop current for different fault types [89].....	67
Table 18. Results obtained from the faulted phase selection logic	70

1 Introduction

In this chapter, a general description of the thesis content is given. Section 1.1 justifies both the context and the motivation for the thesis. Section 1.2 summarises the state-of-the-art and the main novel contributions in this thesis. Section 1.3 describes the background for the thesis. In section 1.4, the main objectives of the thesis are stated. Section 1.5 describes the content of the thesis.

1.1 Context and motivation

The transition to an energy system based on renewable energy resources is already underway. Renewable energy has become increasingly affordable over the past ten years, making it competitively priced with conventional electricity generation in many regions of the world. The global weighted-average levelized cost of electricity (LCOE) of utility-scale solar photovoltaic (PV) for newly commissioned projects fell by 85 % between 2010 and 2020, while for onshore wind projects, the global weighted-average cost of electricity between 2010 and 2020 fell by 56 %, and for offshore wind a reduction of 48 % in 10 years [1].

The significant decrease in greenhouse gas emissions that results from switching to a 100 % renewable energy system is one of the most important advantages. The IPCC (Intergovernmental Panel on Climate Change) emphasizes the necessity for a swift energy revolution based on a considerable increase in renewables to attain the global temperature limit [2]. Many nations have already made progress in achieving this objective. For instance, Iceland uses either geothermal energy and hydropower to provide all its electrical demand. Other nations with strong renewable energy penetration on hydropower-based electric systems include Costa Rica (99 %), Norway (98 %), Brazil (77 %), and Canada (67 %) [3]. Hydropower has been in use for quite a while and is a reasonably affordable renewable energy source, though the geography and natural precipitation of certain areas can limit its usage. Most suitable locations for substantial hydropower resources have already been exploited in many nations, necessitating a switch to intermittent renewable energy sources (i.e., wind and solar PV systems) [4].

The demand for solar power in the European Union has grown significantly in 2021. The 27-member states of the European Union saw around 25.9 GW of new solar PV capacity connected to their grids in 2021 (Figure 1), an increase of 34 % over the 19.3 GW installed the year before. This growth makes 2021 not only another record year for solar in the EU, it was also the best year in history, taking place exactly one decade after the former record was set at 21.4 GW in 2011 [5]. While new wind installations in EU-27 amounted to just 11 GW (10 GW onshore and 0.9 GW offshore) of new wind energy capacity (Figure 2) in 2021 [6].

According to [7], the EU overachieved its target in 2020 with a 22 % share of gross final energy consumption from renewable sources (Figure 3). The definitive figures, reported by the EU countries under the Regulation of the Governance of the Energy Union in April 2022, confirmed the conclusions of Eurostat and revealed that in 2020, the EU reached a share of 22.1 % of renewable energy in gross final energy consumption, thus exceeding the 20 % share aimed at under the 2009 Renewable Energy Directive.

Building on the 20 % target for 2020, the recast Renewable Energy Directive 2018/2001/EU [8] established a new binding renewable energy target for the EU for 2030 of at least 32 %, with a clause for a possible upwards revision by 2023.

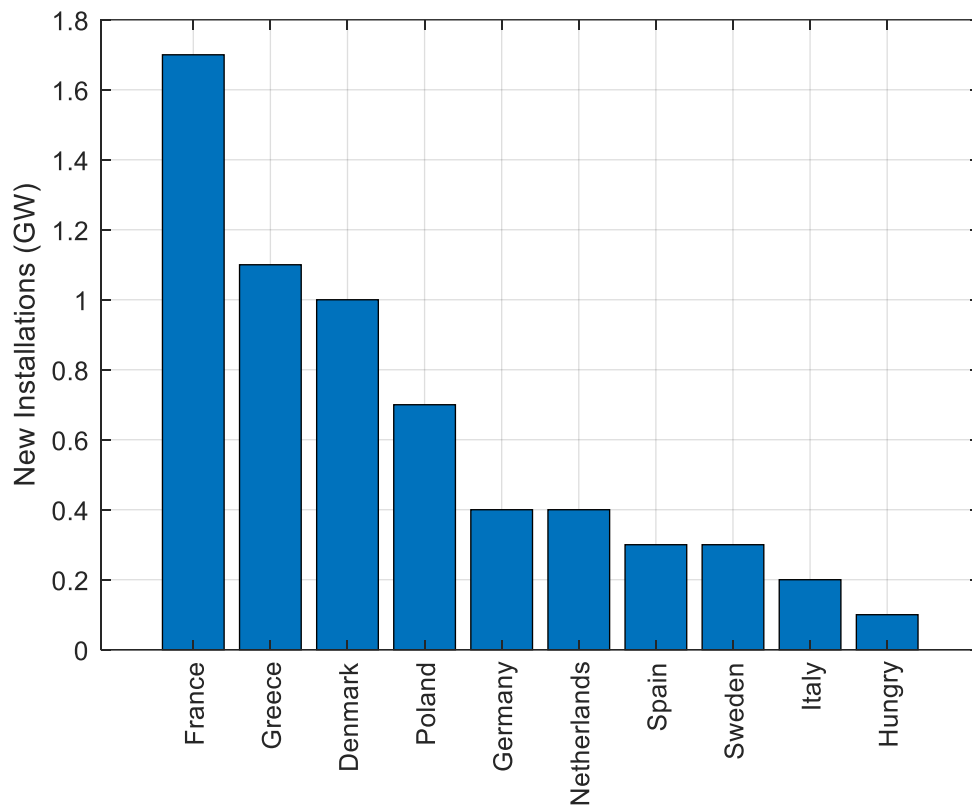


Figure 1. New solar PV installations in EU-27 in 2021 [5]

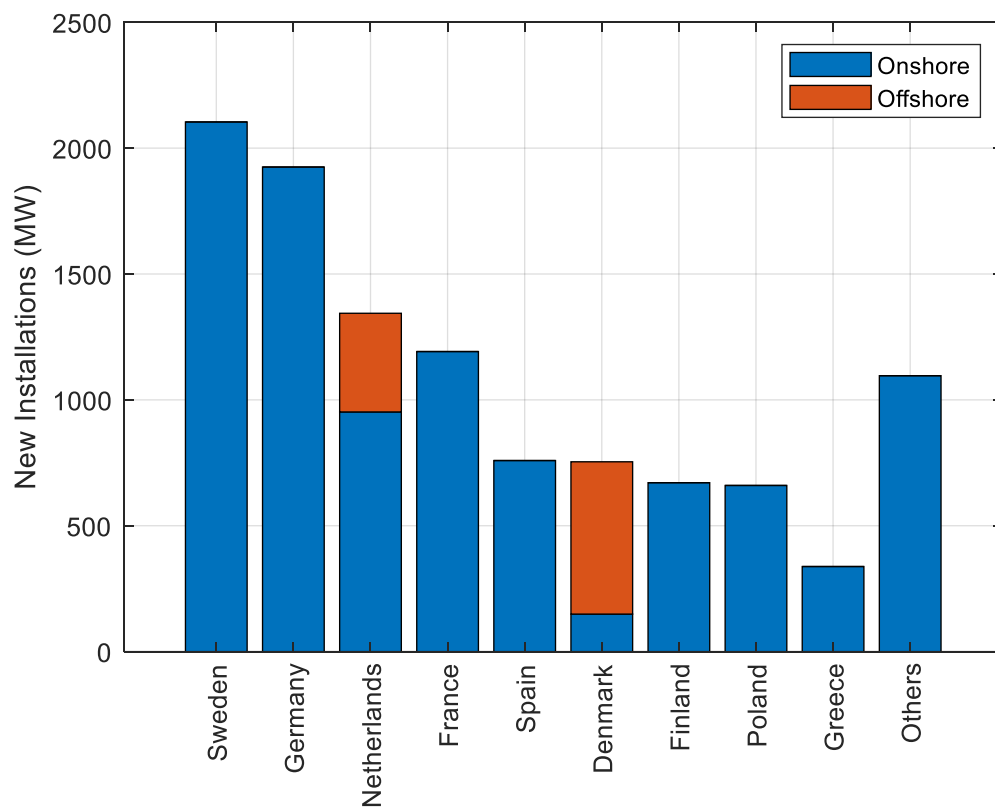
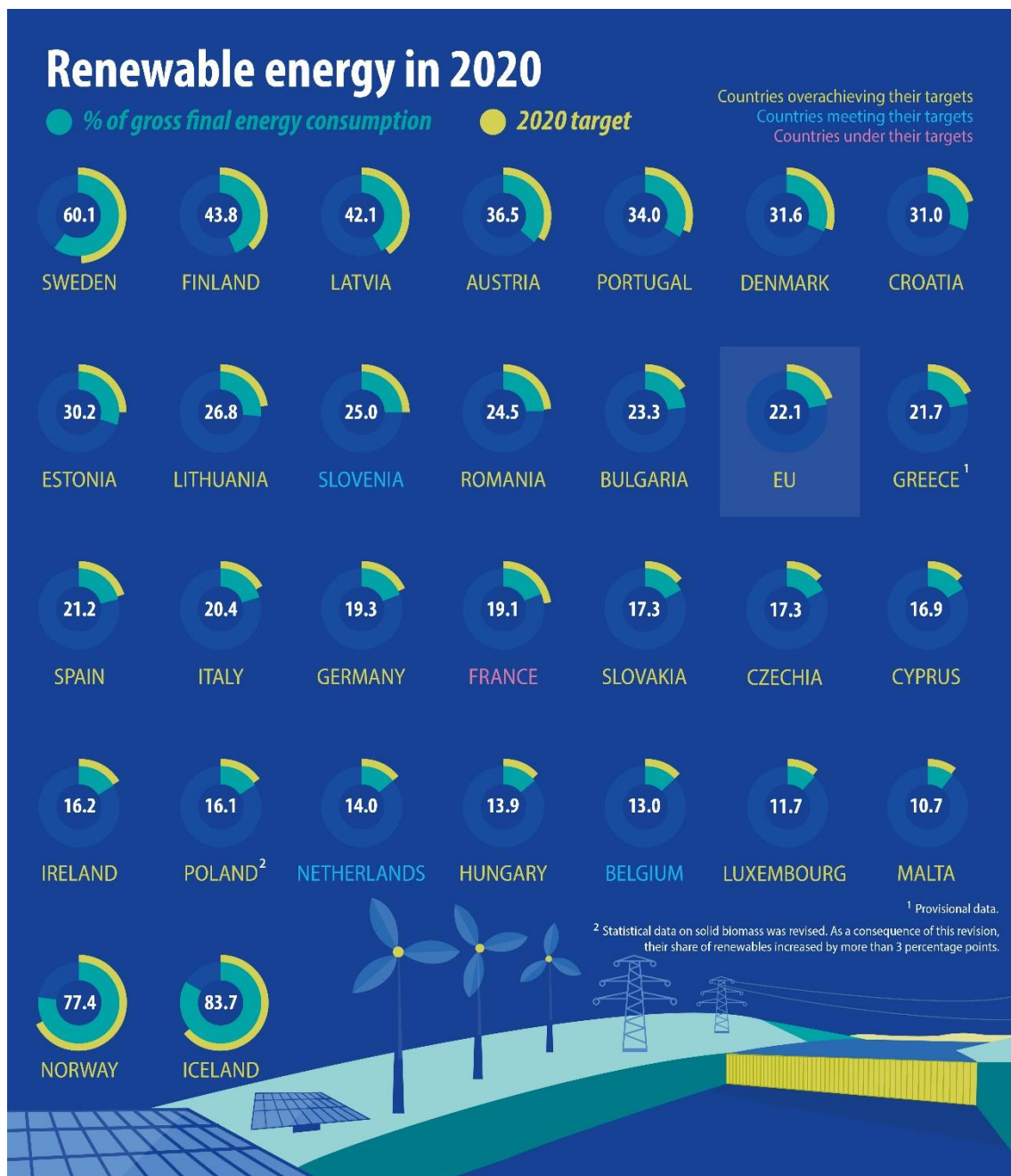


Figure 2. New onshore and offshore wind installations in EU-27 in 2021 [6]



ec.europa.eu/eurostat

Figure 3. Share of energy from renewable sources in EU-27 in 2020 [7]

The Commission presented Europe's new 2030 climate targets, including a proposal for amending the Renewable Energy Directive, on 14 July 2021. It seeks to increase the current target to at least 40 % renewable energy sources in the EU's overall energy mix by 2030.

On 18 May 2022, the Commission published the REPowerEU plan [9], which sets out a series of measures to rapidly reduce EU's dependence on Russian fossil fuels well before 2030 by accelerating the clean energy transition. As part of its scaling up of renewable energy in power generation, industry, buildings and transport, the Commission proposes to increase the target in the directive to 45 % by 2030.

There is still more research to be done on a power system that uses solely intermittent renewable energy, even if certain studies do not show the viability of a 100 % renewable power system owing to intermittent generation of the power sources. There is a good likelihood that 100 % intermittent renewable sources will eventually supply a significant section of the future power grid [4].

The renewable energy sources like wind or solar PV are connected to the grid via power electronics. As a result, the interface with the grid differs significantly from that of a standard power plant, which uses a synchronous machine (SM) to convert energy [10]. SMs are currently in charge of managing the frequency and voltage amplitude. Additionally, they guarantee the stability of the transmission grid since they are physically equipped to handle powerful transient events and maintain the system in a stable environment [11].

When there is a severe fault, SMs inject a strong fault current which facilitates the performance of the overcurrent protection systems. In comparison, converter-interface generators may only inject 1–1,2 (p.u.) of their rated current as fault current. With widespread adoption of converter-based producing units, the short-circuit power level is significantly decreased which leads to malfunctioning of the overcurrent protections [11].

Also, converter-interface generators may significantly affect some input quantities of the distance protection algorithms such as negative-sequence overcurrent pick-up, whereas with synchronous generators (SGs), the negative-sequence current does not present any starting issue because of high negative-sequence current value [12].

1.2 State-of-the-art

The implemented overcurrent protection schemes consider the current to detect the fault condition, it seems obvious that a large reduction of the current by converter-interface generators may cause problems in the fault detection [13]. And in the distance protection algorithm is considered that the currents supplied by the converter-interface generation can lead to underestimation or overestimation of the fault location by the distance relay [14][15][16]. However, it is not considered that the logic of a distance relay requires a start signal to measure the impedance until the fault location. The start procedure has been designed assuming that the negative-sequence current quantities are present in significant levels during a fault, and calculate them by digital relays is simple. Therefore, in case of full penetration of converter-interface generation the start signal fails to pick-up due to the low level of negative-sequence current since the minimum operating current have not reached [12][17][18][19].

Thus, in recent years there have been numerous investigations with different proposals on fault detection in scenarios with high penetration of converter-interface power generation units:

In [20] a fault detection strategy based on voltage sequence components is proposed. The behaviour of the converter control during faults makes the voltage sequence components the best discriminator between normal and fault operation.

In [21] the adaptive protection policy is the most suitable for a grid protection solution. The relay settings can be changed, and the necessary protection can be provided in an adaptive protection system with the topological and operational change.

In [22] the aim of the EU-funded MIGRATE project is to find solutions to the challenges of massive integration of power electronics devices that the grid is currently and especially in

future faced with. The third objective of this project is to establish a design of protection schemes for power systems with high power electronics penetration. Through the work package 4 (WP4): Protection schemes in transmission networks with high power electronics penetration.

Also, there are some paper reviews [16][23][24][25][26][27] that provide a comprehensive overview of the existing proposals for protection design. Apart from describing the most relevant options presented to date and classifying them in specific groups, a comparative analysis is performed. The most important benefits and drawbacks of each approach are presented.

In this thesis, it has proposed a different method from the previous ones seen in the literature. Since the current signals are decomposed using the Wavelet transform for fault detection. The Daubechies mother wavelet is used to give coefficient values that allow for the detection of a fault regardless of the values relied on by traditional protection schemes.

Although there are some papers in the literature that employ the Wavelet transform to detect faults [28][29][30][31][32][33], the novel contributions of this thesis are that control and current limiting are considered in the modelling of the grid-forming converter; the generation scenario is based on 100 % converter-interface penetration; the analysis of both the overcurrent and distance protection scheme; and the distribution network uses a ring topology.

1.3 Background

The Wavelet transform method proposed in this thesis is based on following the research in this area of one of the supervisors of the thesis, Dr. Ricardo Granizo Arrabé [34]. In which focuses on the study and development of new protection methods and systems for power cables used in both AC and DC grids, from generation to distribution or transmission power networks.

1.4 Objectives

The main purpose of this thesis is to investigate the impact on the network protections of converter-interface generation and to develop new methods to mitigate the associated problems.

The main objectives are:

- Studying and analysing the differences between the faults produced by a SG and a converter-interface generator.
- Understand and differentiate the multiple control strategies of a converter.
- Know how to model a complete grid-forming converter control scheme.
- Studying the different existing protection systems.
- Studying and analysing the problems in protection systems caused by a full penetration of converter-interface generation.
- Implementing and developing hardware-in-the-loop (HIL) simulations with real protection relays.
- Studying the theoretical framework of the Wavelet transform and apply it to fault detection.
- Developing a new fault detection method based on Wavelet transform analysis.

1.5 Thesis outline

The chapters are then listed with a brief explanation of each one's contents.

In the **first chapter** a general description of the thesis content is given.

Second chapter includes the literature review of the important fields related to the thesis.

Third chapter describes the modelling of the different elements which need to be considered for the simulations, includes power converters and SGs.

Forth chapter develops the HIL testing platform to test of how the real protection relay behaves. Including wiring and equipment configuration. Also shows the Wavelet implementation in the HIL API.

Fifth chapter shows and analyses the results obtained from the simulations in the IEEE nine-Bus test system for the different fault locations and different generation technology scenarios.

Sixth chapter relates the conclusions of the thesis and suggests some ideas for future research work.

2 Literature review

This section presents a general literature review of the important fields related to the thesis. Section 2.1 presents a brief of the differences between the two main converter control architectures. Section 2.2 explains what impact generation technologies have on fault currents. Section 2.3 describes the equivalent model of converter short-circuit. Section 2.4 summarises the different types of faults in electrical power systems. Section 2.5 introduces the fundamental criteria of protections and the most common protective schemes. Section 2.6 presents the Wavelet transform as a protection algorithm. And section 2.7 describes simulation and HIL tools.

2.1 Power converter control architectures

Converter-interface generators are inevitably becoming a component of electrical power systems due to the increasing need for renewable energy technologies [35]. Grid-following converters and grid-forming converters are two different types of power converters that connect intermittent renewable energy sources to the grid. The main structural differences between the two types of converters are in their control architectures, while they have similar hardware components [36]. Power converters may be controlled either as a current source (i.e., grid-following) or as a voltage source (grid-forming), as shown in Figure 4.

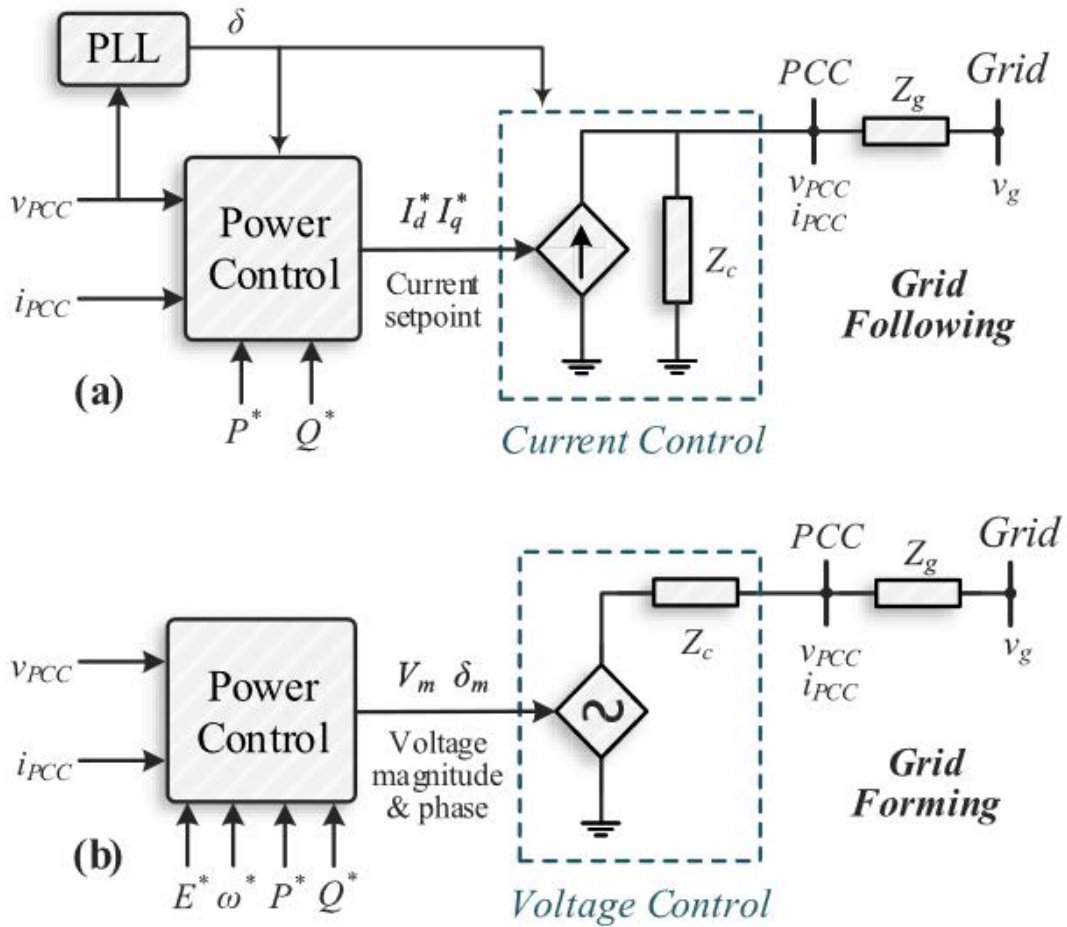


Figure 4. Comparison of control strategy of grid-following (a) and grid-forming (b) [35]

The way the converter is synchronised to the grid differs significantly between grid-forming control and grid-following control. A power converter with a grid-following control has injected

currents that are controlled with a certain phase displacement with relation to the grid voltage at the point of common coupling (PCC). Because of this, it is always necessary to know the fundamental frequency of the grid voltage in order to properly calculate the converter reference currents, whose magnitude and angle with respect to the grid voltage phasor are appropriately modified by outer control loops in order to inject the required amount of active and reactive power. In the case of grid-forming control, the synchronisation technique is fundamentally different. Self-synchronization is achieved once the voltage magnitude has been freely and independently fixed on the grid voltage by a power control loop [4].

However, substituting conventional SGs with voltage-source converters (VSC) can cause instability problems, but if appropriate control loops are enabled with adequate settings, VSCs provide a solution to many problems in the power systems, e.g., low rotational inertia [37].

The grid-forming control technique allows to support the grid operation, since emulate the behavior of SGs. There are different alternatives for grid-forming control implementation. The main ones are Droop Control, Virtual Synchronous Machine (VSM), and Synchronverter (SynC).

- The main foundation of **droop control** is to reproduce the behaviour of a SG governor. In which any increase in the load results in a decrease of the frequency according to its frequency droop characteristic. Similarly, reactive power is related to the voltage magnitude by introducing a voltage droop characteristic.
- The **Virtual Synchronous Machine** (VSM) emulates the mechanical behaviour of the SM by using the swing equation (1).

$$T_a \cdot s \cdot \omega^* \approx P_{set} - P_{mes} - K_d(\omega^* - \omega_{set}) \quad (1)$$

where the input variable is the active power (P_{mes}) generated by VSM; the internal set values are the mechanical time constant (T_a), damping coefficient (K_d), angular frequency (ω_{set}) and active power (P_{set}); and the output variable is the angular frequency reference (ω^*). Being s the derivative operator.

- The **Synchronverter** (SynC) also mimics the behaviour of a SG, but it has the advantage that parameters such as inertia, damping, field inductance, and mutual inductance can be readily modified.

The Synchronverter controller represents the dynamic swing equations of a SG by the equation of the frequency droop (2) and the equation of voltage droop (3) [38].

$$\omega^* = \frac{1}{J_s} (T_m - T_e + D_p(\omega_{set} - \omega^*)) \quad (2)$$

$$M_f i_f = \frac{1}{K_s} (Q_{set} - Q + D_q(V_{set} - V)) \quad (3)$$

where the input variables are of the electromagnetic torque (T_e), reactive power (Q) generated by Synchronverter and grid voltage (V); the internal set values are the moment of inertia (J), integrator gain (K) to regulate the field excitation, frequency droop coefficient (D_p), voltage droop coefficient (D_q), voltage (V_{set}), angular frequency (ω_{set}), active power (P_{set}) and reactive power (Q_{set}); and the output variables are the angular frequency reference (ω^*) and field excitation ($M_f i_f$). The mechanical torque (T_m) can be obtained from the setpoint of active power (P_{set}) by dividing it with the nominal mechanical speed (ω_{set}).

Following, the $\overrightarrow{\cos \theta}$ and $\overrightarrow{\sin \theta}$ are vectors defined as the three-phase angle difference with equal spacing of 120° or $2\pi/3$ in radian, as shown in equation (4).

$$\overrightarrow{\cos \theta} = \begin{bmatrix} \cos \theta \\ \cos \left(\theta - \frac{2\pi}{3} \right) \\ \cos \left(\theta - \frac{4\pi}{3} \right) \end{bmatrix}, \quad \overrightarrow{\sin \theta} = \begin{bmatrix} \sin \theta \\ \sin \left(\theta - \frac{2\pi}{3} \right) \\ \sin \left(\theta - \frac{4\pi}{3} \right) \end{bmatrix} \quad (4)$$

The electromagnetic torque (T_e) is the energy stored in the magnetic field of the machine, by equation (5), where \langle , \rangle denotes the inner product.

$$T_e = M_f i_f \langle i, \overrightarrow{\sin \theta} \rangle \quad (5)$$

where the input variables are the output LC filter current ($i = [i_a \ i_b \ i_c]^T$), $\overrightarrow{\sin \theta}$ vector and field excitation ($M_f i_f$).

The modulated voltage ($e = [e_a \ e_b \ e_c]^T$) is the control signal for the PWM of converter switching devices, by equation (6).

$$e = M_f i_f \dot{\theta} \overrightarrow{\sin \theta} \quad (6)$$

where the input variables are the $\overrightarrow{\sin \theta}$ vector, field excitation ($M_f i_f$) and angular frequency reference (ω^*).

The real active (P) and reactive power (Q) generated by Synchronverter can be given by equation (7), where \langle , \rangle denotes the inner product.

$$P = \dot{\theta} M_f i_f \langle i, \overrightarrow{\sin \theta} \rangle, \quad Q = -\dot{\theta} M_f i_f \langle i, \overrightarrow{\cos \theta} \rangle \quad (7)$$

where the input variables are the output LC filter current (i), $\overrightarrow{\sin \theta}$ vector for the active power, $\overrightarrow{\cos \theta}$ vector for the reactive power, field excitation ($M_f i_f$) and angular frequency reference (ω^*).

2.2 Impact on fault current

The energy transition towards the use of converter-interface generation technologies, such as wind or solar PV, has the effect of reducing the short-circuit currents that these new generation technologies contribute to the electrical power system.

In the case of conventional generation (nuclear, hydro, oil-gas, etc.), i.e. based on SGs, the fault current provided is normally a multiple of between three and six times its rated output current [39]. This is because the presence of SGs in a network causes complex electromagnetic transients to occur during a short-circuit, which must be considered in the short-circuit calculation. These transients are because the magnetic field in the generators cannot vary abruptly, i.e., there is a kind of "magnetic inertia" which is modelled, for short-circuit analysis, as a variation in the internal impedance of the generators, in particular the reactance, which varies throughout the transient. Typically, three values of reactance are considered, which are used depending on the study to be carried out:

1. When the values of currents and voltages in the first instants of time (between 20 and 50 ms) of the short-circuit are to be calculated, the value of the sub-transient reactance, denoted as X'' in unit magnitudes, is used [40].
2. When the values of currents and voltages in the first 0.05-3 seconds of the transient are to be calculated, the value of the transient reactance, denoted as X' in unit magnitudes, is used. The currents that occur during this period of time are those that must interrupt the circuit breakers [40].
3. If the system is to be studied when the short-circuit has already reached steady state, the synchronous reactance value, X_s in unit magnitudes, must be used. Since the steady state is rarely reached when the short-circuit has occurred, as the system protections have been activated by then, this value is rarely used [40].

Typical values for these reactances are as follows:

Table 1. Typical synchronous generator reactance values

Reactance	Value
Synchronous reactance (X_s)	1 – 1.3 p.u.
Transient reactance (X')	0.2 – 0.4 p.u.
Sub-transient reactance (X'')	0.1 – 0.2 p.u.

As can be seen in Table 1, the values of the sub-transient reactance are the lowest of all. This means that during the first moments of the short-circuit, the currents circulating through the elements have a higher value.

Figure 5 shows the time evolution of a typical short-circuit current waveform in a SM in the sub-transient, transient, and permanent periods. In this figure the DC component of the current has been eliminated.

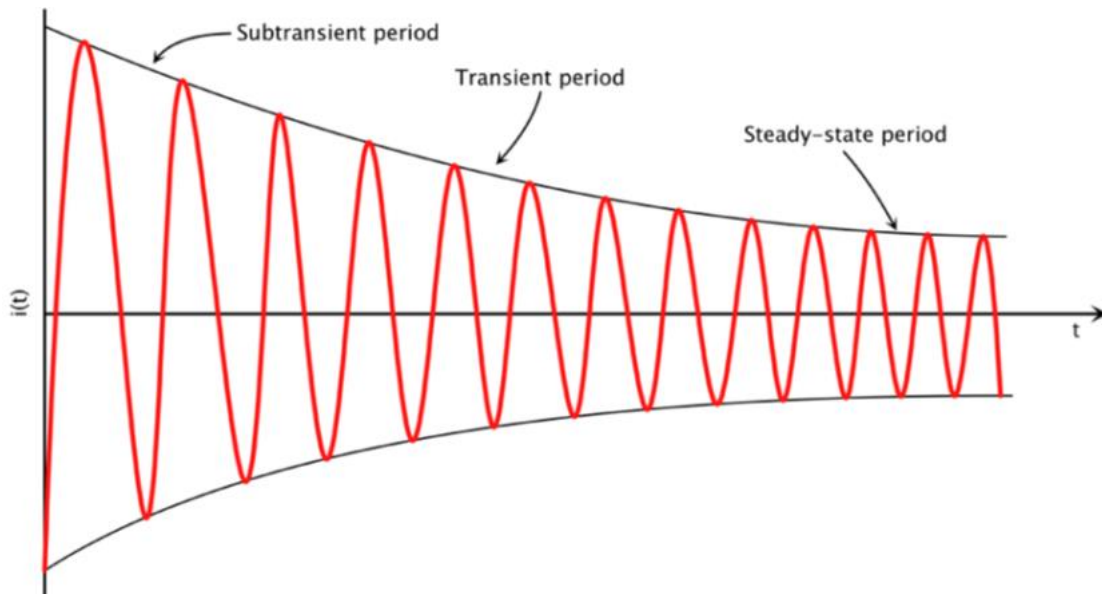


Figure 5. Evolution of the short-circuit current in a synchronous machine, without considering the DC component [41]

In contrast, due to their thermal ratings to protect semiconductor switches, converter-interfaced generators often have extremely limited capacity for short-circuit current, with currents being constrained by the converter controller and built-in protective mechanisms [42].

The fault current delivered depends on the design parameters which differs according to the converter and the manufacturer. Also the converter control as well as the thermal rating of semiconductor switches are relevant to the magnitude of the fault current [15]. The sustained fault current provided by a converter-interfaced source may typically only be around 1.2 times its nominal rating [39].

In [43] the test results between SG and Inverter-Interface Distributed Generator (IIDG) show that in Figure 6(A) the SG outputs quite high sub-transient and transient current before decaying to its steady state value while in Figure 6(B) the IIDG current drops immediately.

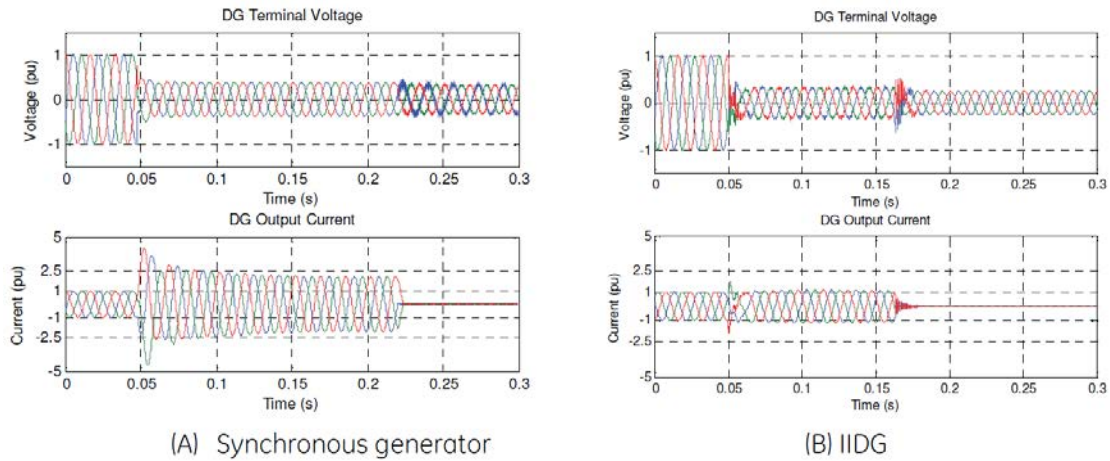


Figure 6. Terminal voltage and output current of SG (A) & IIDG (B) with a 3-phase fault [43]

As a result, in small isolated power systems based on low and medium voltage grids, also known as distribution grids, where protection schemes are based on overcurrent protection devices, such as fuses and relays, this long-established protection technique might be inadequate for grid protection with converter-interface generators since it depends only on the short-circuit current magnitude [14].

Also, if a high penetration of converter-interfaced generation is present, the performance of distance protection can be affected. During the transition period, the waveform of the currents is distorted and deviates from the conventional SG short-circuit current contribution [44][22]. This means that the distance protective relay, which relies on negative-sequence, can potentially malfunction during fault conditions if no negative-sequence current is produced by the converter or if the negative-sequence current produced by the converter does not have the same phase angle relationship as those produced by rotating machines [45][46]. This is due to the negative-sequence current injection suppression control strategy.

It has been observed that negative-sequence control on converter-interface generators has an important effect on power system protection. This is especially significant as the most recent grid codes released by ENTSO-e provide the option to set requirements for negative-sequence current injection [47][22].

For this reason, more sophisticated protection schemes have been explored regarding their suitability for the protection of power systems with high penetration of converter-interface generation [15]. The suitability of such protection schemes is discussed in the section 2.5.

2.3 Converter Short-Circuit Analysis

Electric sources that are integrated into power systems can be modelled in the sequence domain to better understand how they react to disturbances. While the sequence models of SGs are well-known and verified. The fault response of converter-interface generators is significantly different from that of SGs, and their equivalent sequence models must be discussed. In [48][49] the following sequence model has been proposed that can describe the characteristics of grid-forming converters during short-circuit analysis.

2.3.1 Zero-Sequence Model

Since converters are unable to generate zero-sequence current, the magnitude of the zero-sequence output impedance is infinite [48], i.e., the converter represents itself as an open circuit in the zero-sequence network, and its controllers are thus not involved in the zero-sequence circuit [49].

2.3.2 Positive-Sequence Model

The grid-forming converter keeps its output voltage at the nominal value regardless of the three phase currents when the converter currents are below the threshold (I_{th}) on all phases or the current limiter is off. Consequently, the grid-forming converter portrays itself as an ideal voltage source in the positive-sequence circuit. This is illustrated in Figure 7(a).

On the other hand, if the converter current is restricted at the threshold on at least one phase, the converter will no longer be able to maintain its output voltage, causing a voltage sag. This behaviour can be modelled by an impedance (Z_1) at the converter output, as shown in Figure 7(b) [48].

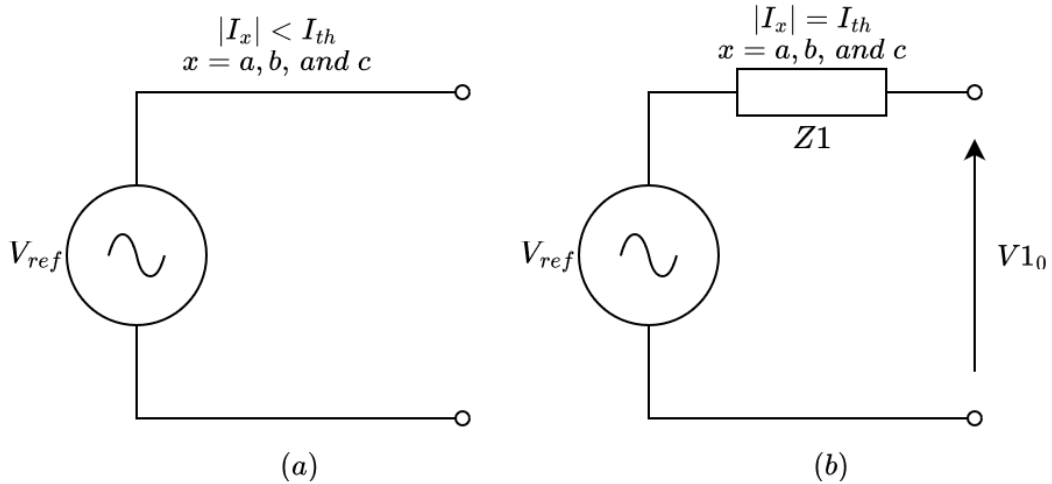


Figure 7. Equivalent model of grid-forming converters in the positive-sequence circuit when the converter currents are (a) below the threshold on all phases (b) limited at the threshold at least on one phase [48]

Measuring the corresponding values at the converter-interface output, denoted by $V1_o$ and $I1_o$, the positive sequence impedance ($Z1$) is calculated through the equation (8) which considers the electric quantities in both pre-fault (denoted by pre_f) and post-fault (denoted by pos_f) conditions.

$$Z1 = -\frac{V1_{o\ pos_f} - V1_{o\ pre_f}}{I1_{o\ pos_f}} \quad (8)$$

2.3.3 Negative-Sequence Model

A negative-sequence current develops in the output current after a fault, yet the output voltage has no negative-sequence. That is, the converter portrays itself as a short-circuit in the negative-sequence circuit. As a result, when the converter current is not restricted, Figure 8(a) depicts the equivalent model of the converter in the negative-sequence circuit.

Three phase currents and voltages will be unbalanced at the output when the converter current is restricted at the threshold on one or more phases. This happens because of the limiter preventing the PI voltage controller from restoring the dq components of the voltage to the reference values, causing a voltage increase. An impedance ($Z2$) can replicate this behaviour, as seen in Figure 8(b).

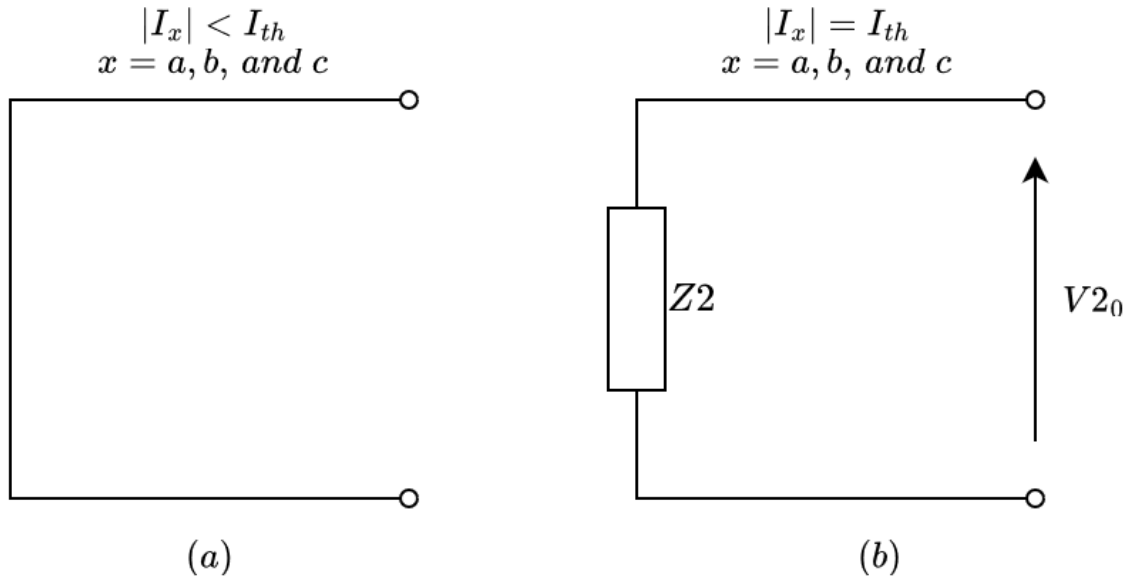


Figure 8. Grid-forming converter in the negative-sequence circuit (a) when all three phase currents are below the threshold (b) when the current is limited at least on one phase [48]

Like the positive-sequence impedance, measuring the corresponding values at the converter-interface output, denoted by $V2_o$ and $I2_o$, the negative-sequence impedance ($Z2$) is obtained through the equation (9).

$$Z2 = -\frac{V2_o}{I2_o} \quad (9)$$

Figure 9 depicts the equivalent model of the grid-forming converter in each sequence circuit when the fault causes converter current to exceed the threshold on at least one phase.

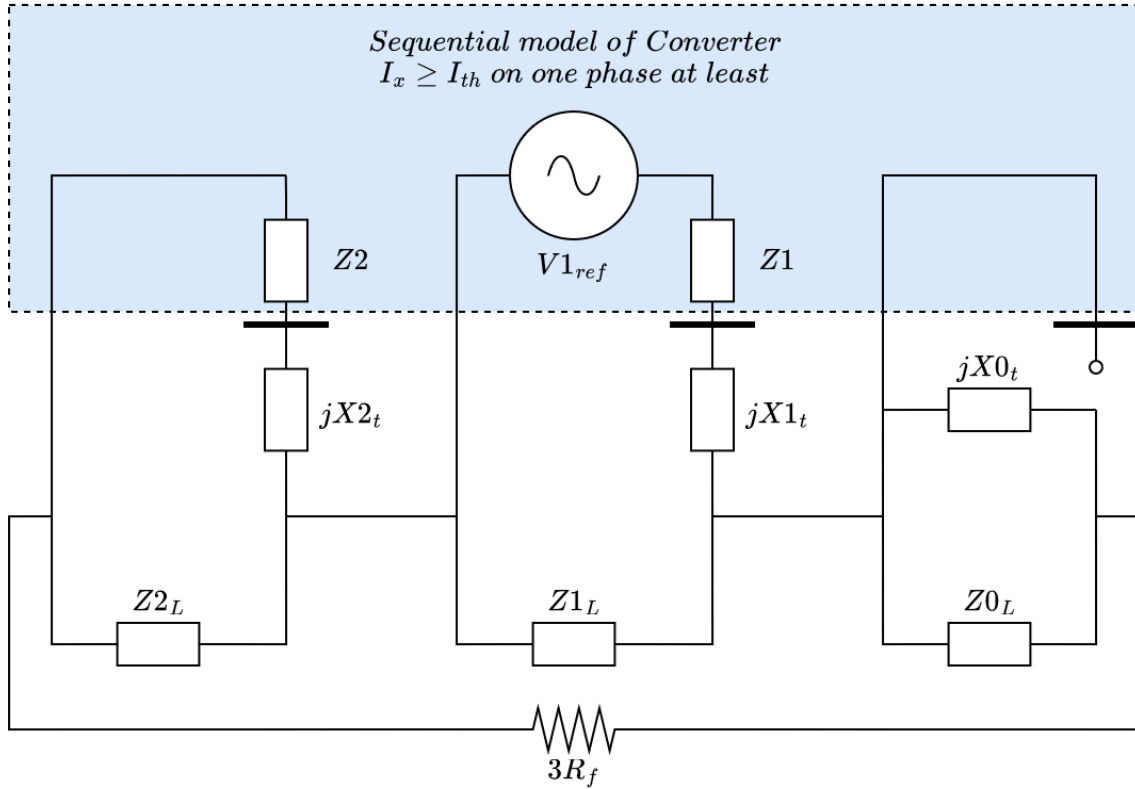


Figure 9. Equivalent model of the grid-forming in each sequence circuit when the fault pushes converter current to exceed the threshold on at least one phase [49]

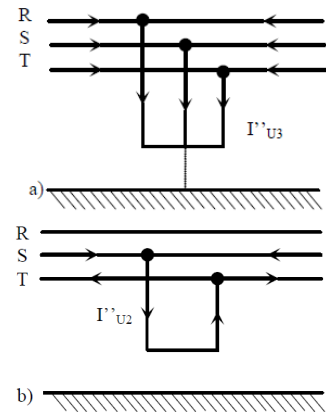
2.4 Faults

A fault may be either symmetrical or asymmetrical, with symmetrical faults affecting all lines simultaneously and asymmetrical faults affecting either one phase or both phases [50]. There are ten different types of faults in electrical power systems:

- Symmetrical faults: 1.
- Asymmetrical phase to phase faults: 3.
- Asymmetrical phase to phase with ground: 3.
- Asymmetrical phase to ground: 3.

Three-phase short-circuit. Three-phase short-circuits are the only ones that behave as balanced systems, as all phases are affected equally. As it is a balanced system, it is only necessary to use the positive-sequence network for its calculation [51].

Two-phase short-circuit. As it occurs in two of the three phases of the system, this short-circuit is no longer balanced and, therefore, both the positive-sequence network and the negative-sequence network must be used for its calculation [51].



Two-phase short-circuit to ground. This has the same characteristics as the two-phase short-circuit without contact to ground, but, in this case, with loss of energy to ground. In the event of this fault, it is necessary to consider, in addition to the positive- and negative-sequence networks, the zero-sequence network, due to the loss of energy [51].

Single-phase short-circuit to ground. For its calculation, as it is an unbalanced short-circuit with energy loss, the three sequence networks (positive, negative and zero) are necessary [51].

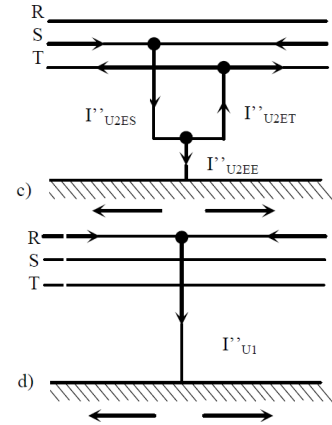


Figure 10. Fault types scheme: a) LLL, b) LL, c) LLG and d) SLG [51]

Three-phase symmetrical faults and single line-to-ground faults are typically the two types of faults that are discussed in the literature. The most frequent fault is single line-to-ground, while three-phase faults are frequently the most severe. Shunt fault data are shown in Table 2 [52].

Table 2. Fault statistics based on fault type [52]

Fault Type	Occurrence Probability (%)	Severity
Single Line to Ground (SLG)	85	Least
Line-Line (LL)	8	
Double Line to Ground (LLG)	5	
Three Phase Bolted (LLL)	2	Most

Additionally, the probability of faults on electrical power system components varies. The transmission and distribution lines that are in open air have the highest risk of developing problems. Indoor equipment is least likely to experience problems (underground cables and power generators). Table 3 displays the fault statistics for the components of the electrical power system [52].

Table 3. Fault statistics based on power systems elements [52]

Power System Element	Probability of Faults (%)
Overhead Lines	50
Underground Cables	9
Transformers	10
Generators	7
Switchgears	12
CT, PT, Relays etc.	12
Total	100

2.5 Protections

Operation and control of electrical power systems require protection as a critical component. If a defect in an electrical power system is not fixed quickly, it can interfere with regular operation and have cascade repercussions. Finding the precise problem location as soon as feasible is one of the key tasks in fault clearing and system restoration. One of the most time-consuming and

important activities performed by operation engineers is identifying and diagnosing problems in an electrical power system. Faster system restoration, increased system dependability, less operational costs and losses, simpler tasks for maintenance staff, and higher customer satisfaction are all benefits of early fault detection and localization [53].

Therefore, protective relays are necessary on a power system to quickly remove any electrical equipment connected to the power system from operation when a short-circuit fault happens or when the power system starts acting abnormally. In a sense, protective relays operate as the brains that decide when the right time is for a circuit breaker to trip. A circuit breaker is a mechanical device that may physically isolate the electrical power system from short-circuit disturbances while detaching the damaged component [50].

The following fundamental criteria must be considered and followed by any network's protective measures [50]:

- a) Selectivity, sometimes referred to as discrimination, is the capacity to preserve supply continuity by cutting off the smallest portion of the network required to isolate the fault and leaving the remaining healthy parts intact.
- b) Reliability, this term describes the capacity of protection to function properly. It is made up of two components: dependability and security, which refer to, respectively, the assurance of a right operation even in the presence of defects and the capacity to prevent erroneous operation while experiencing faults.
- c) Sensitivity, the protective relay needs to be sufficiently sensitive to the current's strength in order to turn on when the pick-up current, a predetermined detection threshold, is just crossed.
- d) Stability, the capacity of the protective system to continue functioning properly even when a significant current is flowing across its protective zone because of an external fault that is not located inside its zone. The relevant circuit breaker fixes the issue.
- e) Speed, to ensure system stability and limit equipment damage, a protective system should promptly disconnect the defective component.
- f) Economics, obtaining the highest level of security at the lowest feasible cost, which is often no more than 5 % of the overall cost of the power system being safeguarded.

There are mainly two options to solve the problem of low short-circuit currents caused by converter-interface generation [14]:

1. Increase the short-circuit current levels. This can be done by using of energy storage systems (e.g., flywheel, supercapacitor, etc.) with high short-circuit capabilities, to satisfy the operating settings of fuses and overcurrent relays [54][55]. Or by increasing the fault current capability of converter interfaced generation units. This can be achieved by increasing their power rating or by applying extensive cooling of their switching devices [14]. The high investment costs of both options rule out their implementation.
2. Replace the actual protective devices with other protective schemes, which provide advanced and accurate protection functionalities for low short-circuit currents [14].

The following are some of the most common protective schemes usually used in modern electrical power systems and could be used to solve the problems caused by converter-interface generators [15]:

2.5.1 Overcurrent protection

It is the most widespread protection in its application, especially in medium voltage distribution networks where it is the main protection against short-circuits. It monitors the current flowing through the protected element and compares it with a set value. If the current flowing through the element is higher than the set value, the relay will trip [23].

2.5.2 Directional overcurrent protection

A directional overcurrent protection decides whether to trip or not based on two quantities: Operating quantity: This is the threshold value of the overcurrent. It monitors if this threshold is exceeded. Polarisation quantity: This is a quantity that serves as a reference for determining the direction of the current [23].

The polarisation magnitude must fulfil two premises: It must not cancel in a short-circuit situation. Even if the direction of current flow changes, the direction of the determined polarisation quantity must remain unchanged [23].

2.5.3 Distance protection

Distance protections, presented in [56], are mainly used in the high-voltage transmission network and mainly for line protection. The protection system must guarantee maximum tripping times irrespective of the existing short-circuit power. This condition cannot be met by overcurrent relays, whose tripping time is a function of the fault current.

The distance protection decides whether or not to trip, within a given time, depending on the impedance between its location and the fault point. To perform its function, the protection measures voltage and current and calculates an impedance from these values.

Normally, distance protection does not require communication between relays [57]. However, the distance protection scheme has several drawbacks, such as problems with measurement accuracy due to the presence of harmonics, inaccuracy in the admittance measurement due to fault resistance, and the difficulty of measuring impedance/admittance in short lines [24].

2.5.4 Differential protection

Differential protection is another common method, and was presented in [58][59][60]. Line differential protection is based on the comparison of the currents at each end of a line. The equipment installed at each end exchanges data via the communication channels. Each device compares the current it measures with the currents coming from the remote ends. Its operation is based on Kirchhoff's law.

This scheme requires protective relays at each end of the line, which increases the cost. In addition, a communication infrastructure is required to send current measurements from both ends of the line, which also increases the cost and compromises the safety of the protection system. Furthermore, measurements need to be synchronised. Finally, unbalanced loads and transients can lead to protection failure [26].

2.5.5 Adaptive protection

An adaptive protection is a relay with dynamic settings since it will automatically update relay settings based on prevailing system conditions. According to this scheme, protection system

continuously monitors the system and applies new protection coordination in case of any changes in topology or operation [61].

Despite of the flexibility that adaptive relays offer it is very expensive to replace all existing relays with adaptive ones. Besides, they always need communication infrastructures for reliable and fast operation [26]. Moreover, after any fundamental change in the distribution system (e.g., addition of new feeder), it is necessary to update the relay coordination algorithm [62].

2.5.6 Voltage-based protection

A voltage-based detection technique, as proposed in [20][63][64], can be used to identify faults with low current levels, since any fault causes a drop in the grid voltage. When the voltage signal measurement is lower than the allowed value of the voltage drop, the protection relay trips [26]. The main disadvantage of voltage-based protection methods is that any voltage drop in the grid can cause unnecessary tripping of the protection relay [24]. Therefore, temporary situations like load switching and/or the energization of dynamic loads might compromise this sort of protection since cannot provide an adequate selective protection [62].

2.6 New protection system proposal: Wavelet transform

Fourier analysis is a standard method for analysing a time-domain waveform in the frequency domain [65]. When obtaining the Fourier transform of a signal with transients, one of the difficulties of this approach becomes apparent. The Fourier transform of the signal is evaluated at a given frequency using a weighted average over the entire period, and since a transient forms only a very small part of the total time duration of the signal, its contribution to the frequency domain representation of the signal may be negligible compared to the contribution from the rest of the signal [66]. Consequently, it is difficult to identify the prominent frequency features of signal transients using a frequency domain representation [67]. In addition, the representation of the signal in the frequency domain does not provide information about the timing of the transients. As a result, the Fourier transform lacks a multi-resolution representation in terms of both time and frequency [68].

In contrast to the Fourier method, the Wavelet transform offers both time and frequency localisation [31]. It therefore detects a wide range of different events, proving to be a powerful tool for assisting in the analysis of electrical power systems [69]. The result is an in-depth study of different components of high-frequency voltages and currents can be thoroughly studied because they have excellent temporal resolution, whereas components of those signals with low frequencies exhibit better frequency resolution [34].

When evaluating increases or decreases, slope changes, discontinuities, etc. in voltage and current waveforms, Wavelet analysis produces coefficients with low values if the changes are not significant enough. However, if the waveforms change significantly, the coefficients obtained are extremely high [34].

Application in the identification of transient events and disruptions in electrical power systems is one of the Wavelet transform's key qualities. Establishing a threshold that permits considering that an event has been detected if it has been surpassed, and, if not exceeded, will not evaluate the different values of the signal or analysed signals [70].

The Wavelet transform can be used to extract information from a transient signal in the time domain by decomposing the signal into a high-frequency band with a short window scale and a

low-frequency band with a long window scale, as opposed to the Fourier transform. This makes it particularly effective for analysing signals with harmonics using the Discrete Wavelet Transform (DWT), as seen in equation 10 [71].

$$DWT(s, m, k) = \frac{1}{\sqrt{a}} \sum_n s(n) \Psi^* \left(\frac{k-b}{a} \right) \quad (10)$$

where $s(n)$ is the input signal to be decomposed, Ψ is the mother Wavelet, and the scaling and translation parameters $a = a_0^m$ and $b = na_0^m$ respectively, are functions of integer parameter m .

The mother Wavelet that is developed for the Wavelet transform analysis must perform well in extracting the primary properties of the analysed signal as well as having appropriate harmonic removal features [34]. There are several mother wavelets such as Harr, Daubechies, Biorthogonal, Coiflets, etc.

The current or voltage signal that is being analysed is divided into several windows with short scales for the high frequency band and long scales for the low frequency band during the transient period when a defect occurs. A magnitude scale and time shift procedures must be used for this decomposition [34].

Depending on the sampling frequency of the original signal, the number of decomposition steps is determined. The first decomposition has two elements: a high-frequency element D_1 and a low-frequency element A_1 . As a function of the sampling frequency f_s , the frequency band of D_1 element is $f_s/2 - f_s/4$ Hz, whereas the frequency band of A_1 element is $f_s/4 - 0$ Hz. In the second decomposition, the A_1 element is decomposed into D_2 element for the high-frequency band ($f_s/4 - f_s/8$ Hz) and A_2 element for the low-frequency band ($f_s/8 - 0$ Hz) [33].

This procedure is repeated until the appropriate frequency band is attained, and the proper information can be retrieved from the assessed signal. In Figure 11, the decomposition developed by the DWT can be seen. A and D represent the approximation and detail coefficients respectively [72].

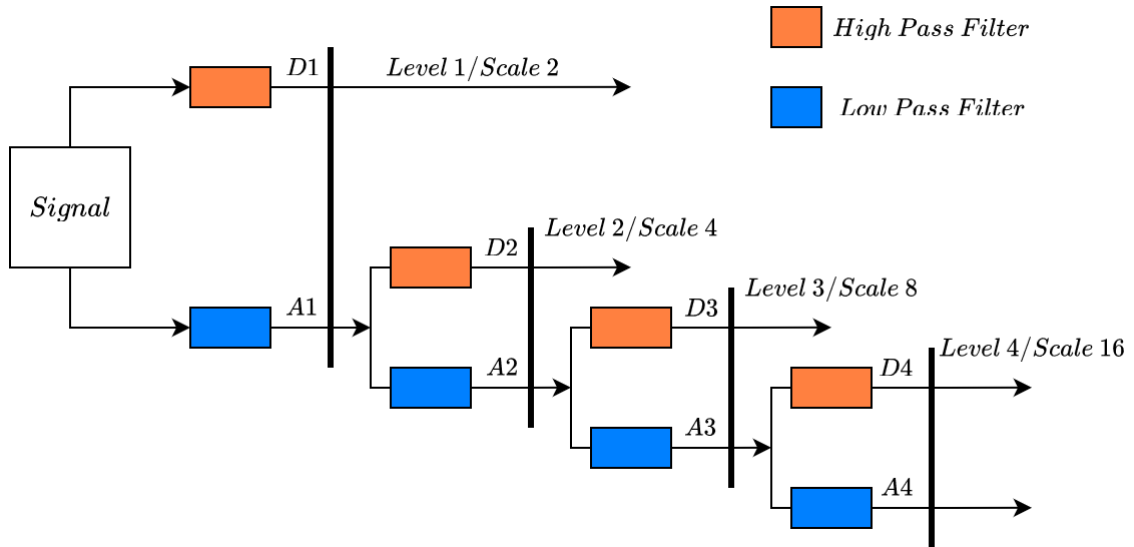


Figure 11. Frequency bands of the discrete Wavelet transform related to decomposition steps [72]

2.7 Simulation and Real-Time Tools

During the development of this thesis, different simulation tools have been used to obtain the results. A brief explanation of their main features and functionalities is given below.

2.7.1 MATLAB/Simulink

Simulink is a simulation and model-based design environment for dynamic and embedded systems, integrated with MATLAB. Simulink is a data flow graphical programming language tool for modelling, simulating, and analysing multi-domain dynamic systems. It is basically a graphical block diagramming tool with customizable set of block libraries [73].

2.7.2 PowerWorld

PowerWorld Simulator is an interactive power system simulation package designed to simulate high voltage power system operation on a time frame ranging from several minutes to several days. The software contains a highly effective power flow analysis package capable of efficiently solving systems [74].

2.7.3 Typhoon HIL

Typhoon HIL provides software for modelling, simulation, monitoring and testing electrical power systems. For real-time simulation and testing, the modules can be used only together with Typhoon devices. Schematic Editor provides the tools for the development of the electrical model, control and data acquisition implementation [75].

Typhoon HIL is based on hardware-in-the-loop (HIL) simulation, which is a technique to test embedded systems in a comprehensive, cost-effective, and repeatable manner. This method is typically used when the embedded system is difficult to thoroughly and repeatably test in its operational environment. To use HIL simulation, developers must create a real-time simulation that models the embedded system under test (SUT) and all its interactions with its environment. The simulation will monitor the SUT's output signals and inject synthetically generated input signals into the SUT at specific points. Output signals from the SUT can include actuator commands and operator display information, while inputs to the SUT may include sensor signals and commands from an operator. The outputs from the embedded system will become inputs to the simulation, and the simulation will generate outputs to become inputs to the embedded system [76].

3 Modelling

The protection system is studied and analysed using a test system that includes power converters and SGs. This chapter describes the models of the elements and devices that comprise the entire test system.

3.1 Grid Model and Characteristics

The grid model chosen for the simulations and the modelling of the different grid elements, the standard IEEE nine-bus test system, is presented below.

3.1.1 IEEE nine-bus System

A 50 Hz grid model has been outlined using the standard IEEE nine-bus test system [77], illustrated in Figure 12, in which the generation units are SGs or grid-forming VSCs. In addition, the positions of the protection relays are also presented in Figure 12.

The three generation units are connected to buses 1, 2, and 3, and the three loads modelled as constant impedances are connected to buses 5, 6, and 8. The grid and the generators are connected through three LV/MV transformers, which are modelled as a three-phase linear transformer. The grid has six transmission lines modelled by a RL model and nine buses. The grid model specifications can be found in Table 4.

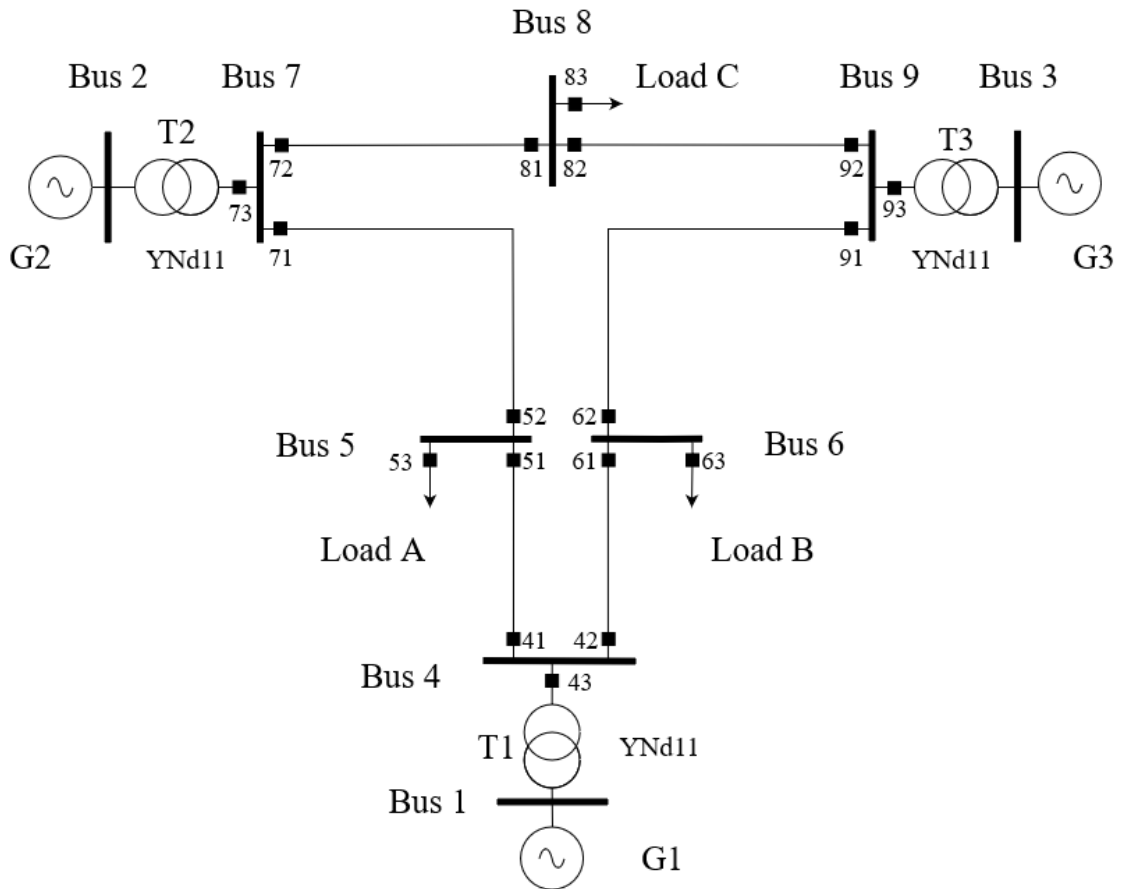


Figure 12. IEEE nine-bus test system scheme

Table 4. Grid model specifications

SG	Load A	Load B	Load C	Transformer	Line
3 MVA	2.25 MW	1.62 MW	1.8 MW	3 MVA	20 km
400 V	0.95 Mvar	0.54 Mvar	0.63 Mvar	400/20000 V	Conductor LA-56
$X'' = 0.13$	20000 V	20000 V	20000 V	$X = 6 \%$	
$X' = 0.17$				$R_g = 23 \text{ ohm}$ (Ground)	
$X_s = 2.11$				YNd11	

The conductor data of the overhead lines considered for this thesis is a conductor type LA-56. Its main data are listed in Table 5.

Table 5. Main features of conductor LA-56 [34]

Conductor	Total section (mm ²)	Resistance at 20°C (Ω/km)	Resistance at 50°C (Ω/km)	Outer diameter (mm)	Max. current (A)
LA-56	54.6	0.613	0.687	9.45	199.35

Next figure shows the dimensions of the tower selected.

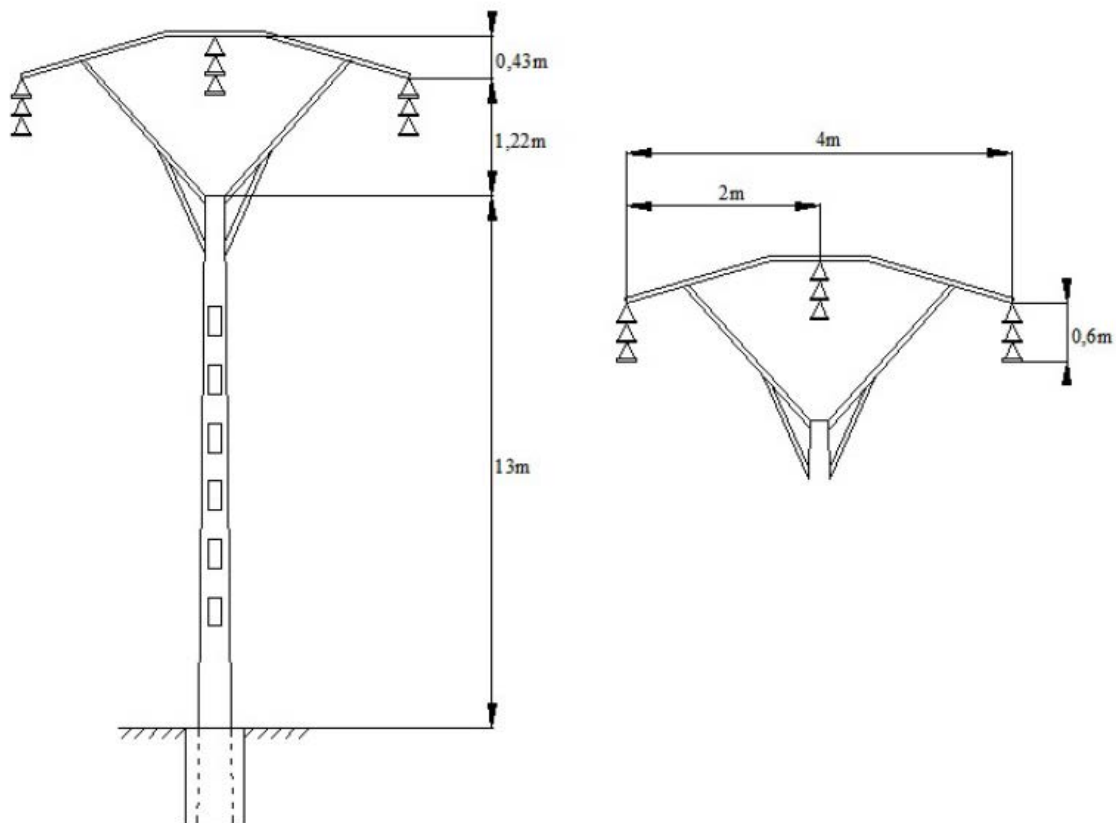


Figure 13. Dimensions of tower used in medium voltage power distribution network [34]

The distribution overhead lines, and electrical tower disposals have the next values:

Table 6. Overhead-line features [34]

Overhead-line features	Values
Length	20 km
Span	100 m
Max. arrow in conductors	1.97 m
Soil resistivity	100 Ω .m

The values obtained for the RL parameters of the overhead lines are:

Table 7. Overhead-line RL features [34]

Overhead-line RL features	Values
Positive resistance sequence (Ω /km)	0.68712
Zero resistance sequence (Ω /km)	0.83102
Positive inductance sequence (H/km)	0.0065445
Zero inductance sequence (H/km)	0.0048614

For the total length of 20 km, the positive- and zero-impedance of the overhead lines have the next values:

$$Z_1 = 13.74 + j4.22 (\Omega) \quad (11)$$

$$Z_0 = 16.62 + j30.53 (\Omega) \quad (12)$$

3.1.2 Synchronous generators

The SGs are three diesel gensets (G1, G2 & G3). For all of them, it has been used the three-phase wound rotor SM model and the IEEE Type 1 exciter model, which provides excitation for a SM and regulates its terminal voltage in generating mode, obtained from the MATLAB/Simulink Simscape library.

The diesel genset active power reference is provided by a local governor that regulates generator speed, closing the active power balance of the grid and maintaining constant the frequency, which it has been modelled as an automatic generation control (AGC) with an internal droop. While, on the other hand, the automatic voltage regulator (AVR) obtains the generator reactive power needed to maintain constant voltage and, thus, closing the reactive power balance of the grid [78].

3.1.3 Voltage Source Converters

As explained in section 2.2, in a grid with 100 % integration of converter-interface generators, the converter control strategy chosen was grid-forming with droop control, and its modelling is presented below.

3.1.3.1 Grid-forming with droop control

An analysis of grid-forming control is essential, as the generation units with converter-interface are the only generators in the grid evaluated here and play a key role in the fault behaviour.

Therefore, the grid-forming control together with the IEEE nine-bus system was modelled in the MATLAB/Simulink environment, to study and verify the proposed detection fault strategy.

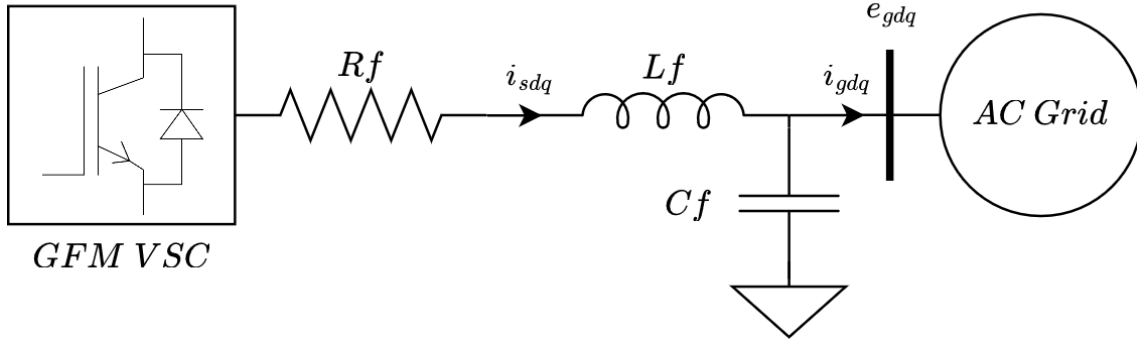


Figure 14. The power stage of a grid-forming (GFM) VSC [35]

Due to the importance of the control of the converter on its fault behaviour, two different control strategies have been implemented to analyse their differences. The first is a cascaded control scheme of the grid-forming in the synchronous rotating reference frame (dq), which is shown in Figure 15. This is more detailed below in the positive-sequence control as it is the same control scheme but with different current and voltage inputs.

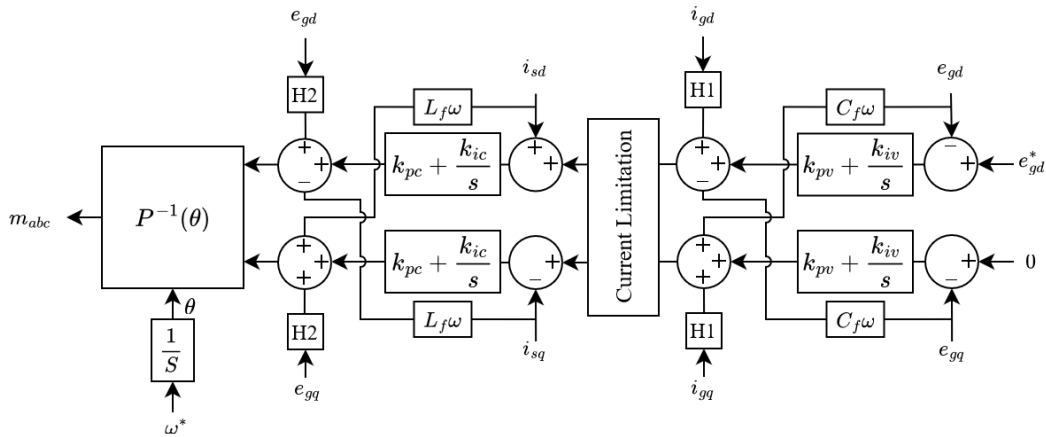


Figure 15. Cascaded control scheme of grid-forming VSC in dq [79]

While the second is also a cascaded control scheme of the grid-forming in dq but for positive-sequence and negative-sequence separately (Figure 16). The positive-sequence control with the inner voltage and current control loops, which are realised in dq , together with the cross-coupling and feed-forward terms. The current references are determined by the voltage loop. They are then passed to the current loop, which produces the modulated voltage for the linearization stage. Finally, the modulation signals are sent to the switching stage of the power converter. An outer control based on the P-f droop control determines the control angle θ by the integral of the angular frequency as shown in (13), and another based on the Q-V droop control gives the voltage reference e_{gd}^* , as shown in (14). The primary control is represented by the equations below [79],[80]:

$$\omega^* = \omega_{set} + m_p(P^* - P_{mes}) \quad (13)$$

$$e_{gd}^* = E_{set} + n_q(Q^* - Q_{mes}) \quad (14)$$

where the active power reference and the output are given by P^* and P_{mes} , respectively; the angular frequency output reference and the set value are given by ω^* and ω_{set} , respectively; m_p is the active power droop gain; the reactive power reference and the output are given by Q^* and Q_{mes} ; e_{gd}^* is the voltage reference; E_{set} is the set voltage value of reactive power droop; n_q is the reactive power droop gain.

Also Figure 16 illustrates the control scheme of the negative-sequence current controller. As Figure 16 indicates, the negative-sequence current controller assumes a structure similar to that of the positive-sequence current controller.

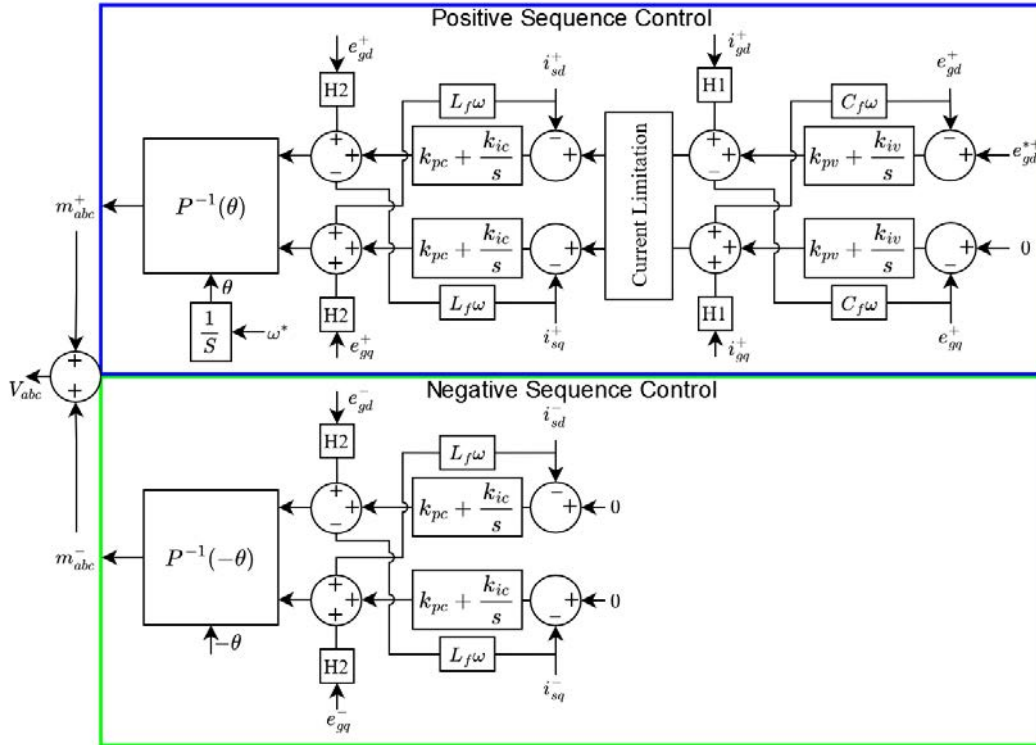


Figure 16. Cascaded control scheme of grid-forming VSC in dq by sequences [79]

The p.u. parameters of the grid-forming VSC used in MATLAB/Simulink simulations are provided in Table 8.

Table 8. Grid-forming VSC parameters (in p.u.)

Parameter	Value	Parameter	Value	Parameter	Value
L_f	0.2	R_f	0.0033	C_f	0.1
K_{ic}	160	K_{pc}	1	H1	0
K_{iv}	78	K_{pv}	1	H2	0

where K_{pc} and K_{ic} are proportional and integral gains of the current controller, respectively; K_{pv} and K_{iv} are proportional and integral gains of the voltage controller, respectively; C_f , L_f and R_f are the filter capacitance, inductance, and resistance, respectively; gains H1 and H2 reduce the disturbances introduced into the control.

To extract the positive- and negative-sequence networks from the measured instantaneous voltages, the positive- and negative-sequence is calculated from the $\alpha\beta$ components and the delay of these components by a quarter of a period ($T/4$) as shown in Figure 17 [81].

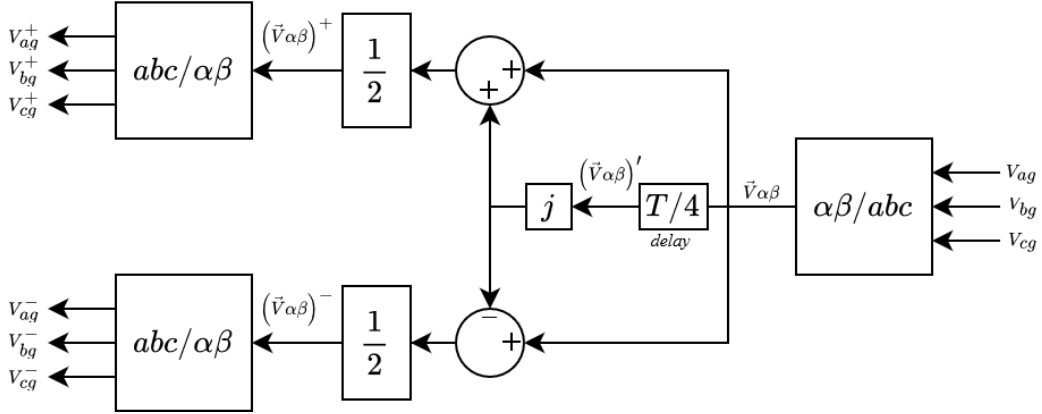


Figure 17. Sequence extraction algorithm [81]

Once the $\alpha\beta$ components of the positive- and negative-sequences are known, the phase magnitudes are obtained using the inverse *Clarke* transform ($\alpha\beta/abc$). As explained above, the P-f droop control determines the control angle θ by the integral of the angular frequency, with that angle the *Park* transform is applied to obtain the positive-sequence dq components for both voltages and currents. The negative-sequence components are obtained by applying the *Park* transform to the same instantaneous voltages and currents as above using the angle of the position of the d-axis of the negative-sequence rotating axis system, angle θ' . Considering that $\theta' = -\theta$, i.e. the negative-sequence axis rotates at the same speed as the positive-sequence axis, but in the opposite direction [81].

Figure 18 shows the block diagram of sequence extraction and *Park's* transformation ($abc/\alpha\beta$) that allows the determination of the positive- and negative-sequence dq components of both currents and voltages [81].

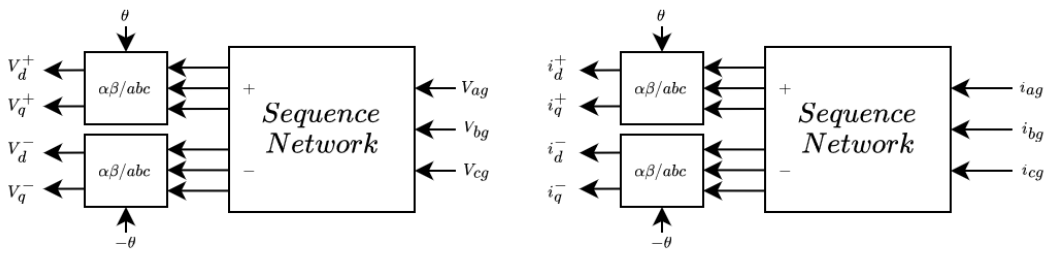


Figure 18. Calculation of sequence components of voltages and currents [81]

Figure 19 below shows the behaviour of the grid-forming control of the converter described earlier in this section against a change in load (10 %) to demonstrate the correct operation of the proposed control strategy.

A current limitation strategy was also designed to prevent damage to the VSC due to overcurrent. This strategy must be included in the control scheme of the converter in order to achieve the main objective of protecting the semiconductor switches. In the following sections, the current limiting strategy is explained.

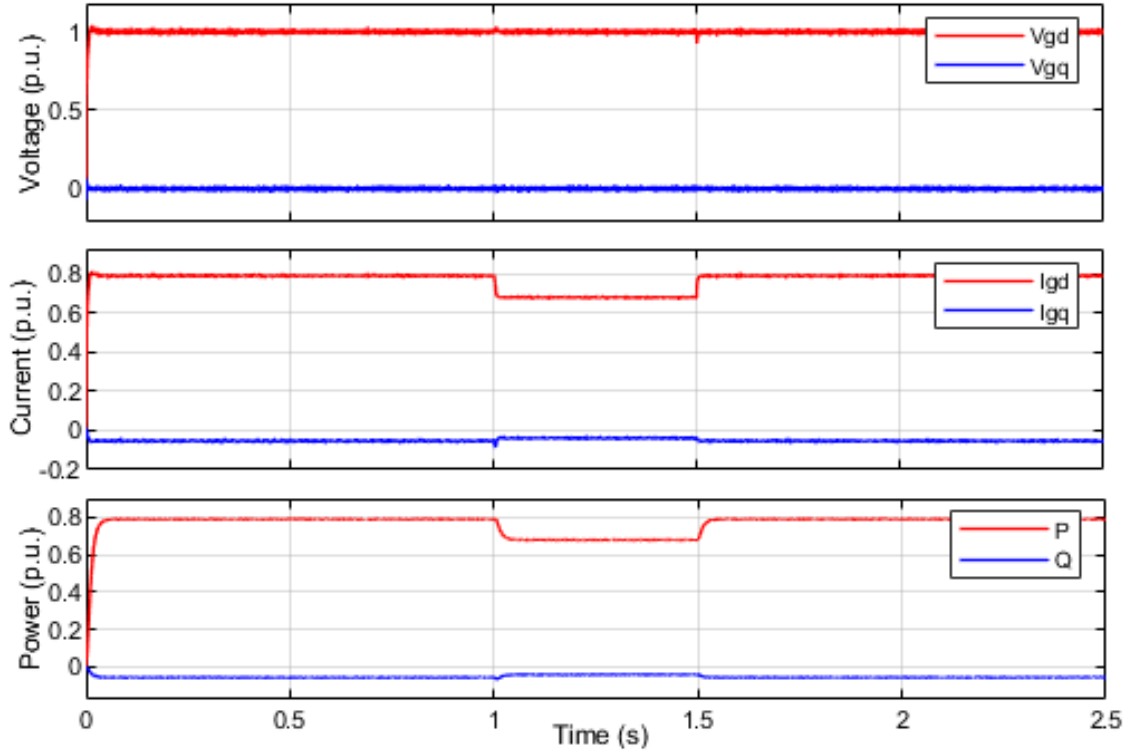


Figure 19. Simulation of the operation of the grid-forming control converter

3.1.3.2 Current Limitation

The main objectives of current limitation are to keep all components of the converter within their rated values and to avoid overcurrent during transient events. By setting the limiting current between the two inner loop controllers, as shown in the *Current Limitation* block in Figures 15 and 16, the reference switching current is limited and its dq components are constrained by vector amplitude saturation [82].

This method requires calculating the current reference amplitude $|\overline{I_{dq}^*}|$ and the vector angle δ_{dq} resulting from the DQ-components using the following equations [82]:

$$|\overline{I_{dq}^*}| = \sqrt{(I_d^*)^2 + (I_q^*)^2} \quad (15)$$

$$\delta_{dq} = \tan^{-1}\left(\frac{I_q^*}{I_d^*}\right) \quad (16)$$

The absolute value of the reference current amplitude $|\overline{I_{dq}^*}|$ can be limited. The current amplitude can be determined and limited according to the ability of the converter components to handle the overcurrent, as shown in Figure 20. The angle is also required for calculating the saturated values of each current component. Thus, like a SG, the grid-forming VSC can give a grid-impedance-dependent P/Q ratio in the event of a fault [82]. Since a limiting value of $I_{max} = 1.2$ (p.u.) is set, the converter can supply a certain amount of overcurrent in the case of a fault.

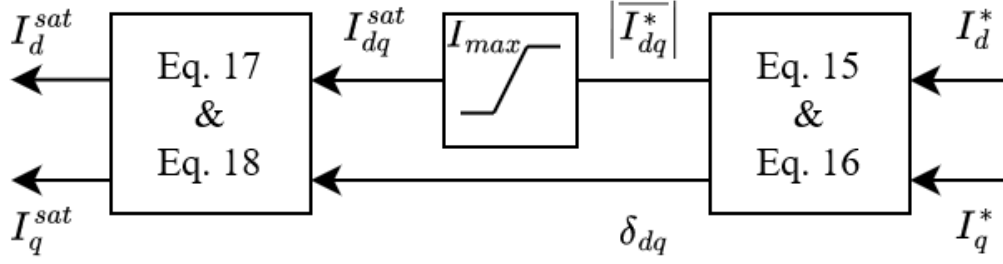


Figure 20. Vector amplitude saturation implementation [82]

where [82]:

$$I_d^{sat} = \cos(\delta_{dq}) \cdot I_{dq}^{sat} \quad (17)$$

$$I_q^{sat} = \sin(\delta_{dq}) \cdot I_{dq}^{sat} \quad (18)$$

3.1.4 Arc Model

Most short-circuits in electrical power systems are ground faults, of which the most common are arcing faults. The investigation of short-circuit faults in [83] shows that more than 80% are arcing faults.

Through the simulation of arcing models, it is possible to better understand the arcing event that appears in high-voltage electrical power systems. Physical models, black box models, and parameter models are the three mathematical models of arcing, and they are described below [84]:

3.1.4.1 Physical Model

This model is based on fluid dynamics rule by the laws of thermodynamics in conjunction with Maxwell's equations, and it has complicated mathematics.

3.1.4.2 Black Box Model

This model describes the behaviour of the arc and is used to simulate arc-circuit interactions. Therefore, the arc is described through one or more differential equations relating the arc conductance to the circuit variables i.e., arc voltage and arc current.

3.1.4.3 Parameter Model

This model is more precise than black box models, but its parameters are acquired from complex equations and tables.

Since the internal conditions of the arc are very complex, a black box model is often used to characterise the arc in order to better understand its electrical characteristics. The *Cassie* model is a classic example, and gives good results for arcs with high currents [84].

Cassie assumed that power losses occur only by convection, which implies that the temperature in the arc remains constant. As a result, the cross-sectional area of the arc is proportional to the current, and the voltage across the arc is constant [84]. The *Cassie* arc model represents the dynamic properties of an arc by the following differential equation:

$$\frac{1}{g} \frac{dg}{dt} = \frac{d \ln g}{dt} = \frac{1}{\tau} \left(\frac{u^2}{U_c^2} - 1 \right) \quad (19)$$

where g is the conductance of the arc, u is the voltage across the arc, τ is the arc time constant, and U_c is the arc voltage constant.

The dielectric breakdown of a gas produces an electric arc by overcoming the dielectric strength of the gas due to a sufficiently high voltage. The voltage leading to the electrical breakdown of a gas is estimated using Paschen's Law, and in the case of dry air, the field strength for breakdown is about 30 kV/cm [85].

The *Cassie* arc is modelled as a voltage-controlled current source, and the differential equation (19) represents the electric arc. Figure 21 shows a block diagram of an implementation of the *Cassie* arc model.

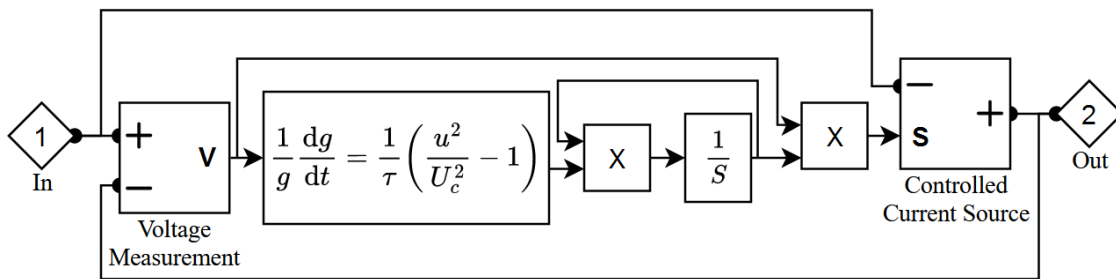


Figure 21. Implementation of the *Cassie* arc model [86]

In the end, the arc fault block diagram shown in Figure 21 was only implemented for the development and research of a journal paper¹. Besides, for the results presented in this thesis the fault has been modelled as an impedance because PowerWorld does not allow arcing to be simulated.

¹ Azuara Grande, L.S.; Granizo Arrabé, R.; Arnaltes, S. Wavelet Analysis to Detect Ground Faults in Electrical Power Systems with Full Penetration of Converter Interface Generation. *Electronics* **2023**, *12*, 1085. <https://doi.org/10.3390/electronics12051085>

4 HIL testing platform implementation

To evaluate the behaviour of the protection relay against different generation technologies (SGs and VSCs), a HIL implementation has been carried out to test of how a real protection relay behaves. Thus, the implementation is divided in two parts:

4.1 Emulated

The case study seen in the previous section is emulated on real-time through the modelling of the full network (Transformers, Transmission lines and Loads) and the generators (SGs or VSCs) by the Typhoon HIL framework modelling. The device in charge of simulate passive components, cables, machines and even semiconductors with optimal fidelity is the HIL 604.

Figure 22 below shows the schematic of the full network modelled through the schematic editor of Typhoon HIL. Also, the grid-forming control explained in section 3.1.3 has been modelled.

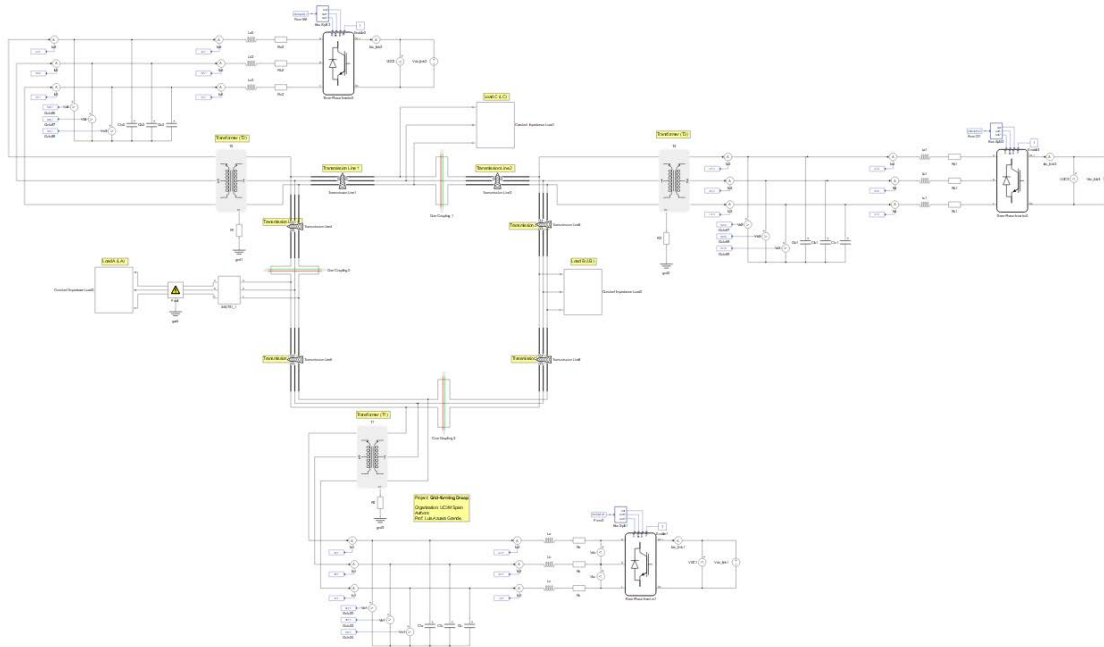


Figure 22. Implementation of the IEEE nine-bus test system in Typhoon HIL real-time simulation framework

4.2 Real

Once the full network and the generation units are emulated on the real-time emulator device, different signals must be sent and received to physically operate the protection relay. Therefore, the real-time emulator (HIL 604) is connected to a power amplifier (Universal HIL Connect) which provides the interface of the analog voltage/current outputs and the digital inputs/outputs with the protection relay (SEL-751). Figure 23 shows a diagram of the connections between the different devices that make up the setup of the HIL testing platform.

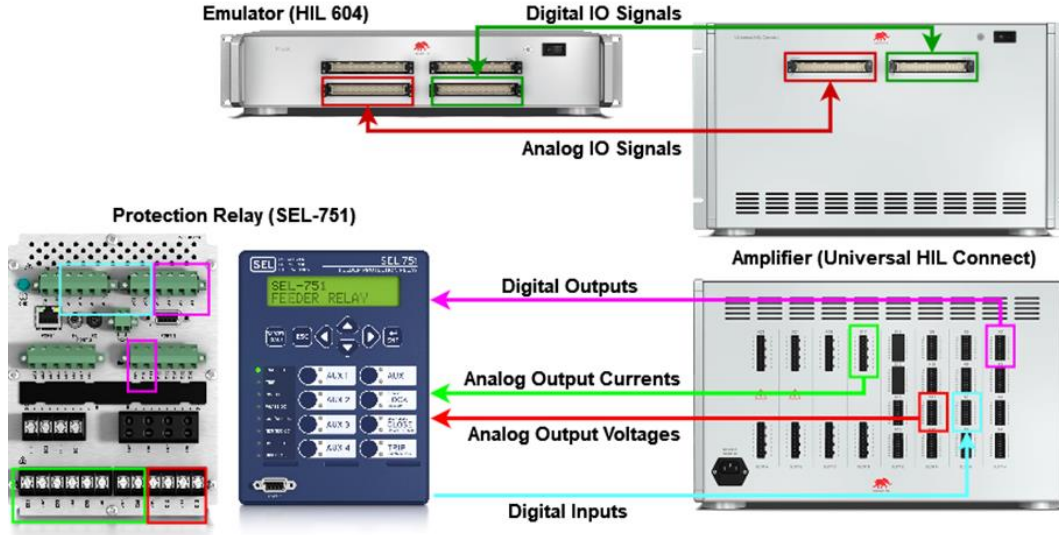


Figure 23. HIL testing platform scheme

In addition, Table 9 specifies the variables of each of the connectors used in the power amplifier (Universal HIL Connect).

Table 9. Inputs and outputs of Universal HIL Connect

Pinouts	Variable	Connector	Pin	HIL Channel
Analog Outputs	Voltage A	X11	1	AO17
	Voltage B	X11	2	AO18
	Voltage C	X11	3	AO19
	Current A	X17	1	AO1
	Current B	X17	3	AO2
	Current C	X17	5	AO3
	Current N	X17	7	AO4
Digital Inputs	Relay Alarm	X5	1	DI1
	Relay Trip	X5	2	DI2
	Relay Trip	X5	3	DI3
Digital Outputs	Not Breaker Status	X1	1	DO1
	Breaker Status	X1	2	DO2
	Wavelet Trip	X1	3	DO3

4.2.1 SEL-751 Configuration

The SEL-751 provides a complete protection for radial and looped distribution circuits with comprehensive protection capabilities, including time-overcurrent, directional overcurrent, autoreclosing, over-/undervoltage, frequency, second- and fifth-harmonic blocking, arc-flash mitigation, fault location, high-impedance fault detection, broken conductor detection, islanding detection, event analysis, and more. The available protection functions of SEL-751 are shown in Table 10 [87].

Table 10. SEL-751 protection functions [87]

ANSI Numbers/Acronyms and Functions			
25	Synchronism Check	51 (P,G,Q)	Time Overcurrent (Phase, Ground, Negative Sequence)
27	Definite-Time Undervoltage	51N	Neutral Time Overcurrent
27I	Phase Undervoltage With Inverse Characteristic	52PB	Trip/Close Pushbuttons
27S	Synchronism-Check Undervoltage	55	Power Factor
32	Directional Power	59 (P,G,Q)	Definite-Time Overvoltage (Phase, Ground, Negative Sequence)
49	IEC Cable/Line Thermal	59I	Overvoltage With Inverse Characteristic
49R	RTD Thermal	59S	Synchronism-Check Overvoltage
50	Adaptive Overcurrent	60	Loss of Potential
50 (P,G,Q)	Overcurrent (Phase, Ground, Negative Sequence)	67 (P,G,Q)	Directional Overcurrent (Phase, Ground, Negative Sequence)
50BF	Breaker Failure	67N	Directional Neutral Overcurrent
50INC	Incipient Cable Fault Detection	78VS	Vector Shift
50N	Neutral Overcurrent	79	Autoreclosing
50N AF	Arc-Flash Neutral Overcurrent	81 (O,U,R,RF)	Over-/Underfrequency (Rate, Fast Rate)
50P AF	Arc-Flash Phase Overcurrent		

In the real implementation, a correct configuration of the protection relay is essential to be able to interact correctly with the emulator as well as to detect and isolate the fault.

Once all the wiring has been done, the next step is to establish the voltage and current transformer ratios of the relay based on the signals it receives from the power amplifier. Next, the digital inputs and outputs of the relay must be enabled, and the corresponding variables assigned (Table 11).

Table 11. Variables of SEL-751 configuration

Variable	Value
CT Ratio (CTR & CTRN)	1000 A
Phase LEA Ratio (LEA_R & LEA_S_R)	2760 V
Transformer Connection (DELTA_Y)	WYE
OUT101	HALARM OR SALARM
OUT102	TRIP
OUT103	TRIP
52A Breaker Status N/O Contact	IN101
52B Breaker Status N/C Contact	IN102
Remote Trip (REMTrip)	NOT IN301

The SEL-751 was configured as the protection relay 53 of the Load A with an overcurrent scheme (50).

Finally, the results of the HIL simulations could not be verified due to problems in the validation process of the data provided by the protection relay. And since time and resources were very limited, there was no possibility to solve the validation problems in time because this work was carried out during the 3 months of the PhD student's mobility in the laboratory of Professor Francisco Gonzalez-Longatt at the University South-Eastern of Norway (Figure 24).



Figure 24. Protection Laboratory of the University South-Eastern of Norway

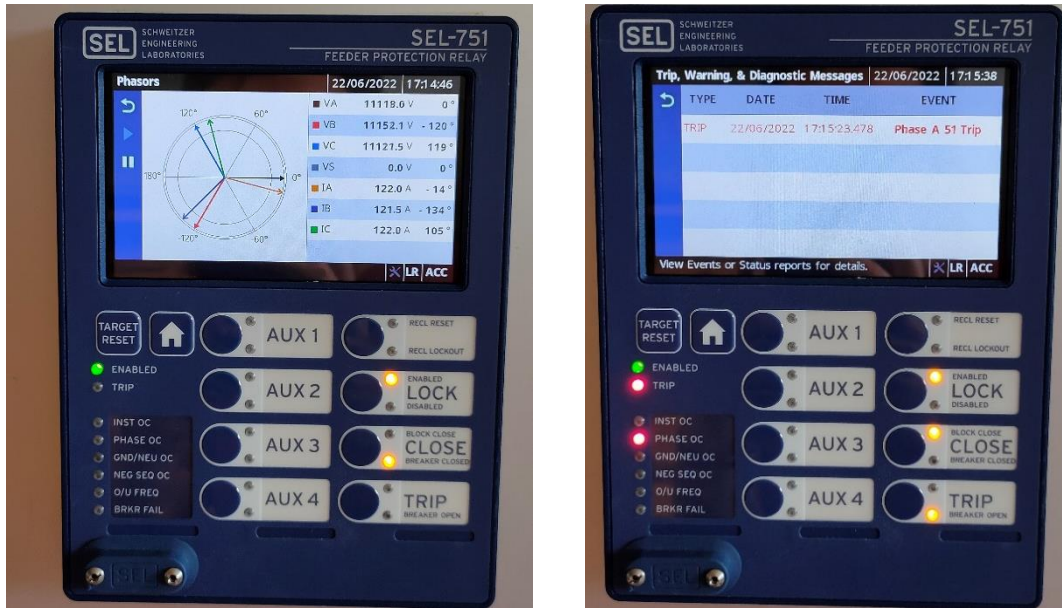


Figure 25. Protection relay SEL-751

4.3 Wavelet Implementation

Although no conclusive results were available, a first simple implementation of the Wavelet transform analysis on voltage and current waveforms was carried out, through a free Open-Source library for Wavelet transforms in Python (PyWavelets), in one-dimensional multi scale to detect faults, thanks to the integration of Python scripts in Typhoon HIL, through the HIL API.

Thus, the Wavelet implementation in the HIL API is developed within a rolling horizon algorithm scheme that periodically updates input data information. The Wavelet transform analysis is solved at each time step to determine the detail coefficients of the voltage and current waveforms separately over a fixed time horizon. At the next time step, it repeats the process, solving a new Wavelet transform analysis with the time horizon shifted one step forward.

In this case the time horizon is 2 seconds, and the time step is 250 ms (minimum execution time allowed by the HIL API). The minimum execution time being too long for the requirements of the MV/HV protection systems. The sequence of the proposed Wavelet implementation is illustrated in Figure 26, which shows the steps to be carried out by the Wavelet implementation algorithm.

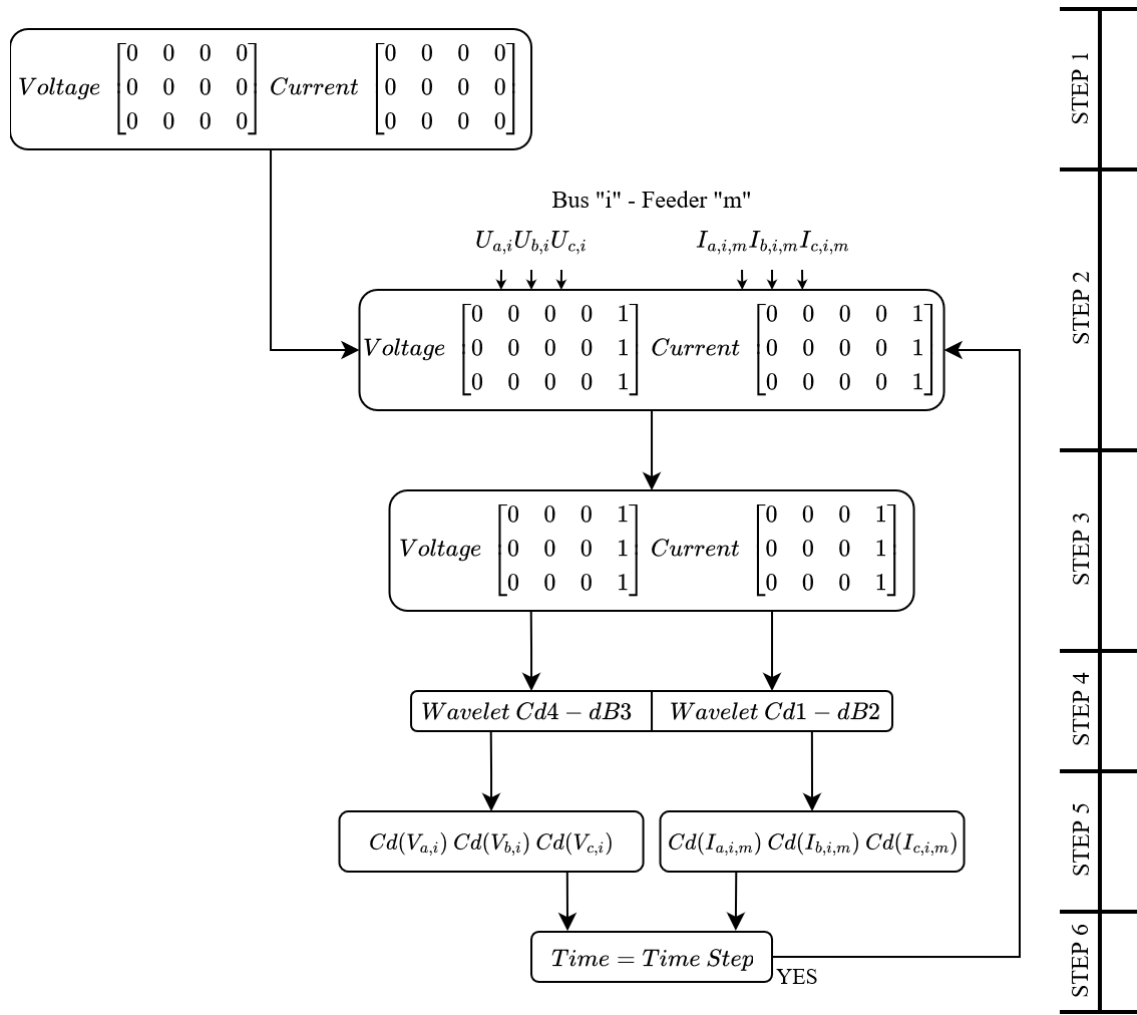


Figure 26. Flowchart of Wavelet implementation in Typhoon HIL

The operational sequence consists of six steps, as follows.

1. Initialize the algorithm by preloading values into the vectors where the values of the voltage and current waveform readings are to be saved. The size of this vector will be conditioned by the amount of read values that the processor is capable of accepting in the set time horizon.
2. Read and save the value of the voltage and current waveforms in the last position of their respective vector.
3. Delete the value stored in the first position of the voltage and current vector, as it is the oldest data. Back to the original size of both vectors.
4. Execute the Wavelet transform on the voltage and current vectors, according to the mother Wavelet and the level established.
5. Obtain the values of the coefficients for both voltage and current vectors.
6. When the next time step is reached, return to step 2.

5 Results

After modelling the IEEE nine-bus system (Section 3), the fault behaviour of the electrical power system is analysed. The results obtained from the different simulations are shown in this section.

5.1 Short-circuits Analysis 100 % SG Scheme

Before setting the trip thresholds of the relays and testing them in the different scenarios established, it is necessary to perform an analysis of the operating and short-circuit currents of the whole system in order to have a reference when setting the trip thresholds of the protection relays.

Using the PowerWorld tool, the nominal currents of the system are obtained through the resolution of a load flow, and the fault currents through the calculation of the short-circuit currents. Previously, it was necessary to implement the nine-bus model in the tool as shown in Figure 27 and to establish the different parameters of the elements according to the values in Table 4.

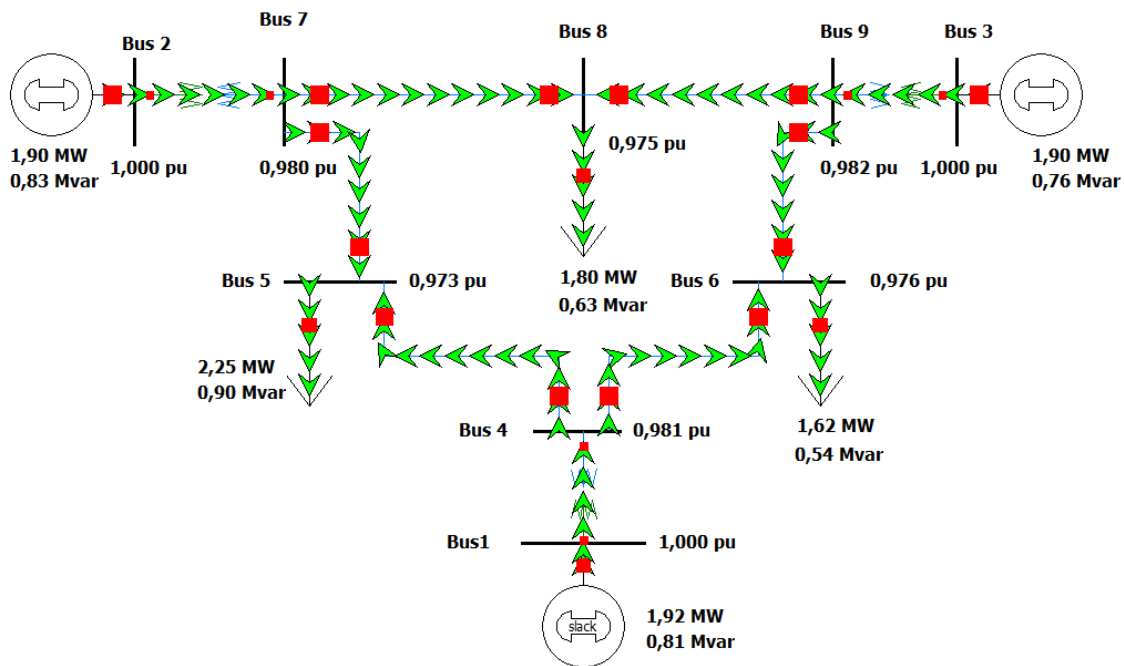


Figure 27. IEEE nine-bus test system implemented in PowerWorld

To ensure a correct configuration of the trip thresholds and avoid false tripping of the protections, apart from solving the system load flow with all the transmission lines enabled, three contingency scenarios have been established in which in each of them a different transmission line is out of service (Line 5-7, line 6-4 or line 8-9). The maximum operating currents of the system are shown in Table 12 below.

Table 12. Nominal and contingency currents in 100 % SG scheme

	From Bus	To Bus	Nominal	Contingency Line 5-7	Contingency Line 6-4	Contingency Line 8-9	Max
Line	4	5	38,68	73,19	58,07	66,27	73,19
Line	5	7	35,45	0,00	16,60	12,92	35,45
Line	7	8	26,37	56,34	46,45	57,29	57,29
Line	8	9	31,48	9,00	12,94	0,00	31,48
Line	9	6	26,46	59,21	51,02	56,27	59,21
Line	6	4	24,83	11,34	0,00	9,98	24,83
SG	4		63,51	66,55	58,07	60,83	66,55
SG	7		61,81	56,34	59,93	64,80	64,80
SG	9		57,88	59,32	62,15	56,27	62,15
Load	5		74,13	73,19	74,67	79,19	79,19
Load	6		51,29	47,87	51,02	46,29	51,02
Load	8		57,85	47,34	59,39	57,29	59,39

The short-circuit currents have then been obtained for the four established locations of a single-phase to ground fault with an impedance of 1 Ω , i.e., at Line 7-5, Bus 7, Line 8-9, and Bus 9 (Table 13).

Table 13. Fault currents in 100 % SG scheme

	From Bus	To Bus	SLG Line 7-5	SLG Bus 7	SLG Line 8-9	SLG Bus 9
Line	4	5	321,38	270,45	91.89	34.18
Line	5	7	276,64//445,17	221,41	36.46	34.02
Line	7	8	150,29	226,27	313.39	262.31
Line	8	9	192,71	265,37	277.92//443.29	223.20
Line	9	6	81,32	24,26	150.64	226.68
Line	6	4	38,93	23,01	188.51	261.53
SG	4		284,97	292.61	280.04	294.16
SG	7		306,37	336.91	285.34	292.77
SG	9		273,77	287.81	302.55	332.33
Fault (A)			719.047 < -57.91°	758.308 < -62.41°	719.559 < -58.19°	759.824 < -62.47°
Fault (B)			0 < -113.58°	0 < -117.09°	0 < 89.99°	0 < 164.88°
Fault (C)			0 < -113.58°	0 < -117.09°	0 < 89.99°	0 < 164.88°

Once the maximum operating currents of the system and the short-circuit currents have been obtained, the trip thresholds of the overcurrent relays placed on the generation buses are calculated (Table 14). For correct sensitivity and selectivity of the protections, the trip thresholds should be higher than the maximum operating current and lower than the minimum short-circuit current.

Table 14. Relays trip threshold values in 100 % SG scheme

Relay Number	43	73	93
Trip Threshold	320 A	320 A	320 A

5.2 Short-circuits Analysis 100 % VSC Scheme

After analysing the behaviour of the short-circuit currents with a 100 % SG generation scenario, the short-circuit currents are then studied for a 100 % VSC generation scenario (Table 15).

Again, the short-circuit currents are obtained for the four established locations of a single-phase to ground fault. As in the previous scenario, the values of the currents have been obtained from the PowerWorld simulations. However, in this scenario, the sequence impedance values of the SG (Table 4) have been replaced by those of the converter, which have been obtained through the converter sequence model previously presented in section 2.3, whose impedance values are as follows:

$$Z_1 = 0.55 + j0.24 \text{ (p. u.)} \quad (20)$$

$$Z_2 = 0.85 + j0.16 \text{ (p. u.)} \quad (21)$$

As discussed in Section 2.3.1 above, the converters cannot produce any zero-sequence current, which in turn means that the magnitude of the zero-sequence is infinite.

Table 15. Fault currents in 100 % VSC scheme

	From Bus	To Bus	SLG Line 7-5	SLG Bus 7	SLG Line 8-9	SLG Bus 9
Line	4	5	170,93	140,21	49,37	18,16
Line	5	7	146,85//233,60	113,67	18,94	17,50
Line	7	8	77,96	115,54	165,33	134,73
Line	8	9	101,58	136,52	146,28//232,60	113,68
Line	9	6	42,30	11,56	78,75	116,32
Line	6	4	18,92	12,90	99,95	135,06
VSC	4		152,51	152,77	149,29	152,98
VSC	7		156,81	164,61	149,87	150,16
VSC	9		143,78	147,41	154,22	161,94
Fault (A)			380.037 < -44.24°	392.148 < -44.93°	378.863 < -44.07°	391.53 < -44.57°
Fault (B)			0 < -38.12°	0 < -11.02°	0 < 177.8°	0 < 137.85°
Fault (C)			0 < -38.12°	0 < -11.02°	0 < 177.8°	0 < 137.85°

In this case, the converter control scheme in dq has been used, without considering the control of positive- and negative-sequences, to facilitate the calculation of the impedance values of the converter model (Equations 20 and 21) entered in PowerWorld to obtain the fault current values.

5.3 Comparison between 100 % SG and 100 % VSC Scheme

Once the short-circuit current values for the 100 % VSC generation scenario (Table 15) have been obtained, it is verified that the trip thresholds previously established (Table 14) for the 100 % SG generation scenario are valid and do not cause false tripping due to the modification of the generation technology.

For this purpose, two cases will be analysed according to the location of the faults established above, the overcurrent protection relays (Relays 43, 73 and 93) of the generation buses (Bus 4, 7 and 9), and the distance protection relays (71/52, 51/41, 42/61, 62/91, 92/82 and 81/72) of the transmission lines (7-5, 5-4, 4-6, 6-9, 9-8 and 8-7), comparing the operation of the protection relays in the different generation technology scenarios.

5.3.1 Generation bus: overcurrent protection relays

Starting with the first case study, the generation bus overcurrent protection relays, when comparing the short-circuit current values obtained in Table 13 with respect to the trip thresholds in Table 14, it is detected that these thresholds are too high due to the reduction of the short-circuit current caused by the presence of the VSCs. Therefore, an initial attempt is made to solve this problem by modifying the trip thresholds with new values, which are shown in Table 16.

Table 16. Relays trip threshold values in 100 % VSC scheme

Relay Number	43	73	93
Trip Threshold	160 A	160 A	160 A

Once the trip thresholds have been modified, Table 15 also shows a sensitivity and selectivity problem in these relays, again caused by the sharp reduction in short-circuit current compared with the 100 % SG scenario. The difference between the current measured by these relays when there is a fault on a generation bus and when the fault is on the line adjacent to the generation bus is barely 8 A in the 100 % VSC scenario, while in the 100 % SG scenario it is 30 A. Therefore, the loss of selectivity to differentiate between these two faults can cause a false tripping of the relays when a fault occurs on the adjacent line, leaving the corresponding generator out of service, with the serious problem this would cause to the power system.

Figures 28, 29, 30, 31, 32, 33, 34 and 35 below show the short-circuit current flows for the generation bus overcurrent protection relays at the four locations of a single-phase to ground fault (Line 7-5, Bus 7, Line 8-9, and Bus 9) and under the two generation technology scenarios (100 % SG and 100 % VSC).

5.3.1.1 SLG Fault in Bus 7

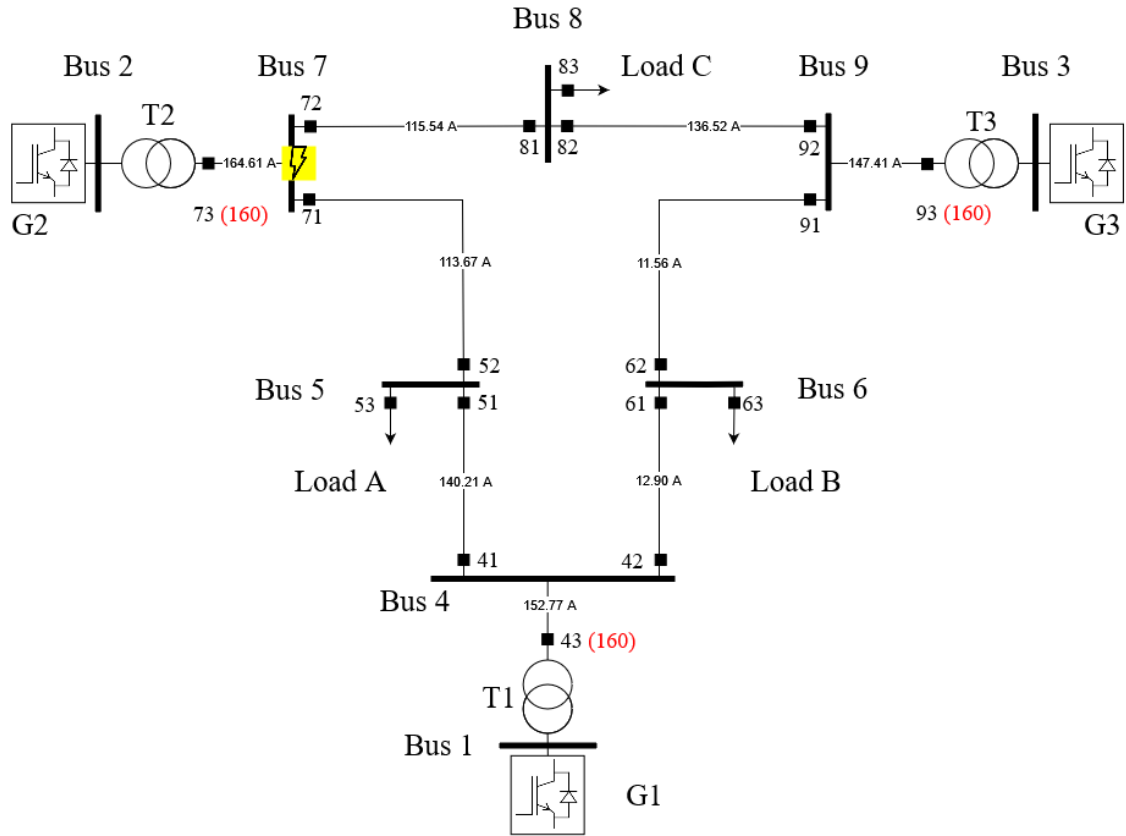


Figure 28. Fault currents & tripping thresholds during a SLG fault in Bus 7 for 100 % VSC

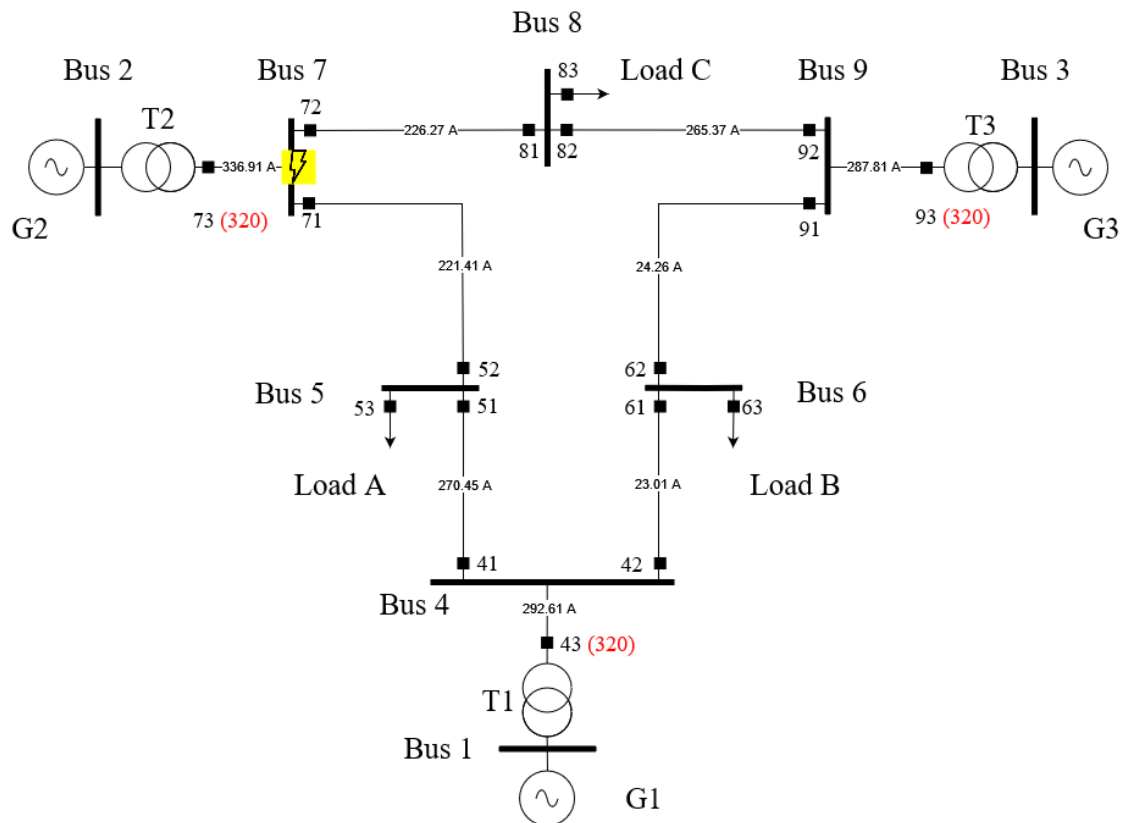


Figure 29. Fault currents & tripping thresholds during a SLG fault in Bus 7 for 100 % SG

5.3.1.2 SLG Fault in Line 7-5

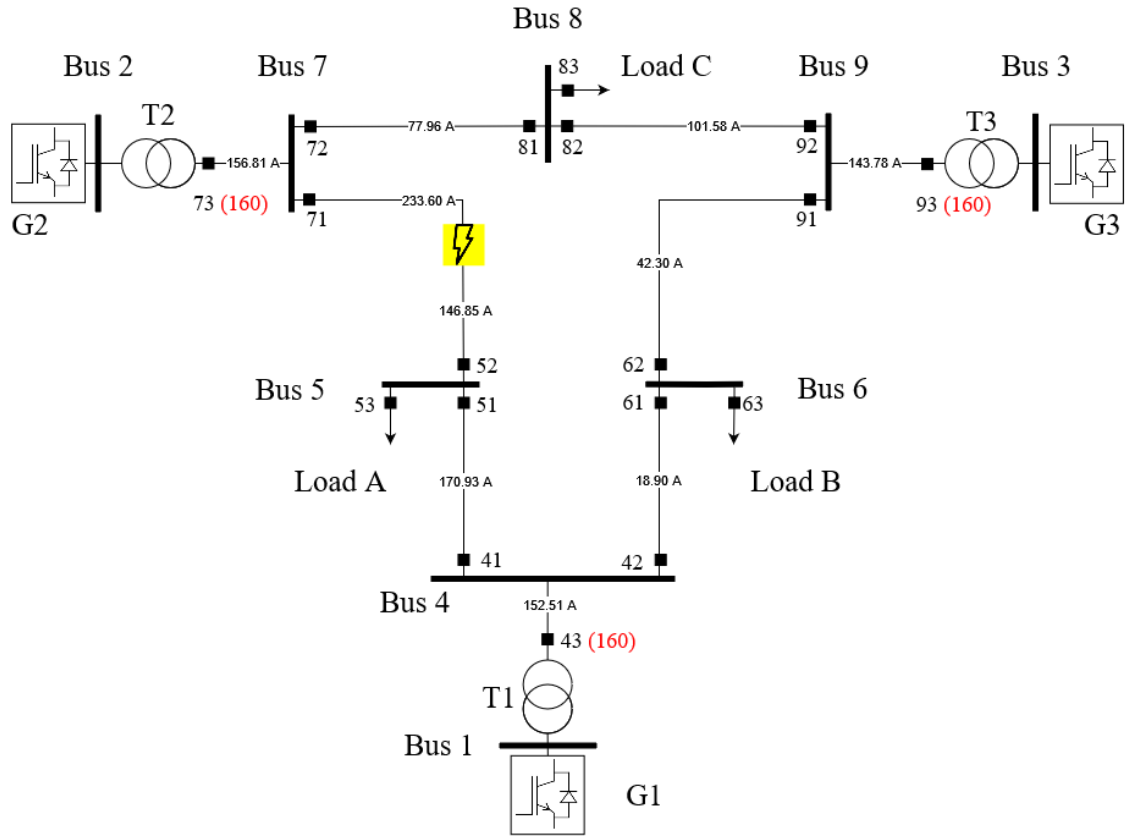


Figure 30. Fault currents & tripping thresholds during a SLG fault in Line 7-5 for 100 % VSC

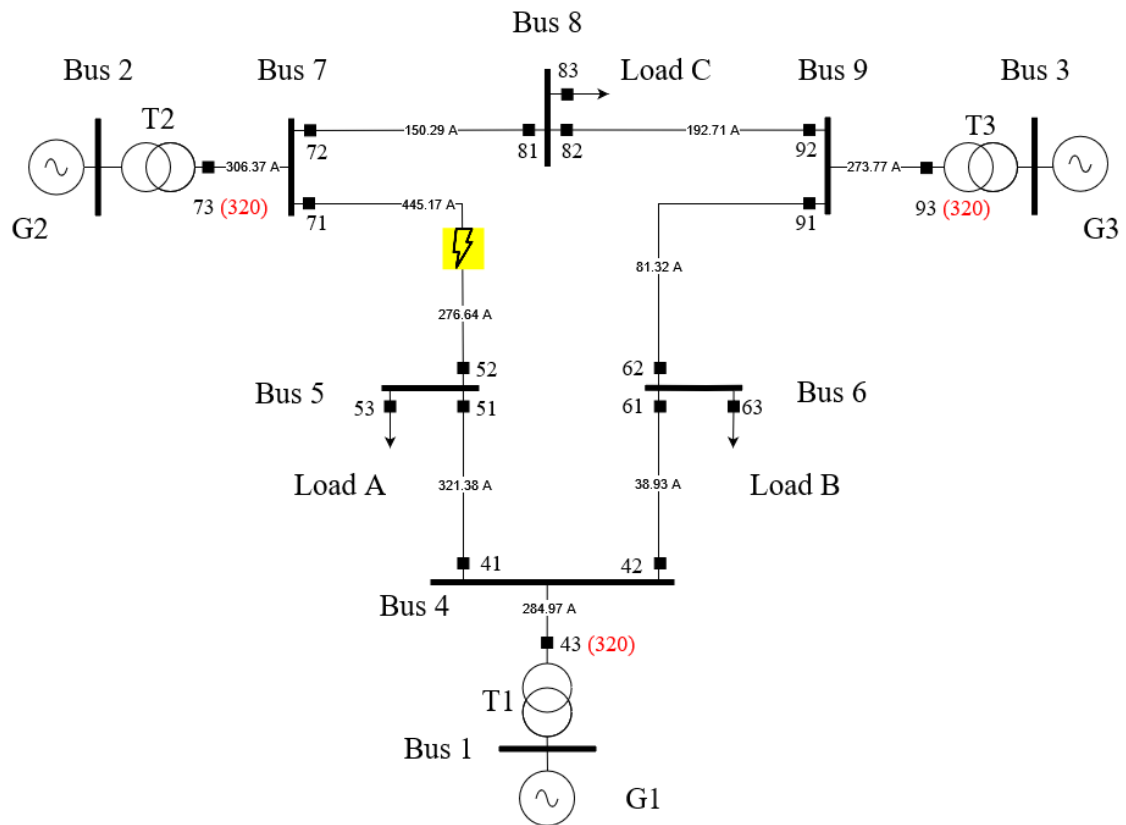


Figure 31. Fault currents & tripping thresholds during a SLG fault in Line 7-5 for 100 % SG

5.3.1.3 SLG Fault in Bus 9

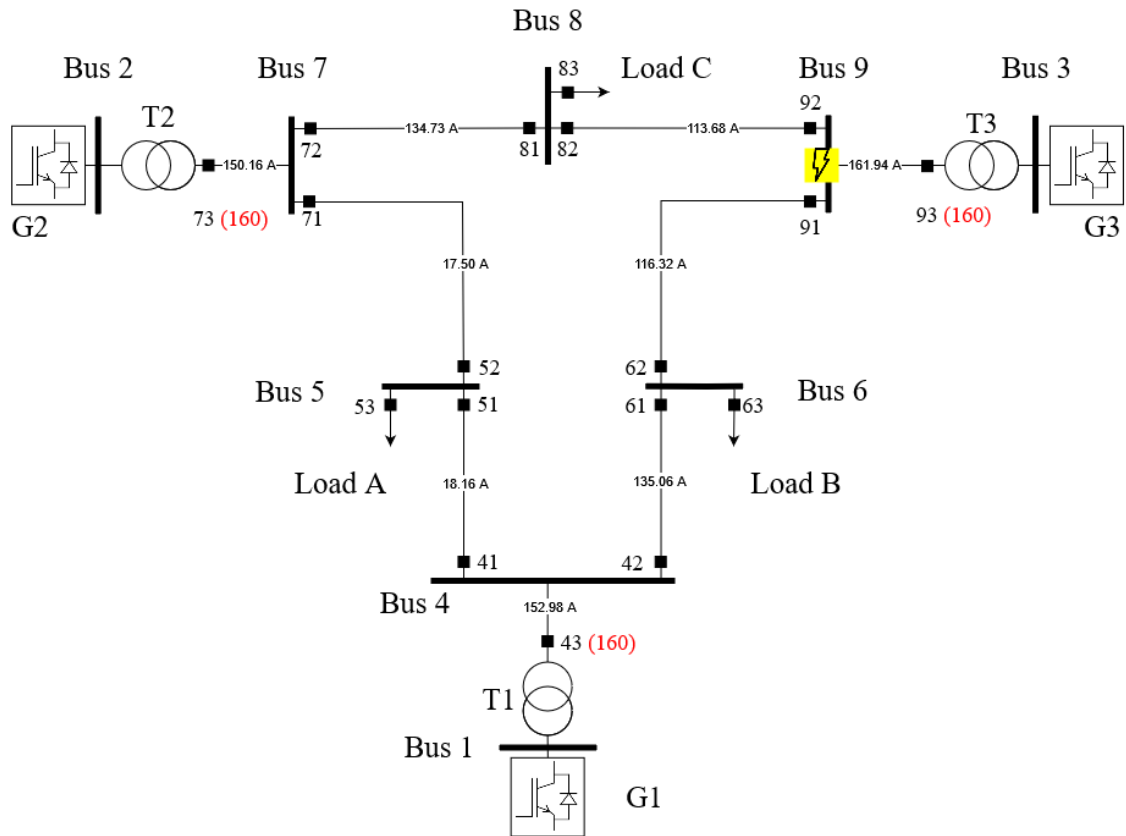


Figure 32. Fault currents & tripping thresholds during a SLG fault in Bus 9 for 100 % VSC

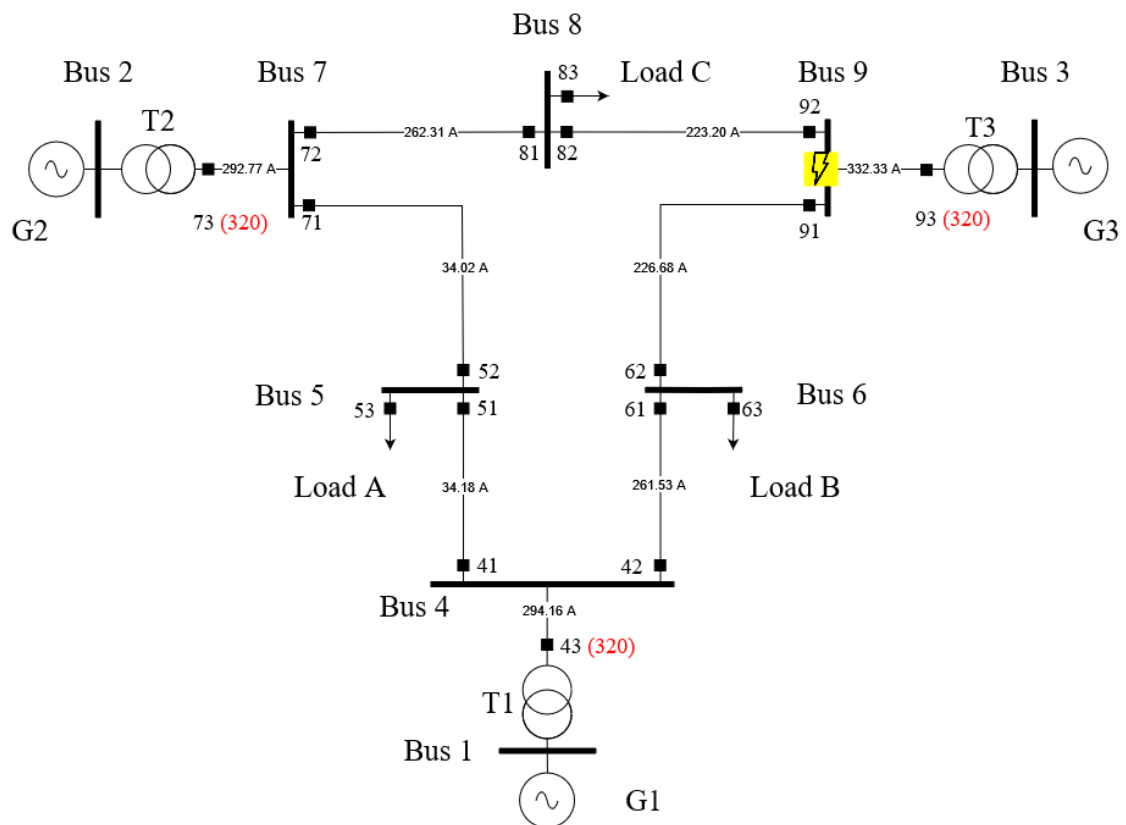


Figure 33. Fault currents & tripping thresholds during a SLG fault in Bus 9 for 100 % SG

5.3.1.4 SLG Fault in Line 8-9

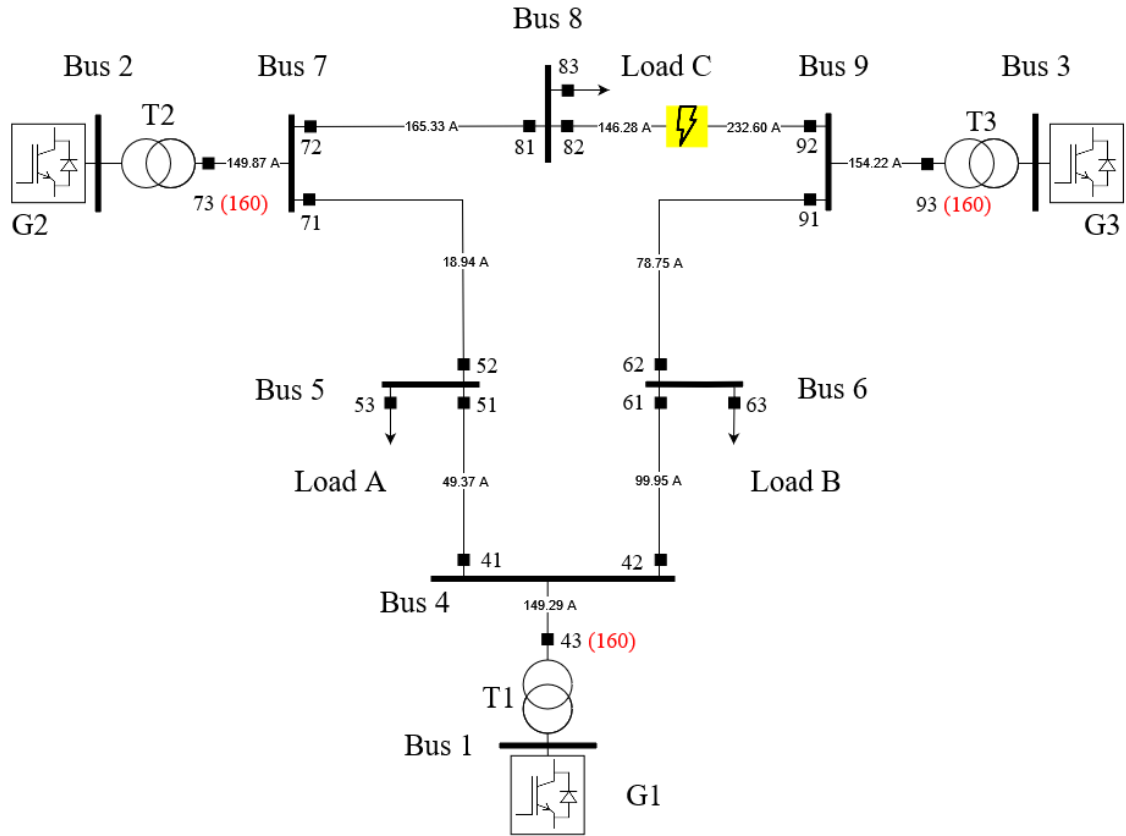


Figure 34. Fault currents & tripping thresholds during a SLG fault in Line 8-9 for 100 % VSC

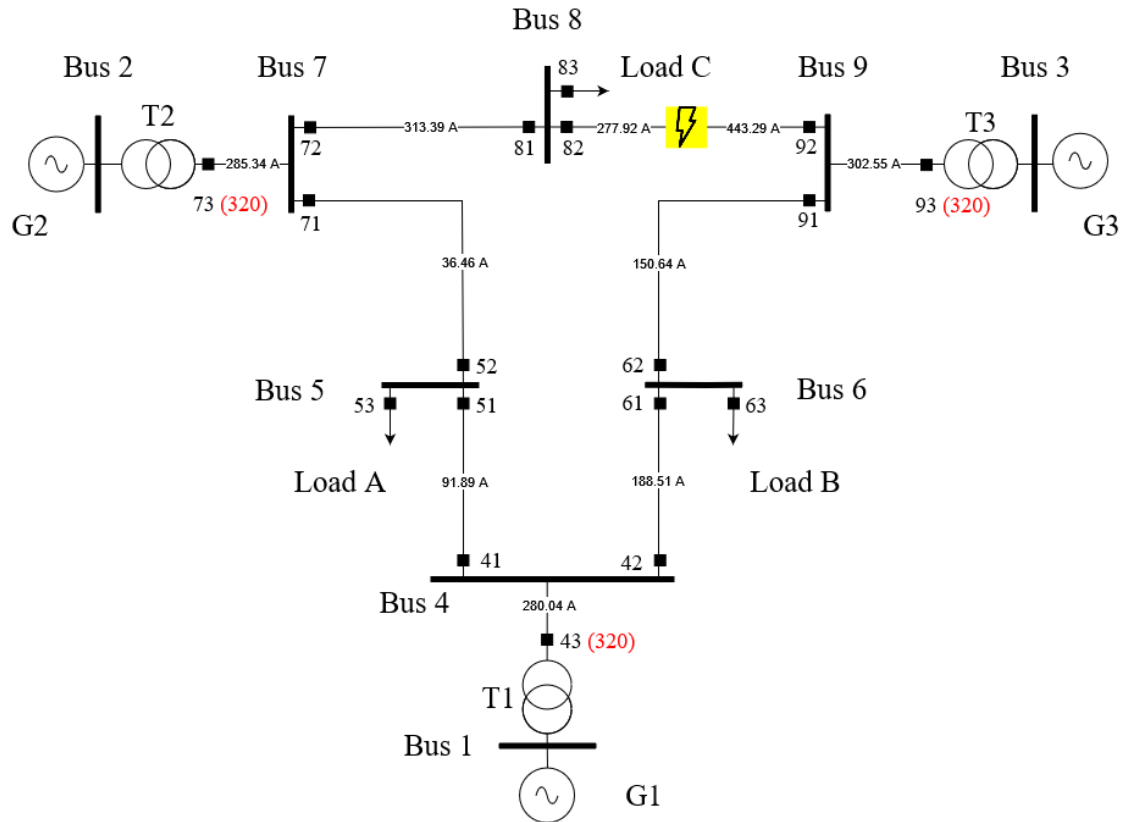


Figure 35. Fault currents & tripping thresholds during a SLG fault in Line 8-9 for 100 % SG

5.3.2 Transmission line: distance protection relays

In the second and last case study, the transmission line distance protection relays respond to the impedance between the relay location and the fault location [88]. They have been designed assuming that the negative-sequence quantities are present in significant levels in the case of synchronous generation during unbalanced fault conditions. Thus, the operation of a distance relay is commonly supervised by negative-sequence overcurrent. This element ensures that distance relay impedance measuring get activated only when the pick-up negative-sequence current is larger than a pre-specified threshold. The low level of fault negative-sequence current under converter-interface generation may result in lack of enough pick-up current, thus leading to maloperation of the distance protection [17][18].

Then, if the pick-up negative-sequence current is present in significant level, through the voltage and current values, the relay will measure the positive-sequence impedance to the fault. Once this is achieved, the zone settings of all relays can be based upon the total positive-sequence impedance of the line, regardless of the type of the fault [79].

For distance relays, the measured apparent impedance seen by a relay is given by the following equation [89]:

$$Z_{app} = \frac{V_r}{I_r} = Z_F + \Delta Z = xZ_{1L} + \left(\frac{I_F}{I_r}\right) \cdot R_F \quad (22)$$

where V_r and I_r are the operating voltage and current for the relay, respectively, and I_F represents the faulted loop current. Table 17 provides V_r , I_r , and I_F for different fault types. Also, K_0 is the zero-sequence compensation factor for the transmission line, expressed as $K_0 = (Z_0 - Z_1/Z_1)$, with 1, 2, and 0 in subscript representing the positive-, negative-, and zero-sequence components, respectively.

Table 17. Distance relay operating measurement and faulted loop current for different fault types [89]

Fault Type	V_r	I_r	I_F
AG	V_{AG}	$I_A + K_0 \cdot I_0$	I_{AF}
BG	V_{BG}	$I_B + K_0 \cdot I_0$	I_{BF}
CG	V_{CG}	$I_C + K_0 \cdot I_0$	I_{CF}
ABG	V_{AB}	$I_A - I_B$	$I_{AF} - I_{BF}$
BCG	V_{BC}	$I_B - I_C$	$I_{BF} - I_{CF}$
CAG	V_{CA}	$I_C - I_A$	$I_{CF} - I_{AF}$
ABC	V_{AG}	I_A	I_{1F}

In equation (22), Z_{app} includes the line impedance to the fault ($Z_F = x \cdot Z_{1L}$), where Z_{1L} represents the positive impedance of transmission line and a fault is considered at a distance of x p.u. from relay bus, plus an additional impedance ($\Delta Z = (I_F/I_r) \cdot R_F$) which is the fault resistance and it may contribute an error to the measured apparent impedance seen by a relay.

In Figure 36 the R–X diagram example illustrates the need to shape the trip zone of a distance relay to include the area around the apparent impedance. It is important to note that an expansive protection zone in the R–X plane allows for higher fault path resistance while also limiting the loadability of the relay [88].

As can be seen in Table 17, the calculation of apparent impedance seen by a relay differs according to the type of fault. Therefore, distance protections use a faulted phase selector to identify the type of fault.

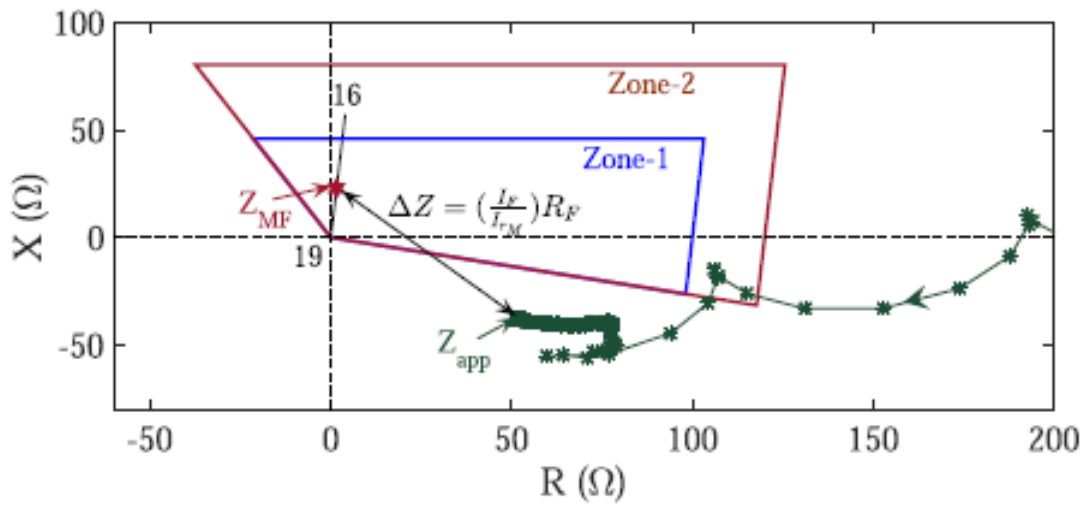


Figure 36. Example of a R-X diagram of distance relaying [89]

A first classification of the fault is carried out by utilizing the flowchart in Figure 37. According to it, if zero-sequence current is present, the unbalance fault can either be SLG or LLG, as both faults exhibit negative-sequence current, so it is impossible to differentiate between them using negative- and zero-sequence current. If no zero-sequence current is measured, the fault will be either LL or LLL. However, if a negative-sequence current is detected, then the fault can be narrowed down to LL, as LL faults show negative-sequence current while LLL faults do not [13]. Following this step, the faulted phase selector stage applies a further criterion to the initial classification.

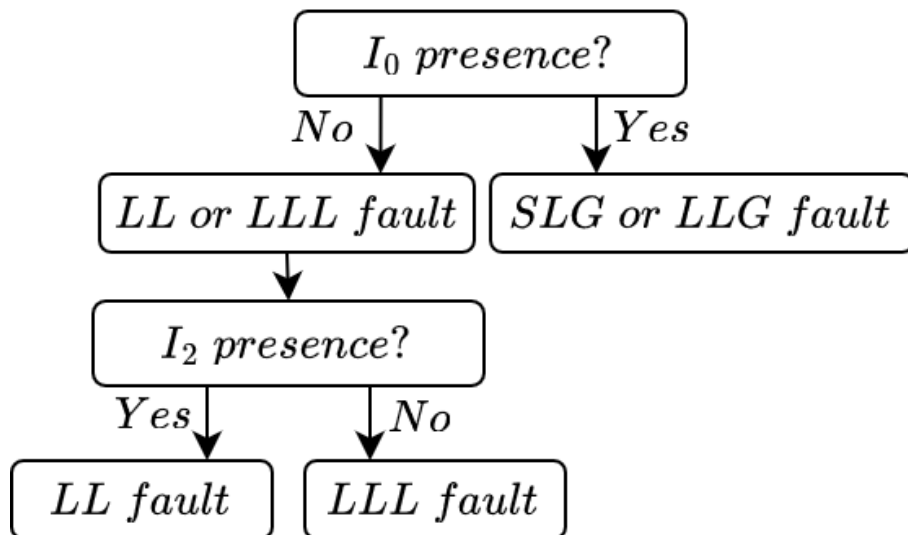


Figure 37. Flowchart of fault classification [13]

This protection principle is based on the theory of sequence networks and has been used traditionally by protection relay manufacturers [13]. It is based on the comparison of phasor angles of positive- and negative-sequence currents, which can be obtained by using the fast

Fourier transform (FFT). In this step, the algorithm calculates the difference between positive- and negative-sequence phasor (phase A) and compares it with the angular sectors shown in Figure 38. Figure 38(a) displays sectors corresponding to SLG and LLG events involving any combination of phases and Figure 38(b) is for LL faults.

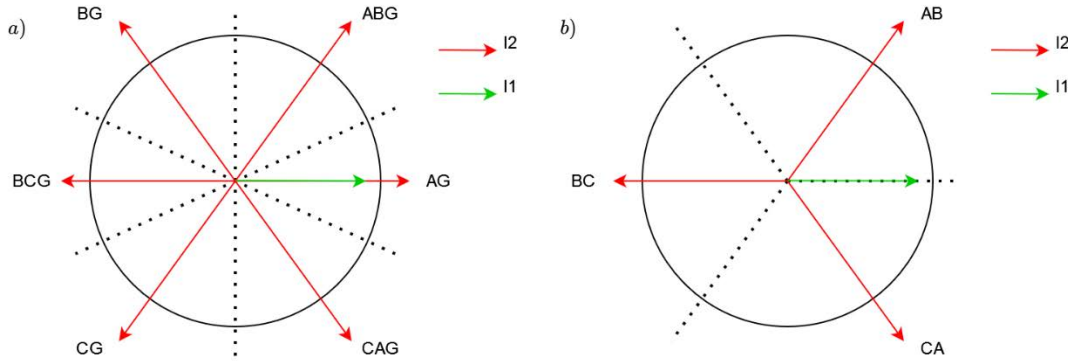


Figure 38. Angular relationship between the negative current (I_2) and the positive-sequence current (I_1): (a) Single-phase and two-phase-to-ground fault diagram; (b) two-phase fault diagram [46]

Therefore, the right operation of the faulted phase selection logic described in Figure 38 depends on the angular relationship between I_2 and I_1 , which is based on the fault current contribution behaviour.

But when the fault current comes from renewable generators connected to the grid by means of power electronic devices can affect to the supervision of the negative-sequence overcurrent in the distance relay algorithm. As can be seen in the figures below (Figures 39 and 40), the implementation of negative-sequence control on converter-interface generators has a strong impact on distance protection since the low level of fault negative-sequence current may result in lack of enough pick-up current.

In order to analyse the reduction of negative-sequence current by the converter-interface generators with respect to the SGs, several simulations have been carried out and are shown in Figures 39 and 40, in which it can be seen that before the fault ($t = 1$ s) an unbalance has been caused in the Load A ($t = 0.5$ s). The negative-sequence current difference between unbalance and fault is 18-110 A for 100 % SG scenario and 13-36 A for 100 % VSC scenario. This indicates that the pick-up negative-sequence current must be a sufficiently high value to differentiate between unbalance and fault, avoiding false tripping.

Because in the 100 % VSC scenario the current range is very small, reducing the pick-up current threshold would not be the most suitable solution, since can cause sensitivity problems. Therefore, other solutions must be proposed.

Despite having detected the problem with the pick-up current, phase identification and impedance calculation are then performed to rule out other problems arising from the presence of converter-interface generation. Table 18 shows the results obtained from the faulted phase selection logic for the two proposed generation scenarios in this thesis, and it is observed that despite the differences in the positive- and negative-sequence values of both current and voltage, the faulted phase detection algorithm works correctly.

Table 18. Results obtained from the faulted phase selection logic

Fault Type	100 % SG Scenario		100 % VSC Scenario	
	Phase Angle I2 & I1	Identification	Phase Angle I2 & I1	Identification
AG	0 – 5°	Yes	5 – 10°	Yes
BG	120 – 125°	Yes	125 – 130°	Yes
CG	240 – 245°	Yes	245 – 250°	Yes

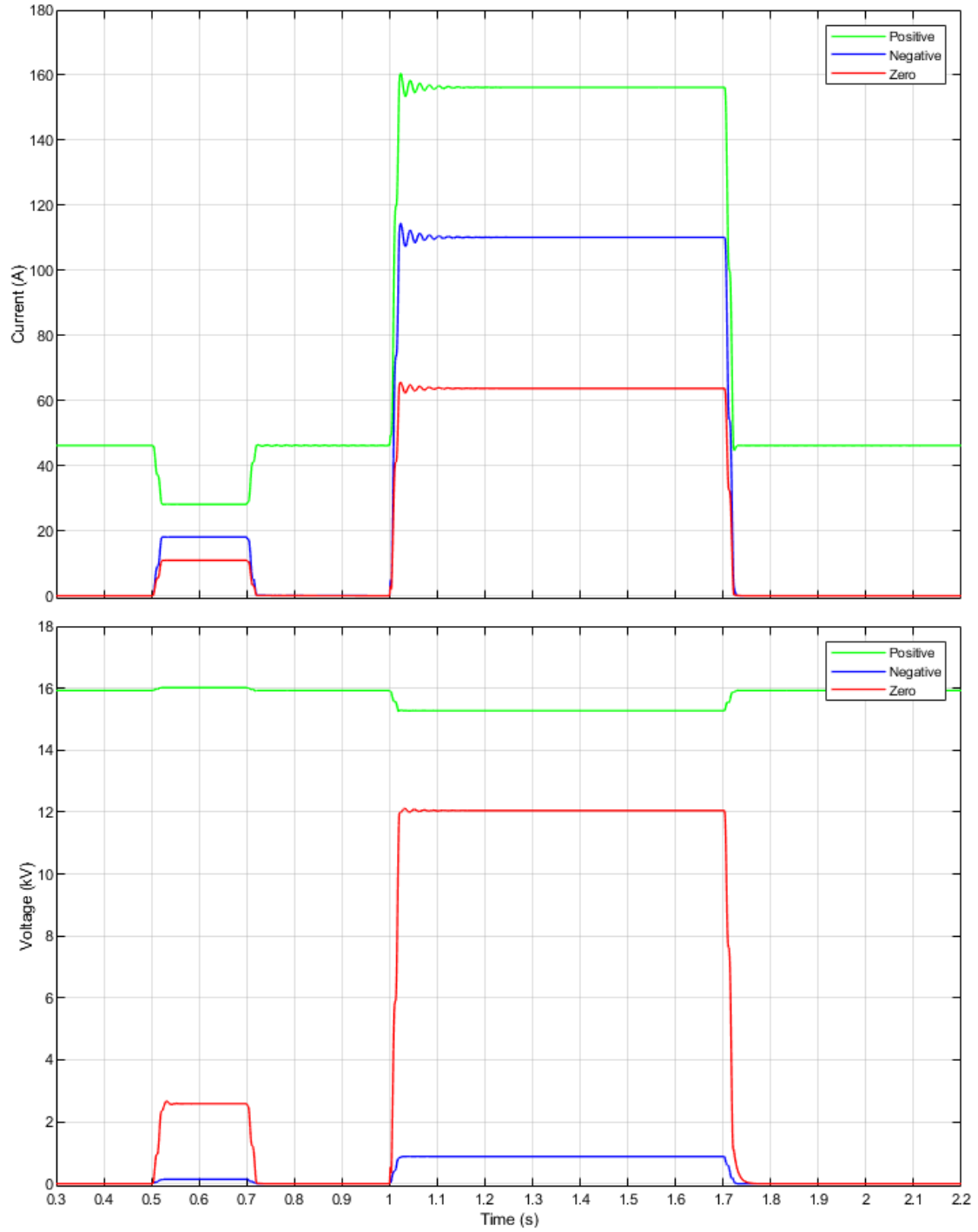


Figure 39. Sequence voltages and currents during an unbalance and a SLG fault in relay 71 for 100 % SG

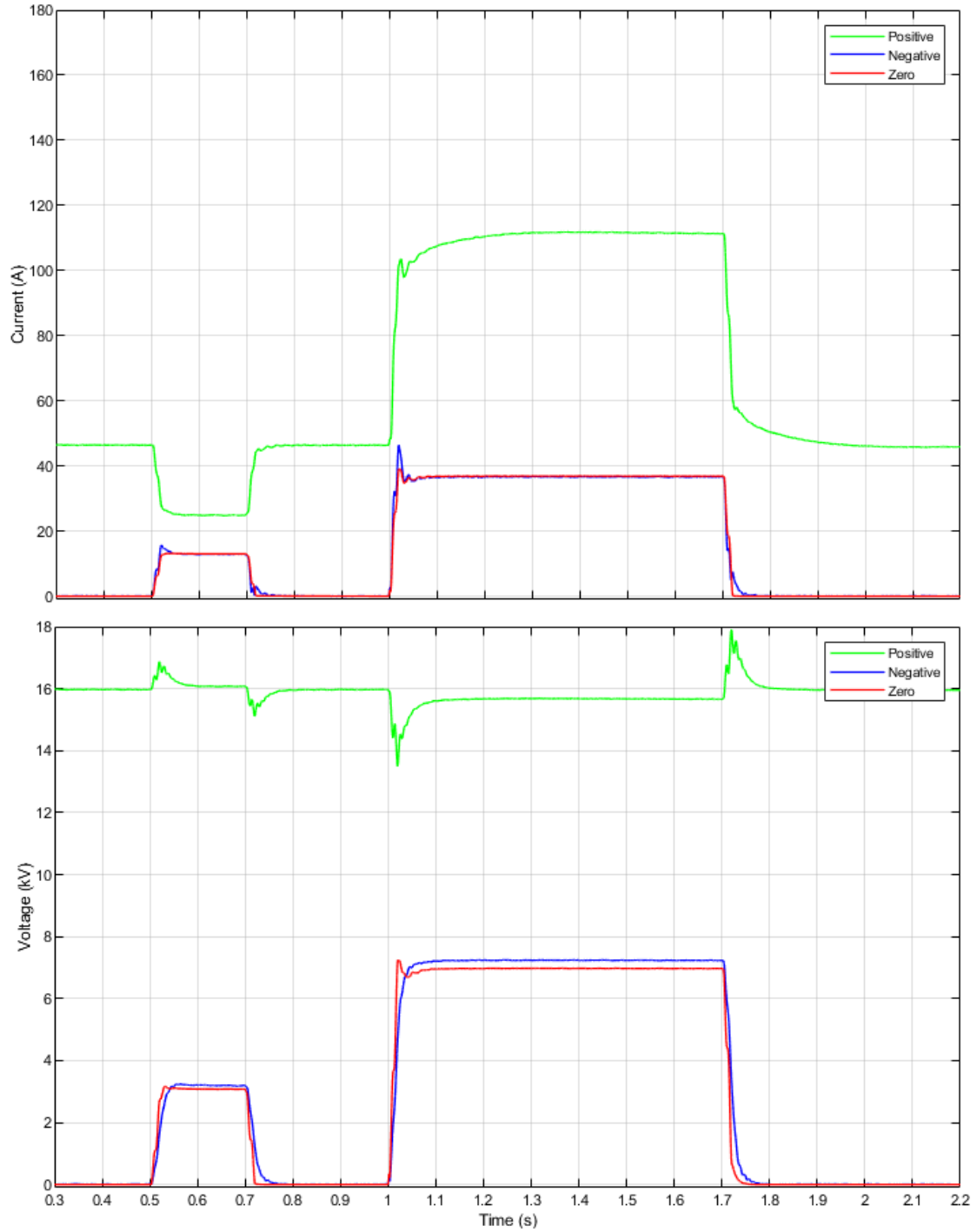


Figure 40. Sequence voltages and currents during an unbalance and a SLG fault in relay 71 for 100 % VSC

Once the faulted phase identification is done (Table 18), the calculation of the impedance from the relay to the fault is performed applying the correct variables from Table 17, as it is described in the following paragraphs.

For a phase-to-ground fault in the middle of Line 7-5 for 100 % SG scenario, the appropriate voltage, and current inputs to be used for the distance relay (71) are shown below through equations (22-26) [88].

The phase A voltage and current at the relay location (71) are:

$$E_a = 2771.48\angle -55.24^\circ (V) \quad (22)$$

$$I_a = 329.74\angle -56.04^\circ (A) \quad (23)$$

The zero-sequence current compensation factor m is given by:

$$m = \frac{Z_0 - Z_1}{Z_1} = \frac{(16.62 + j30.53) - (13.74 + j4.22)}{13.74 + j4.22} = 1.405\angle 51.75^\circ \quad (24)$$

And the compensated phase A current is:

$$I'_a = I_a + m \cdot I_0 = 349.46\angle -70.78^\circ (A) \quad (25)$$

Thus, the fault impedance seen by the relay in this case is:

$$Z_{1f} = \frac{E_a}{I'_a} = \frac{2771.48\angle -55.24^\circ}{349.46\angle -70.78^\circ} = 7.63 + j2.12 (\Omega) \quad (26)$$

The obtained value of Z_{1f} is $Z_1/2$ which indicates that the fault has occurred in the middle of the line 7-5.

While for a phase-to-ground fault in the middle of Line 7-5 for 100 % VSC scenario, the fault impedance seen by the distance relay (71) is calculated through equations (27-31) [88].

The phase A voltage and current at the relay location (71) are:

$$E_a = 1284.72\angle -45.99^\circ (V) \quad (27)$$

$$I_a = 164.85\angle -46.10^\circ (A) \quad (28)$$

The zero-sequence current compensation factor m is given by:

$$m = \frac{Z_0 - Z_1}{Z_1} = \frac{(16.62 + j30.53) - (13.74 + j4.22)}{13.74 + j4.22} = 1.405\angle 51.75^\circ \quad (29)$$

And the compensated phase A current is:

$$I'_a = I_a + m \cdot I_0 = 155.90\angle -63.07^\circ (A) \quad (30)$$

Thus, the fault impedance seen by the relay in this case is:

$$Z_{1f} = \frac{E_a}{I'_a} = \frac{1284.72\angle -45.99^\circ}{155.90\angle -63.07^\circ} = 7.86 + j2.42 (\Omega) \quad (31)$$

The obtained value of Z_{1f} almost match with the position where the fault has occurred. Therefore, the impedance values will not be affected by converter-interface generation despite the measured impedance of the distance relay depends on the feeder currents and these change with respect to the currents supplied by SG.

5.4 Wavelet Protection System Proposal

5.4.1 Generation bus: overcurrent protection relays

To solve the problem of lack of sensitivity and selectivity in the overcurrent protection relays of the generation buses, it is proposed to apply the Wavelet transform analysis, previously described in section 2.7, on the waveforms of the current measured by relay 73. These waveforms are shown in Figures 41, 42, 43, and 44, which show the behaviour of the current and voltage seen by relay 73 when a single-phase to ground fault occurs on Bus 7, Line 7-5, Line 8-9, and Load A.

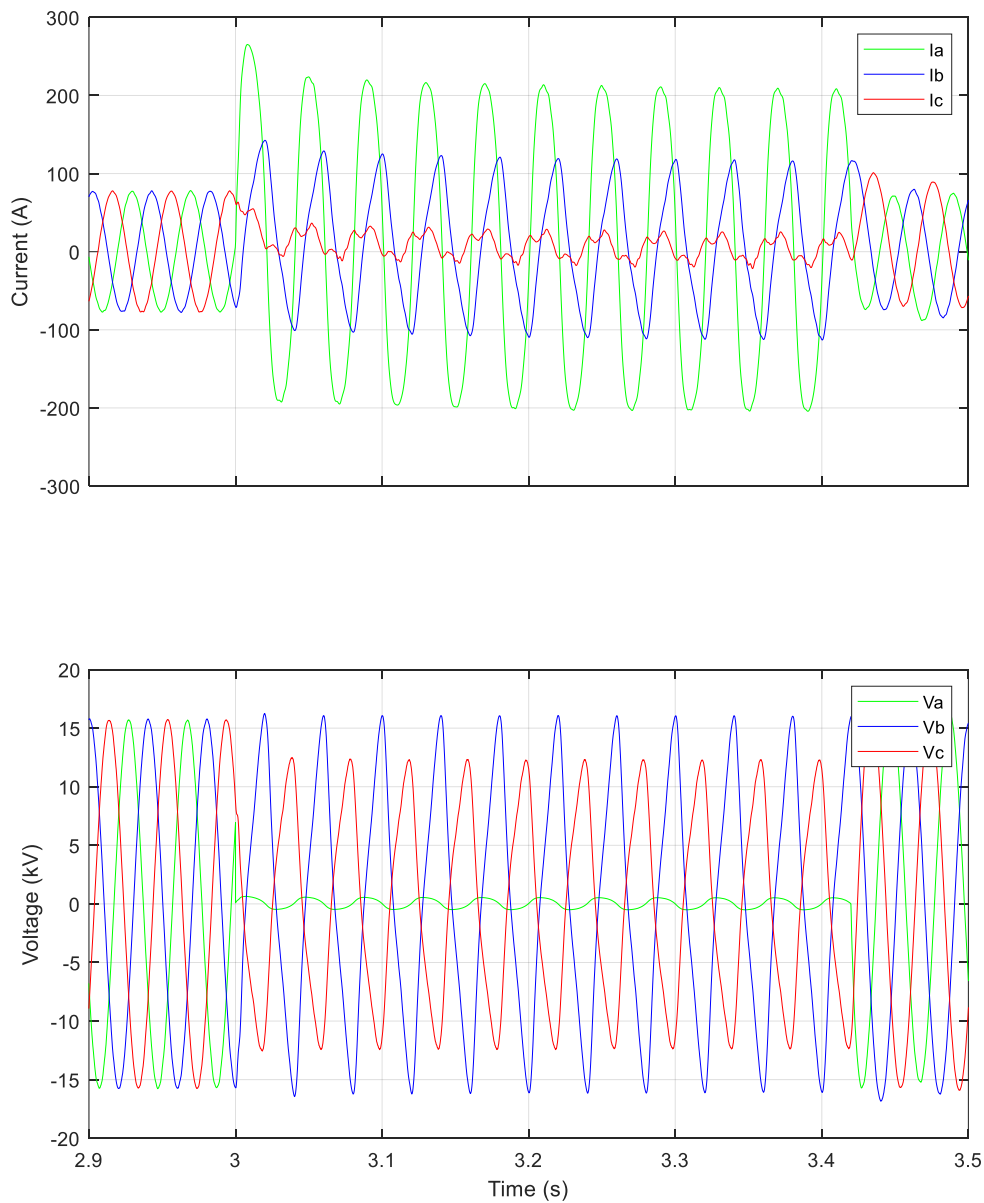


Figure 41. Currents and voltages in relay 73 during a SLG fault in Bus 7 for 100 % VSC

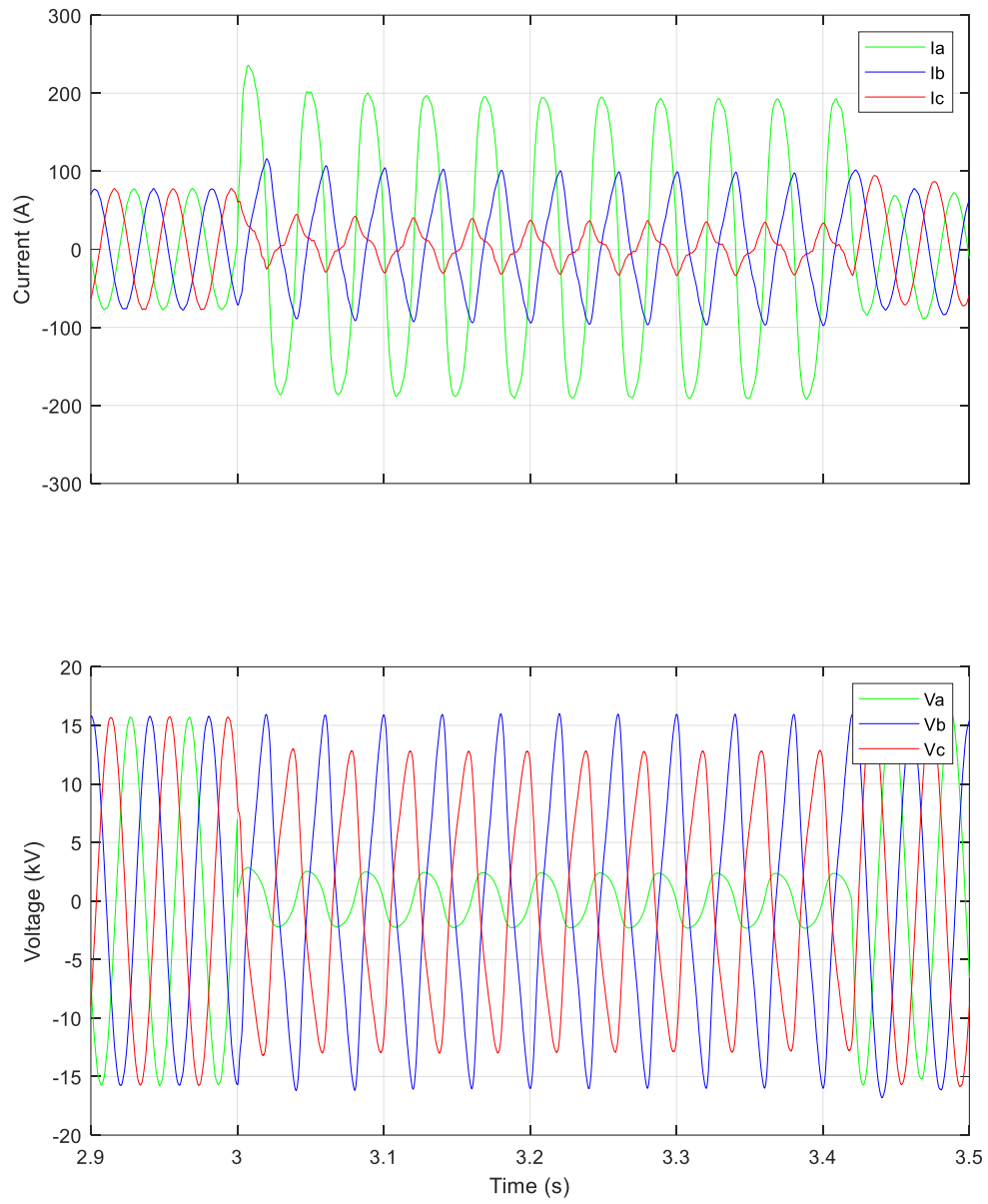


Figure 42. Currents and voltages in relay 73 during a SLG fault in Line 7-5 for 100 % VSC

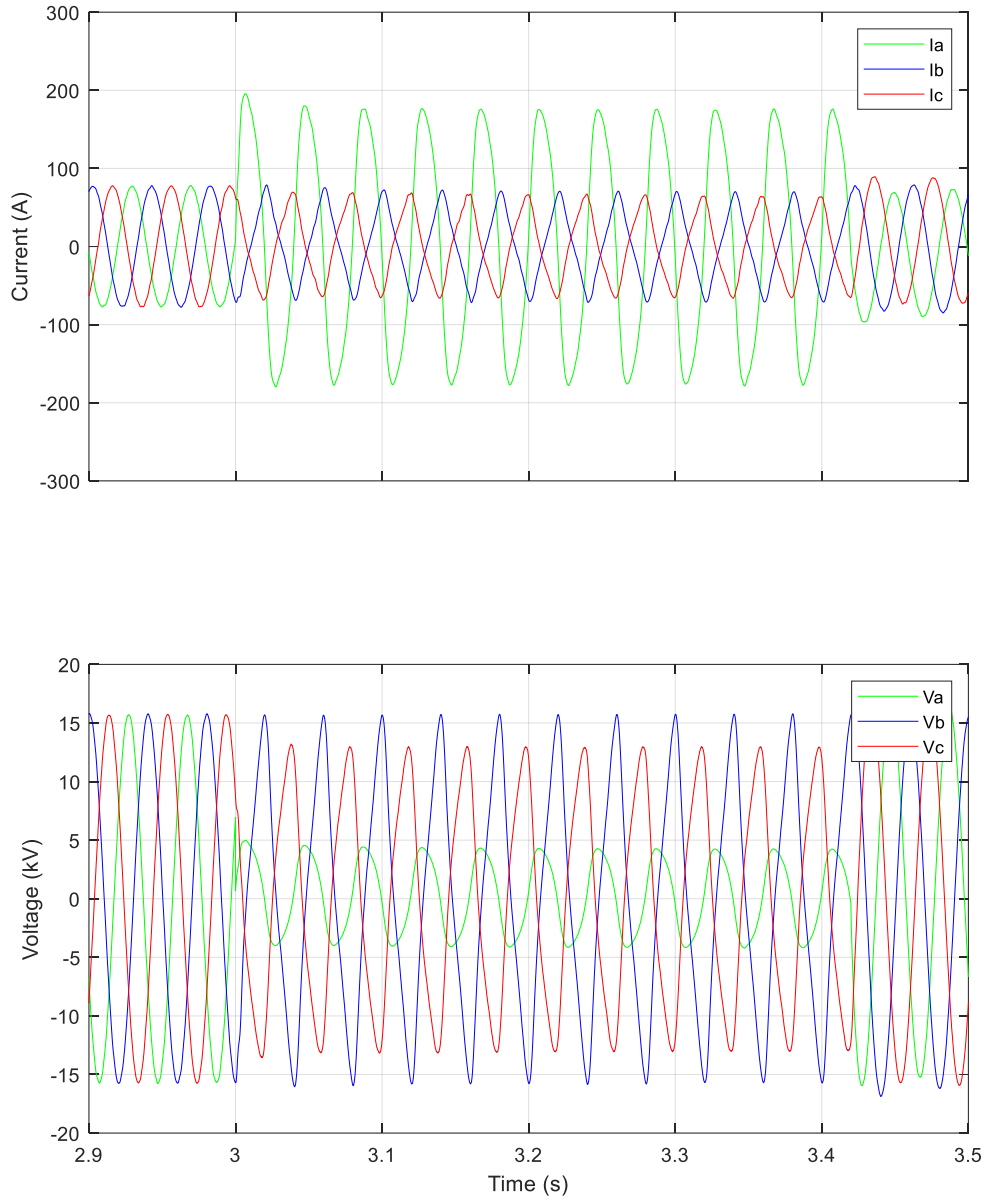


Figure 43. Currents and voltages in relay 73 during a SLG fault in Line 8-9 for 100 % VSC

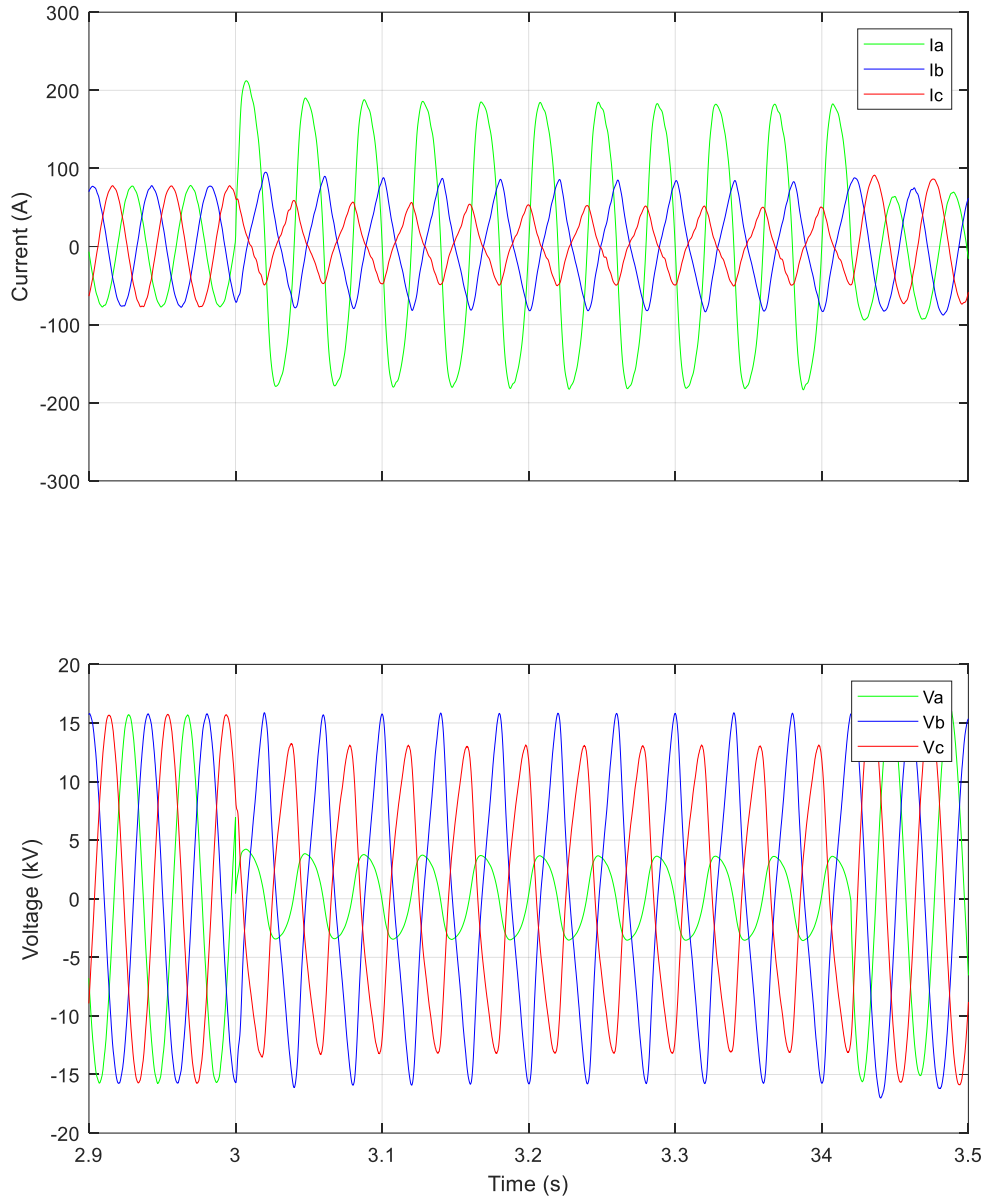


Figure 44. Currents and voltages in relay 73 during a SLG fault in Load A for 100 % VSC

The Daubechies mother Wavelet chosen was the dB1 at level 8. The choice of mother Wavelet will depend on the type of signal to be analysed and the information to be obtained from it. In particular, for the analysis of electrical power systems, the Daubechies family gives the most suitable and reliable results, in addition to outstanding performance in the detection of waveform discontinuities [90][91][92]. Fast and short transient disturbances will be detected at lower scales (dB1), while slower and longer transient disturbances will be detected at higher scales (dB12).

Figure 45 shows the results obtained after applying the Wavelet transform analysis to the current waveforms in phase A, i.e., the phase at fault (SLG), using the Wavelet toolbox in MATLAB. It is observed that the detail coefficient obtained (Cd8 – dB1) is higher when the fault occurs on Bus 7 (533.8) than when it occurs on line 7-5 (468.3), which allows the relay 73 to differentiate between both short-circuit currents with greater sensitivity (12.27 % difference) than with the conventional overcurrent scheme (4.73 % difference), thus avoiding false tripping.

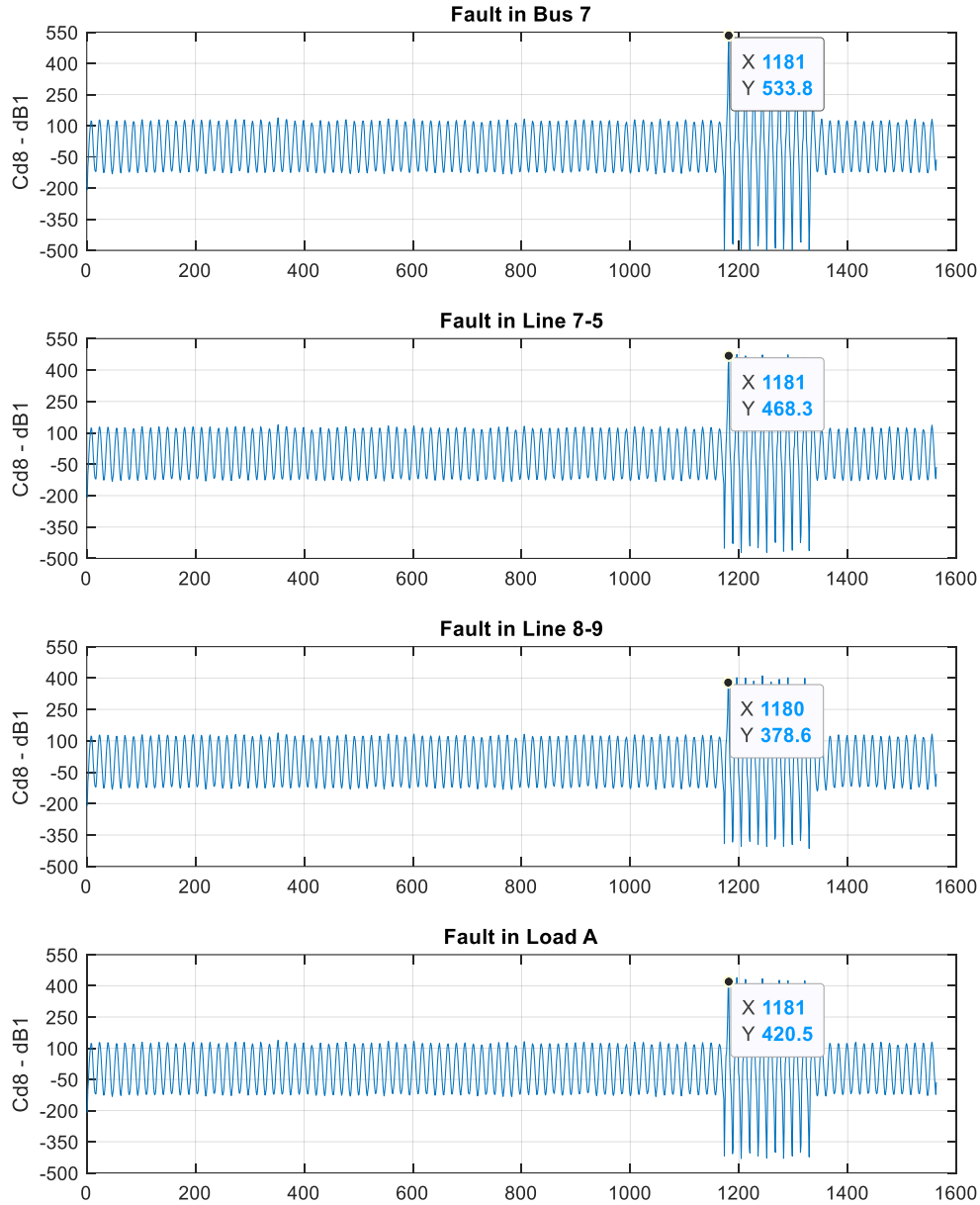


Figure 45. Wavelet coefficients Cd8 – dB1 in relay 73 at different fault locations, phase A

Figure 46 shows the results of the Wavelet transform analysis for the current waveforms in phase B. The detail coefficients obtained (Cd8 – dB1) are lower in all cases with respect to those obtained in Figure 45 for the waveforms of the current in phase A.

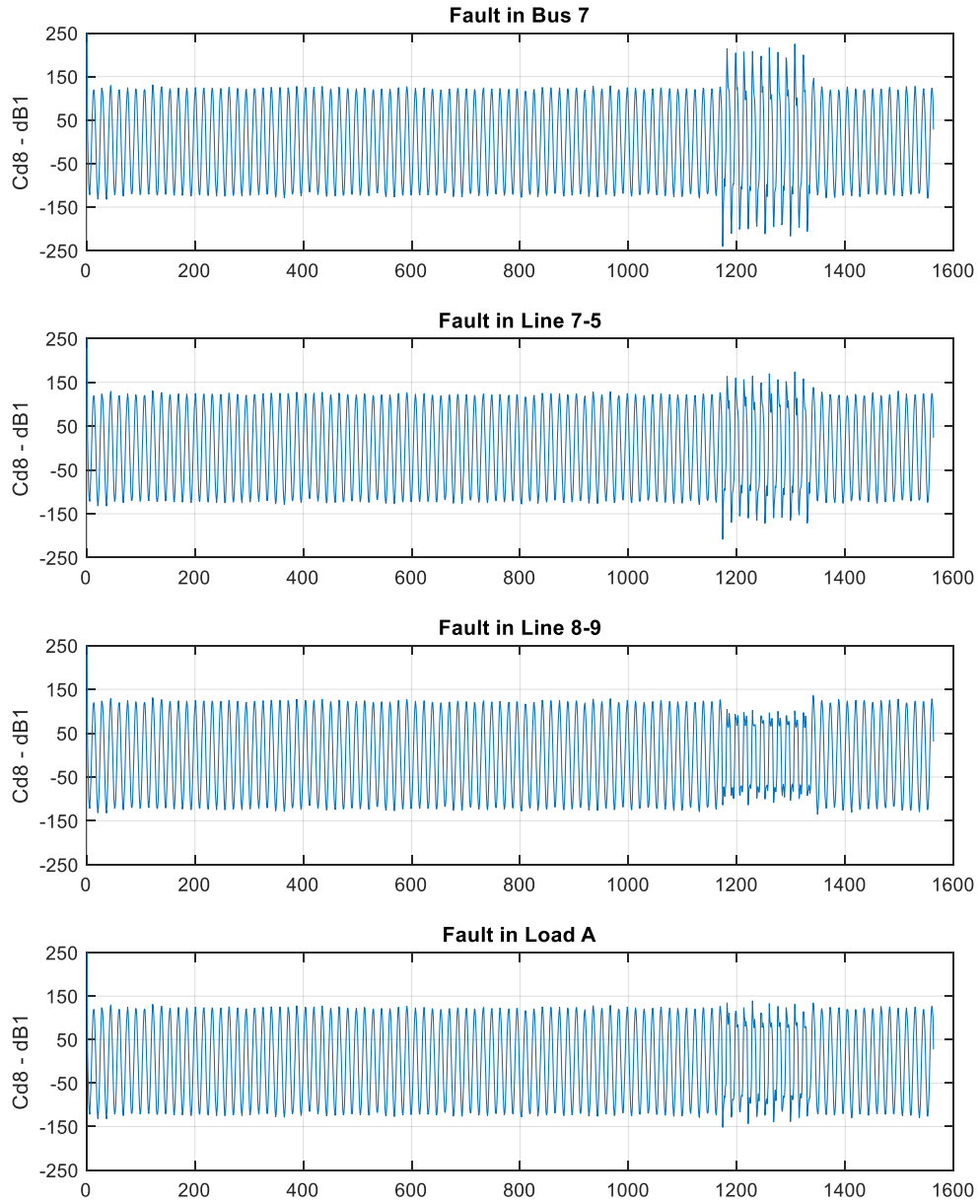


Figure 46. Wavelet coefficients Cd8 – dB1 in relay 73 at different fault locations, phase B

Figure 47 shows the results of the Wavelet analysis for the current waveforms in phase C. And again, it is observed that the detail coefficients obtained ($Cd8 - dB1$) are lower in all cases with respect to those obtained in Figure 45 for the waveforms of the current in phase A. Therefore, the analysis of the Wavelet transform allows us to know which is the faulty phase.

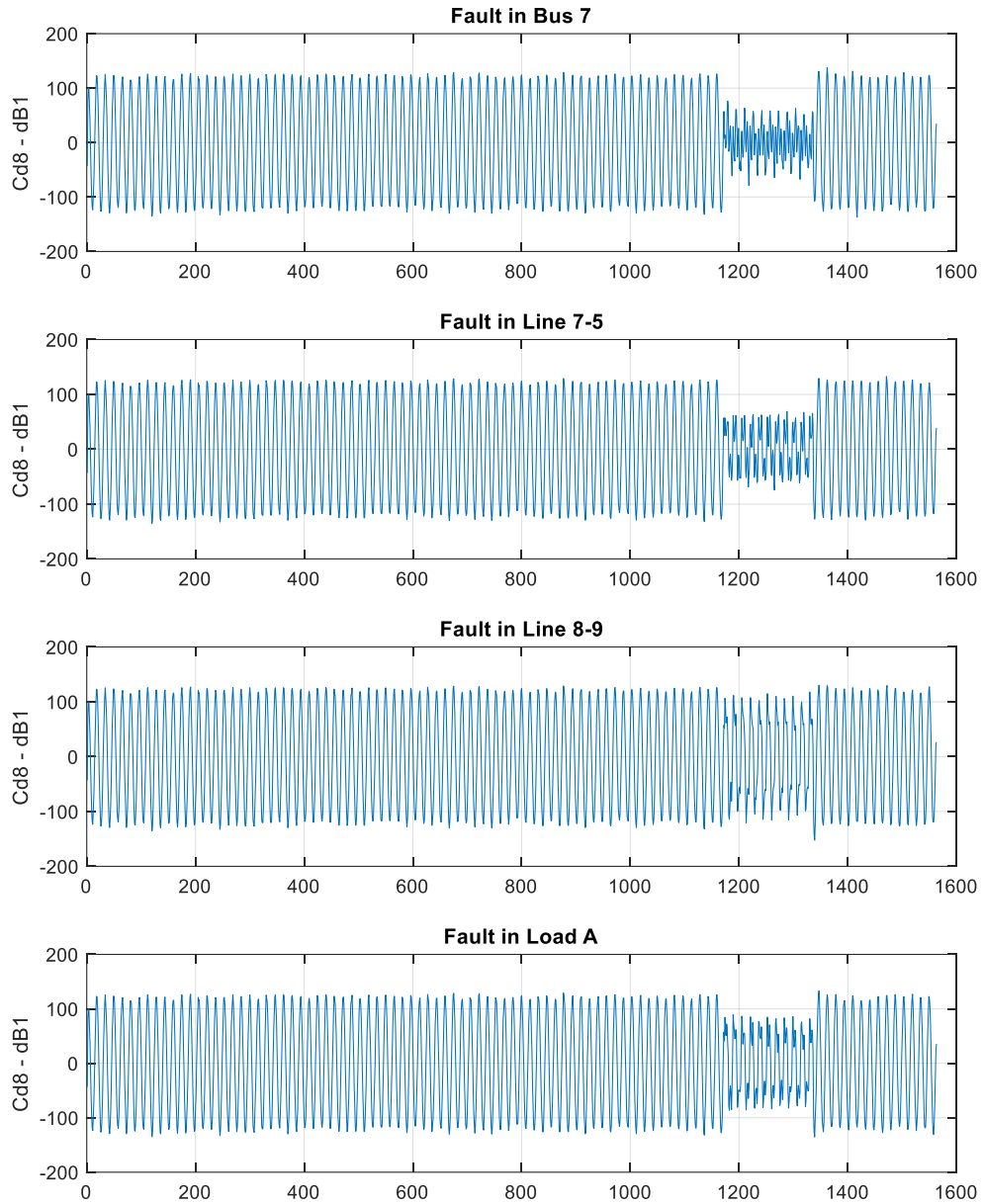


Figure 47. Wavelet coefficients $Cd8 - dB1$ in relay 73 at different fault locations, phase C

After analysing the detail coefficients obtained by relay 73 in Figures 45, 46, and 47 for the different fault locations in the nine-bus system, a detail coefficient trip threshold for relay 73 of 500 is set at $Cd8 - dB1$.

Solved the problem of sensitivity and selectivity in overcurrent protection relays of the generation buses by applying the Wavelet transform analysis to the current waveforms. It is proposed to add a second check in the new protection algorithm to guarantee selective fault detection. By means of a second Wavelet transform analysis using again the Wavelet toolbox in MATLAB, shown in Figures 48, 49, and 50, on the current waveforms in phases A, B, and C of relay 73, providing greater reliability to the protection algorithm. In this case, the Daubechies mother wavelet chosen was the dB3 at level 7.

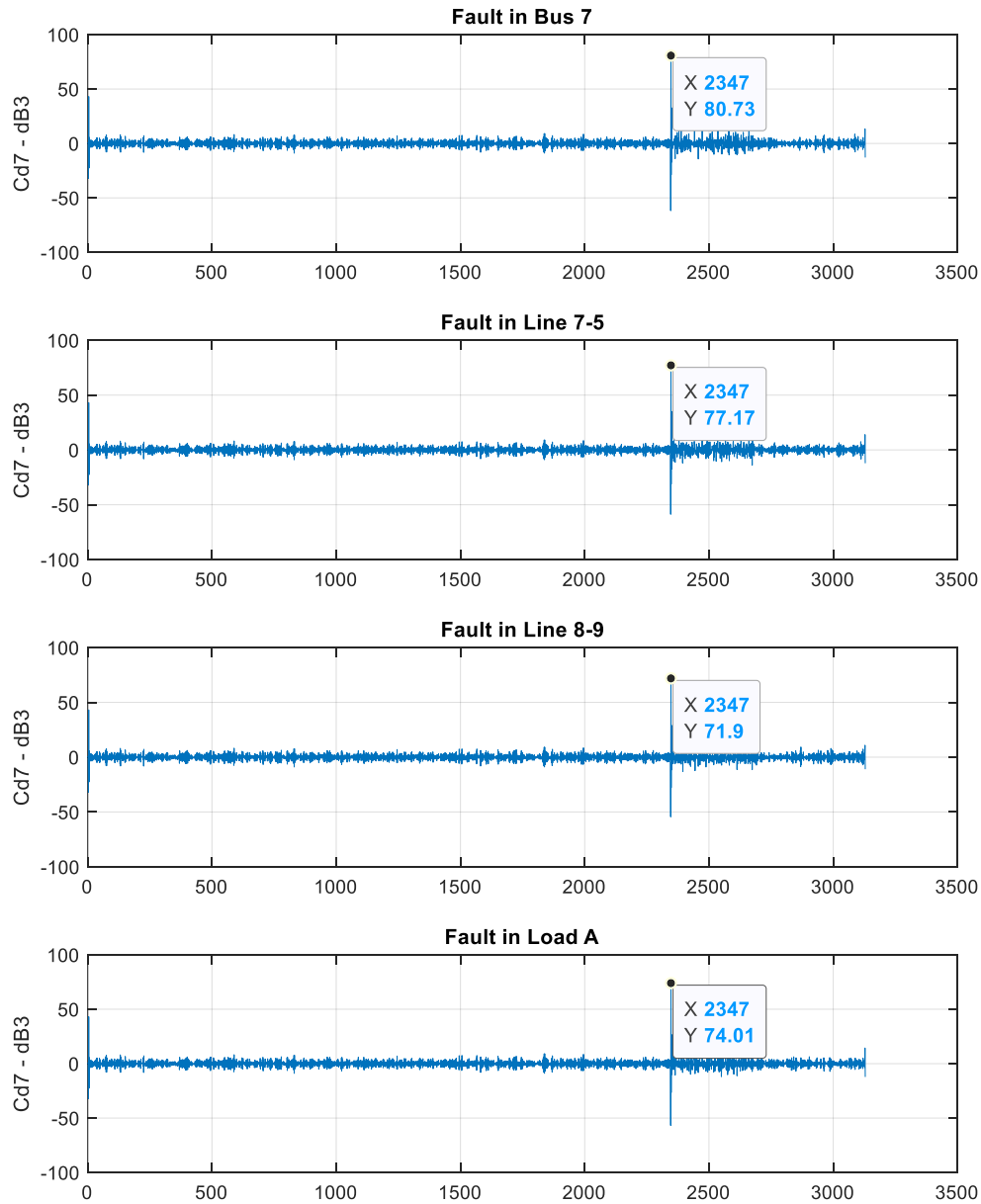


Figure 48. Wavelet coefficients $Cd7 - dB3$ in relay 73 at different fault locations, phase A

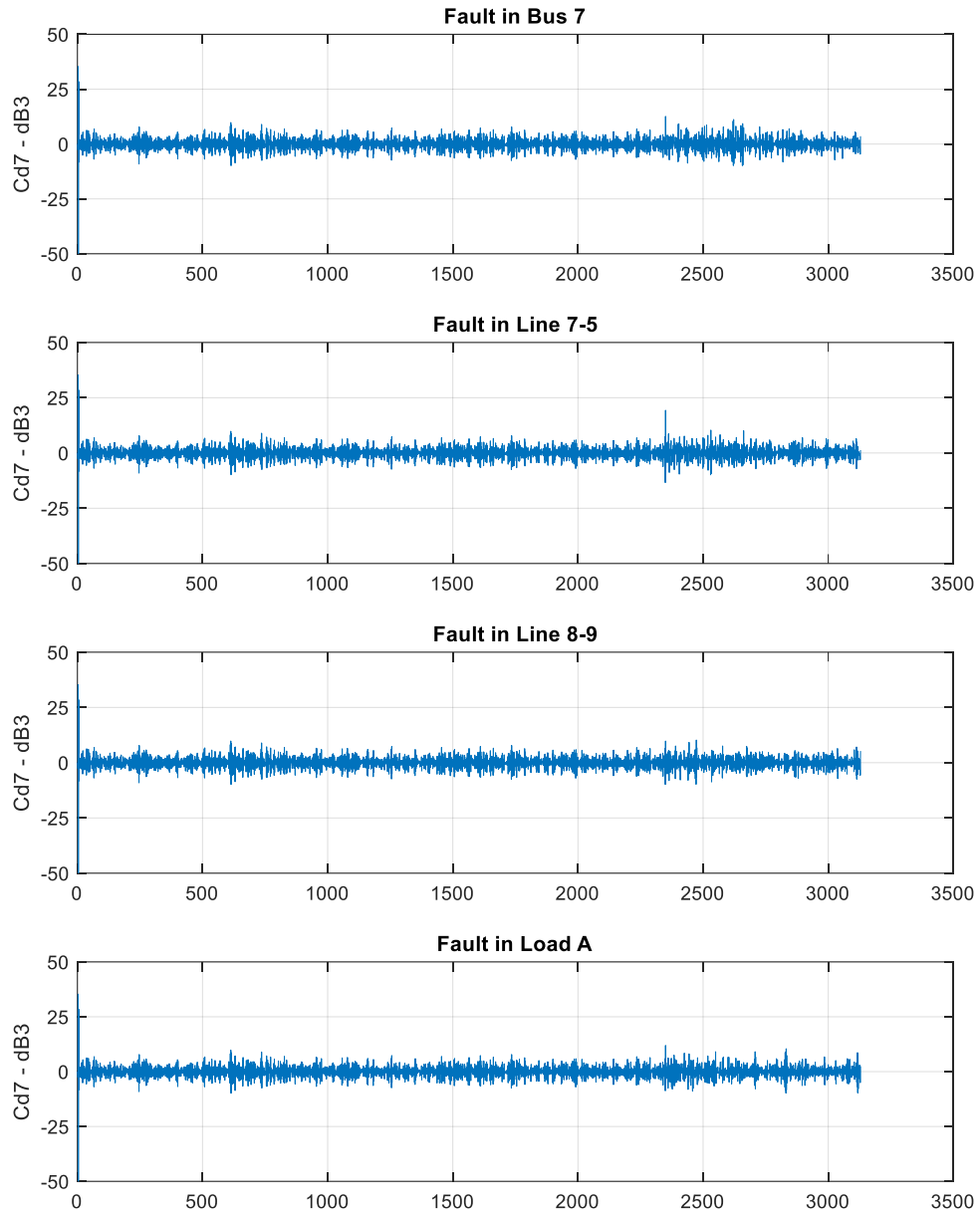


Figure 49. Wavelet coefficients $Cd7 - dB3$ in relay 73 at different fault locations, phase B

In Figure 48, unlike in Figures 49 and 50, there is a strong variation of the detail coefficients obtained in relay 73 because it is in the phase in which the fault (SLG) has occurred, as indicated by the markers in that figure.

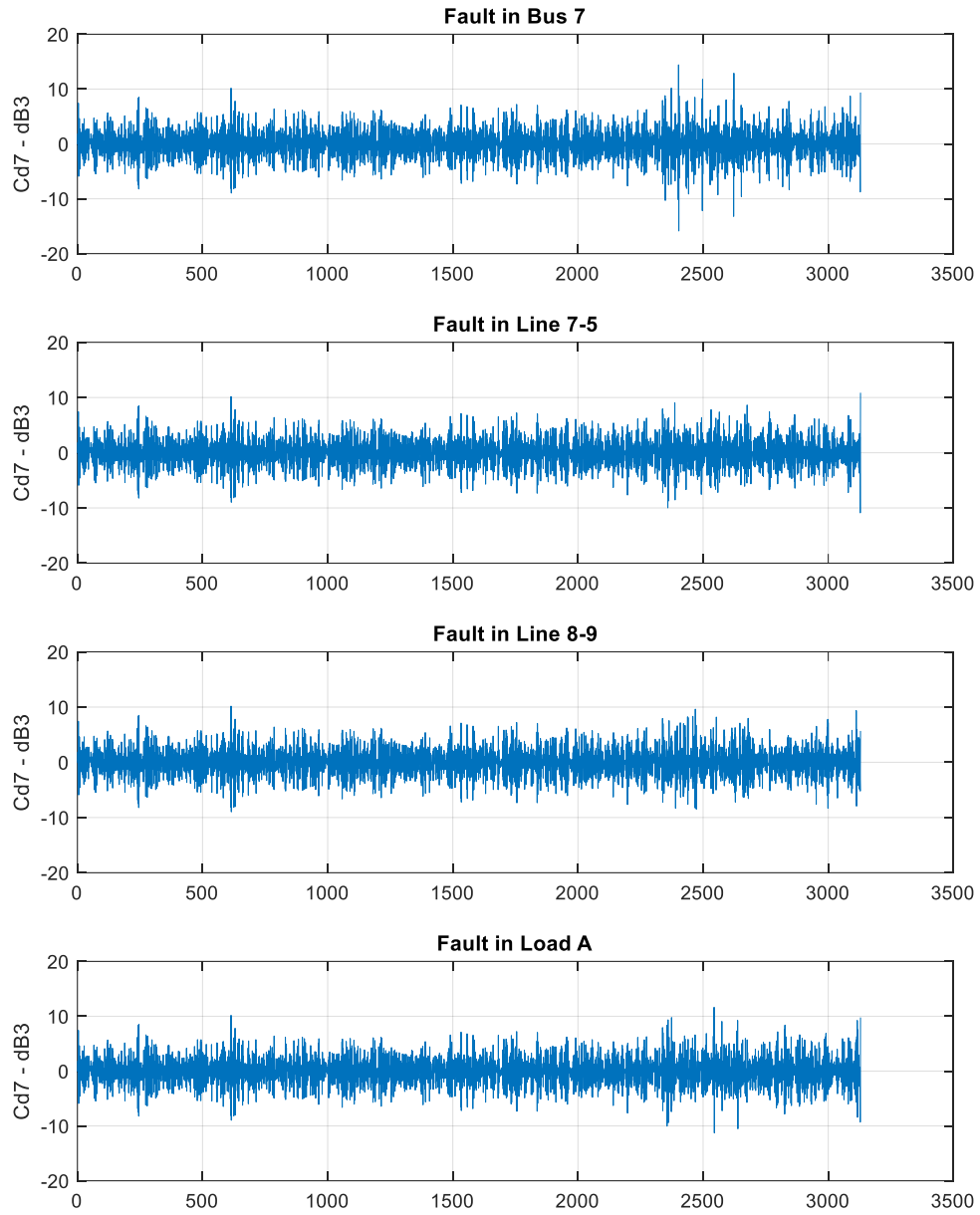


Figure 50. Wavelet coefficients $Cd7 - dB3$ in relay 73 at different fault locations, phase C

After analysing the detail coefficients obtained by relay 73 in Figures 48, 49, and 50 for the different fault locations in the nine-bus system, a detail coefficient trip threshold for relay 73 of 50 is set at $Cd7 - dB3$.

The sequence of operation of the proposed fault detection method is illustrated in Figure 51, which shows the steps to be carried out by the protection algorithm at each generation bus relay (43, 73, and 93).

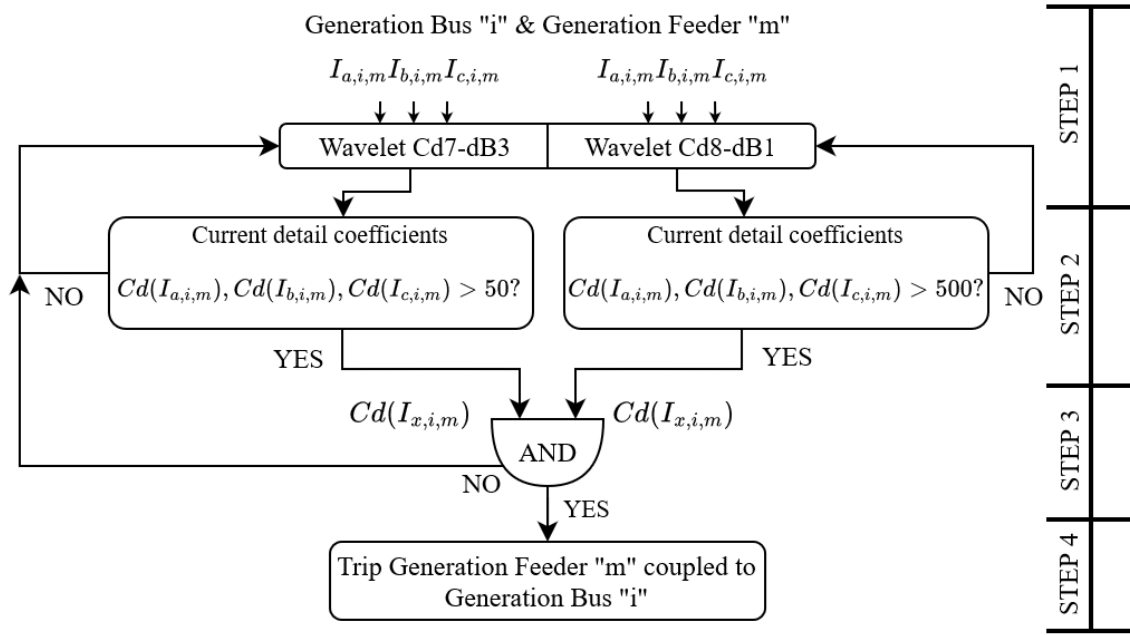


Figure 51. Flowchart of the operational sequence of the generation bus overcurrent protection relays

The operational sequence consists of four steps, as follows.

1. Measure the three-phase current waveform for a generation feeder m coupled to generation bus i and calculate their current detail coefficients by applying the Wavelet transform Cd7 – dB3 & Cd8 – dB1.
2. Check whether the current detail coefficients obtained in Step 1 are higher than the threshold values 50 & 500 for Wavelet transforms Cd7 – dB3 & Cd8 – dB1 respectively.
3. Check whether both Wavelet transforms have detail coefficients that have exceeded their established thresholds and have the same phase sub-index x .
4. Trip generation feeder m coupled to generation bus i .

5.4.2 Transmission line: distance protection relays

To solve the problem of the pick-up current in the transmission line distance protection relays caused by the lack of negative-sequence current in 100 % converter-interface generation scenario, it is proposed to apply the Wavelet transform analysis, previously described in section 2.7, on the negative-sequence current signal from the distance relays (71 and 52). These signals are shown in Figures 52 and 53, which show the behaviour of the negative-sequence current seen by relay 71 and 52 respectively, when a single-phase to ground fault occurs in the middle of Line 7-5 ($t = 1$ s) and an unbalance in Load A ($t = 0.5$ s).

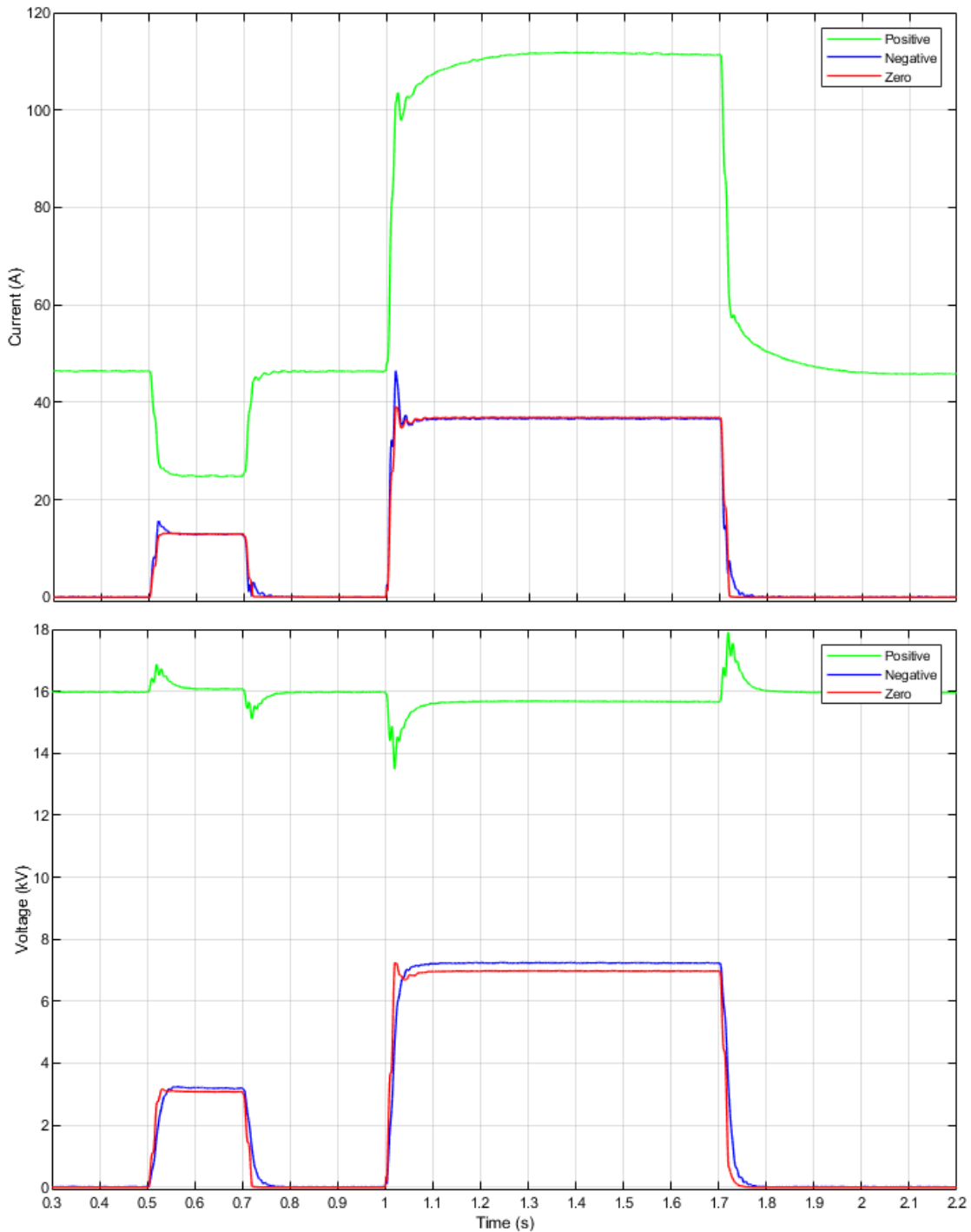


Figure 52. Sequence voltages and currents during an unbalance and a SLG fault in relay 71 for 100 % VSC

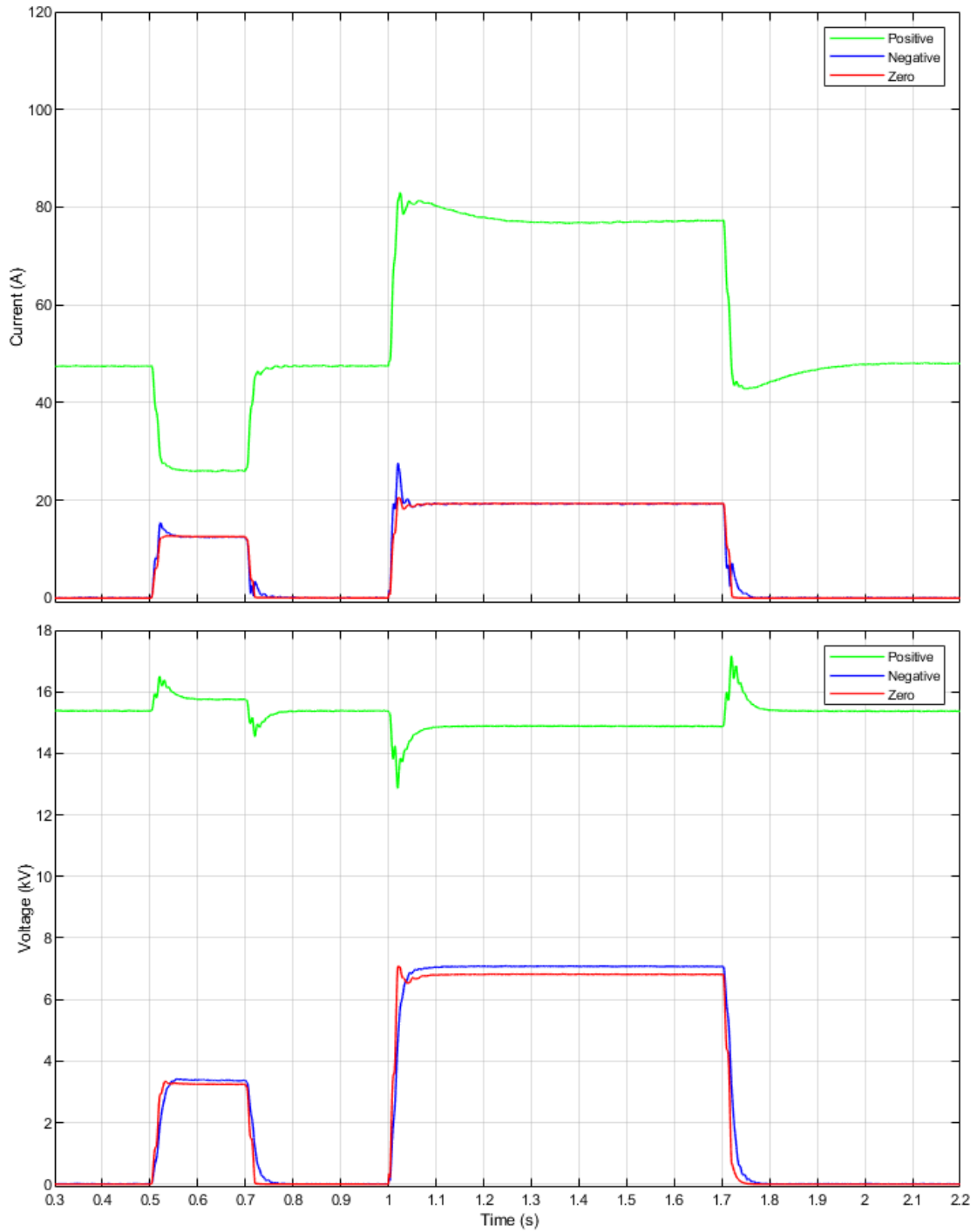


Figure 53. Sequence voltages and currents during an unbalance and a SLG fault in relay 52 for 100 % VSC

In this case, the Daubechies mother wavelet chosen was the dB4 at level 11. As mentioned above, the choice of mother Wavelet will depend on the type of signal to be analysed and the information to be obtained from it.

Figure 54 shows the results obtained after applying the Wavelet transform analysis to the negative-sequence current signals using the Wavelet toolbox in MATLAB. It is observed that the detail coefficients obtained (Cd11 – dB4) are higher when the fault occurs (297.7 & 182.2) than when the unbalance occurs (57.18 & 55.99), which allows relays 71 and 52 to discriminate between fault and unbalance. In addition, the wavelet transform analysis provides higher

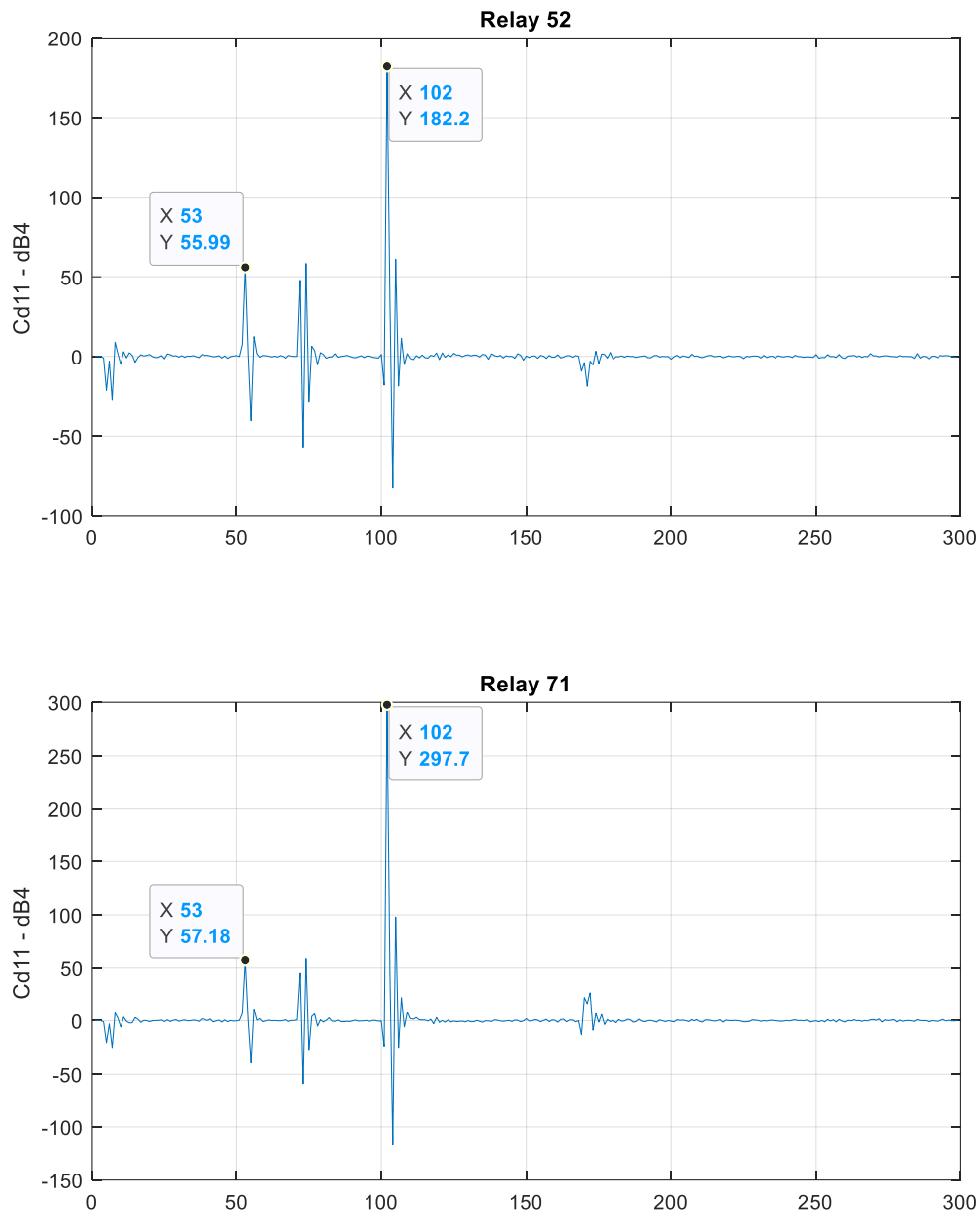


Figure 54. Wavelet coefficients Cd11 – dB4 in relays 52 & 71

sensitivity to pick-up (80.79 & 69.27 % difference) than with the classic negative-sequence overcurrent scheme (63.88 & 34.50 % difference), thus avoiding false tripping.

After analysing the detail coefficients obtained by relays 52 and 71 in Figure 54 for an unbalance in Load A and a fault on Line 7-5, a detail coefficient pick-up threshold is set for relay 52 of 91 at Cd11 – dB4 and for relay 71 of 148 at Cd11 – dB4. Such thresholds are taken as half of the maximum values of the detail coefficient for negative-sequence currents.

The sequence of the proposed pick-up method is illustrated in Figure 55, which shows the steps to be carried out by the pick-up algorithm for distance protection at each distance relay.

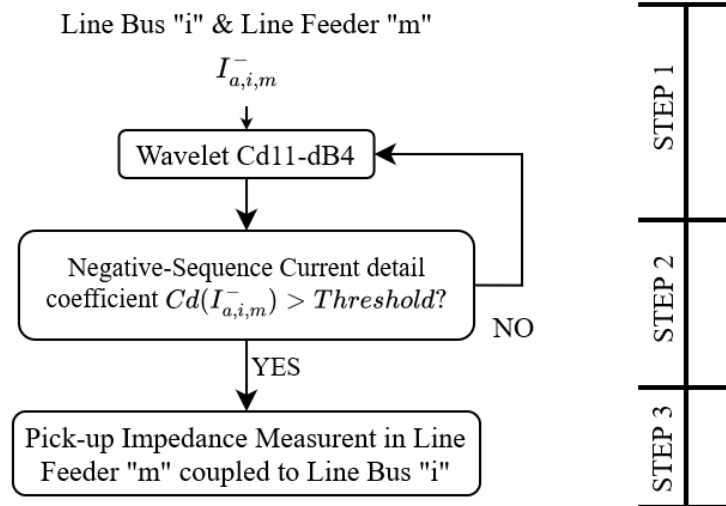


Figure 55. Flowchart of the pick-up sequence of the transmission line distance protection relays

The pick-up sequence consists of three steps, as follows.

1. Measure the negative-sequence current for a line feeder m coupled to line bus i and calculate its detail coefficient by applying the Wavelet transform Cd11 – dB4.
2. Check whether the negative-sequence current detail coefficient obtained in Step 1 is higher than the assigned threshold value for Wavelet transforms Cd11 – dB4.
3. Pick-up the impedance measurement of the line feeder m coupled to line bus i .

6 Conclusions

This thesis presents the Wavelet transform analysis as a solution for: detection problems of generation bus overcurrent protection relays caused by the low fault current contribution of converter-interface generation, and pick-up negative-sequence current problem of transmission line distance protection relays caused by the low negative-sequence current contribution of converter-interface generation. To develop the Wavelet transform analysis, the IEEE nine-bus test system was employed to simulate a grid with 100 % RES, based on power electronic converter-interface generation. A full modelling of grid-forming converter control and its current limitation were designed to replicate the role of grid sources in an electrical power system.

The protection algorithm performs a Wavelet transform analysis to decompose the voltage and current waveforms measured at the generation bus overcurrent protection relays, and the signal of negative-sequence current measured at the transmission line distance protection relays. Simulations have shown that this technique is able to differentiate between non-fault and fault scenarios with more accuracy than the conventional protection schemes; this is due to the ability of the Wavelet transform analysis to detect singularities in both high and low frequency signals and classify them according to their time and magnitude.

In the case of generation bus overcurrent protection relays, for example relay 71, the difference between the current measured by the relay when there is a fault on a generation bus and when the fault is on the line adjacent to the generation bus is barely 8 Amps, whereas the detail coefficients provide differences of up to 66 p.u. In this way, the problems with sensitivity and selectivity that prevent generation bus overcurrent protection relays from detecting ground faults with low current contribution are solved. And in the case of transmission line distance protection relays the difference between the negative-sequence current of an unbalance and a fault is much larger when the detail coefficients are used, reaching up to 240 p.u. compared to the 23 Amps of the conventional pick-up negative-sequence overcurrent scheme on transmission line distance protection relays.

Therefore, the Wavelet transform solution can address the problems of sensitivity and selectivity that prevent generation bus overcurrent protection relays from detecting ground faults with small current contributions. Similarly, it can be used to solve the issues related to sensitivity and selectivity that hinder the transmission line distance protection relays from picking up the impedance measurement sequence with low negative-sequence current contributions.

In addition, the real protection relays installed today to protect power systems are usually segregated line differential relays, distance relays and directional earth fault relays whose minimum trip times are not usually less than 30 ms. Thanks to the use of the Wavelet transform, the ground fault detection times do not exceed one complete cycle, so the tripping time of the new proposed method will not exceed the tripping times of the currently installed protection systems.

However, it is necessary to study each scenario thoroughly to select the best Wavelet configuration for all applications, as generalised configurations cannot be established for all cases. Based on the results and experience obtained from the application of this Wavelet transform to fault detection, generalised configurations cannot be established for all cases and applications, and a rigorous depth study is therefore required for each scenario to choose the best Wavelet configuration.

Despite of the obtained results from HIL simulations were not validate, HIL simulation technique is the most suitable method for testing new protection algorithms. Also, the Wavelet implementation through the HIL API showed us the potential of the Wavelet transform analysis for detecting faults in a 100 % power electronic converter-interface generation scenario. Although it was limited by the minimum execution time step (250 ms) of the HIL API embedded in Typhoon HIL. This problem could be solved with a more powerful processing unit to read the voltage and current waveforms and then obtain their respective detail coefficients to detect faults in less than 250 ms. Since this tripping time is unacceptable for a MV/HV electrical protection system.

Future works will focus on study other types of faults like phase-to-phase faults, validate the real-time tests with a HIL tool (e.g. Typhoon HIL), and develop a new processing unit to implement real-time Wavelet transform analysis using Python (PyWavelets).

References

- [1] IRENA (International Renewable Energy Agency), “Renewable Power Generation Costs in 2020,” 2021.
- [2] H.-O. Pörtner *et al.*, “IPCC, 2022: Climate Change 2022: Impacts, Adaptation, and Vulnerability. Contribution of Working Group II to the Sixth Assessment Report of the Intergovernmental Panel on Climate Change,” Cambridge, UK and New York, USA, 2022. doi: 10.1017/9781009325844.
- [3] “Share of electricity production from renewables,” 2022. <https://ourworldindata.org/energy> (accessed Nov. 25, 2022).
- [4] Taoufik Qoria, “Grid-forming control to achieve a 100% power electronics interfaced power transmission systems,” HESAM Université, 2020.
- [5] SolarPower Europe, “EU Market Outlook for Solar Power 2021-2025,” 2021.
- [6] WindEurope, “Wind energy in Europe: 2021 Statistics and the outlook for 2022-2026,” 2021.
- [7] ec.europa.eu/eurostat, “Renewable energy statistics,” 2022. https://ec.europa.eu/eurostat/statistics-explained/index.php?title=Renewable_energy_statistics (accessed Nov. 25, 2022).
- [8] European Parliament, *Directive (EU) 2018/2001 of the European Parliament and of the Council of 11 December 2018 on the promotion of the use of energy from renewable sources (recast)*, vol. 2018, no. L 328. 2018, pp. 82–209.
- [9] European Commission, *COMMUNICATION FROM THE COMMISSION TO THE EUROPEAN PARLIAMENT, THE EUROPEAN COUNCIL, THE COUNCIL, THE EUROPEAN ECONOMIC AND SOCIAL COMMITTEE AND THE COMMITTEE OF THE REGIONS REPowerEU Plan*. 2022, p. 21.
- [10] Y. Pan, I. Voloh, and W. Ren, “Protection issues and solutions for protecting feeder with distributed generation,” *2013 66th Annu. Conf. Prot. Relay Eng. CPRE 2013*, pp. 92–111, 2013, doi: 10.1109/CPRE.2013.6822030.
- [11] C. Jimenez, “Large Scale Analysis of Massive Deployment of Converter-based Generation equipped with Grid-forming Strategies Large Scale Analysis of Massive Deployment of Converter-based Generation equipped with Grid- forming Strategies,” Royal Institute of Technology (KTH), 2021.
- [12] J. C. Quispe and E. Orduña, “Transmission line protection challenges influenced by inverter-based resources: a review,” *Prot. Control Mod. Power Syst.*, vol. 7, no. 1, pp. 1–17, 2022, doi: 10.1186/s41601-022-00249-8.
- [13] E. M. Carrasco, M. P. C. Moreno, M. T. V. Martínez, and S. B. Vicente, “Improved faulted phase selection algorithm for distance protection under high penetration of renewable energies,” *Energies*, vol. 13, no. 3, 2020, doi: 10.3390/en13030558.
- [14] D. Lagos, V. Papaspiliotopoulos, G. Korres, and N. Hatziaargyriou, “Microgrid Protection against Internal Faults: Challenges in Islanded and Interconnected Operation,” *IEEE Power Energy Mag.*, vol. 19, no. 3, pp. 20–35, 2021, doi: 10.1109/MPE.2021.3057950.
- [15] M. J. Reno, S. Brahma, A. Bidram, and M. E. Ropp, “Influence of Inverter-Based Resources on Microgrid Protection: Part 1: Microgrids in Radial Distribution Systems,”

IEEE Power Energy Mag., vol. 19, no. 3, pp. 36–46, May 2021, doi: 10.1109/MPE.2021.3057951.

- [16] S. Brahma, “Protection of distribution system islands fed by inverter-interfaced sources,” *2019 IEEE Milan PowerTech, PowerTech 2019*, pp. 1–6, 2019, doi: 10.1109/PTC.2019.8810544.
- [17] A. Haddadi, E. Farantatos, I. Kocar, and U. Karaagac, “Impact of inverter based resources on system protection,” *Energies*, vol. 14, no. 4, 2021, doi: 10.3390/en14041050.
- [18] A. Haddadi, I. Kocar, and E. Farantatos, “Impact of Inverter-Based Resources on Protection Schemes Based on Negative Sequence Components,” *Electric Power Research Institute (EPRI)*, 2019.
<https://www.epri.com/research/products/000000003002016197> (accessed Nov. 25, 2022).
- [19] ABB, “Distance Protection REF 542plus: Application and Setting Guide,” 2008.
https://library.e.abb.com/public/602e9601f9afb4f2c1257520002ca2d8/appl_REF542plus_distance_protection_756605_ENa.pdf (accessed Nov. 25, 2022).
- [20] M. Brucoli, “Fault behaviour and fault detection in islanded inverter-only microgrids,” Imperial College London, 2008.
- [21] M. N. Emon, “Microgrid Protection,” Tampere University, 2020.
- [22] “MIGRATE.” www.h2020-migrate.eu (accessed Dec. 16, 2022).
- [23] G. Buigues, A. Dyśko, V. Valverde, I. Zamora, and E. Fernández, “Microgrid protection: Technical challenges and existing techniques,” *Renew. Energy Power Qual. J.*, vol. 1, no. 11, pp. 222–227, 2013, doi: 10.24084/repqj11.262.
- [24] S. Mirsaiedi, D. M. Said, M. W. Mustafa, M. H. Habibuddin, and M. R. Miveh, “A comprehensive overview of different protection schemes in micro-grids,” *Int. J. Emerg. Electr. Power Syst.*, vol. 14, no. 4, pp. 327–332, 2013, doi: 10.1515/ijeeps-2013-0051.
- [25] H. Karimi, G. Shahgholian, B. Fani, I. Sadeghkhani, and M. Moazzami, “A protection strategy for inverter-interfaced islanded microgrids with looped configuration,” *Electr. Eng.*, vol. 101, no. 3, pp. 1059–1073, 2019, doi: 10.1007/s00202-019-00841-6.
- [26] N. A. Mohamed and M. M. A. Salama, “A review on the proposed solutions to microgrid protection problems,” *Can. Conf. Electr. Comput. Eng.*, vol. 2016-Octob, pp. 1–5, 2016, doi: 10.1109/CCECE.2016.7726697.
- [27] N. Hussain, M. Nasir, J. C. Vasquez, and J. M. Guerrero, “Recent developments and challenges on AC microgrids fault detection and protection systems-a review,” *Energies*, vol. 13, no. 9, 2020, doi: 10.3390/en13092149.
- [28] S. Devi, N. K. Swarnkar, S. R. Ola, and O. P. Mahela, “Detection of transmission line faults using discrete wavelet transform,” *Conf. Adv. Signal Process. CASP 2016*, pp. 133–138, 2016, doi: 10.1109/CASP.2016.7746152.
- [29] M. F. Guo, N. C. Yang, and L. X. You, “Wavelet-transform based early detection method for short-circuit faults in power distribution networks,” *Int. J. Electr. Power Energy Syst.*, vol. 99, no. July 2017, pp. 706–721, 2018, doi: 10.1016/j.ijepes.2018.01.013.
- [30] R. Escudero, J. Noel, J. Elizondo, and J. Kirtley, “Microgrid fault detection based on wavelet transformation and Park’s vector approach,” *Electr. Power Syst. Res.*, vol. 152,

pp. 401–410, 2017, doi: 10.1016/j.eprsr.2017.07.028.

- [31] F. H. Magnago and A. Abur, "Fault location using wavelets," *IEEE Trans. Power Deliv.*, vol. 13, no. 4, pp. 1475–1480, 1998, doi: 10.1109/61.714808.
- [32] F. H. Magnago and A. Abur, "A new fault location technique for radial distribution systems based on high frequency signals," *1999 IEEE Power Eng. Soc. Summer Meet. PES 1999 - Conf. Proc.*, vol. 1, pp. 426–431, 1999, doi: 10.1109/PSS.1999.784386.
- [33] H. Jung, Y. Park, M. Han, C. Lee, H. Park, and M. Shin, "Novel technique for fault location estimation on parallel transmission lines using wavelet," *Int. J. Electr. Power Energy Syst.*, vol. 29, no. 1, pp. 76–82, 2007, doi: 10.1016/j.ijepes.2006.05.002.
- [34] R. Granizo Arrabé, "New methods and protection systems for AC and DC power networks," Universidad Politécnica de Madrid, 2018.
- [35] D. B. Rathnayake *et al.*, "Grid Forming Inverter Modeling, Control, and Applications," *IEEE Access*, vol. 9, pp. 114781–114807, 2021, doi: 10.1109/ACCESS.2021.3104617.
- [36] A. Sajadi, R. W. Kenyon, M. Bossart, and B. M. Hodge, "Dynamic interaction of grid-forming and grid-following inverters with synchronous generators in hybrid power plants," *2021 IEEE Kansas Power Energy Conf. KPEC 2021*, 2021, doi: 10.1109/KPEC51835.2021.9446204.
- [37] S. D'Arco, J. A. Suul, and O. B. Fosso, "A Virtual Synchronous Machine implementation for distributed control of power converters in SmartGrids," *Electr. Power Syst. Res.*, vol. 122, pp. 180–197, 2015, doi: 10.1016/j.eprsr.2015.01.001.
- [38] Q. C. Zhong and G. Weiss, "Synchronverters: Inverters that mimic synchronous generators," *IEEE Trans. Ind. Electron.*, vol. 58, no. 4, pp. 1259–1267, 2011, doi: 10.1109/TIE.2010.2048839.
- [39] R. Li *et al.*, "Protection challenges in future converter dominated power systems: Demonstration through simulation and hardware tests," *IET Conf. Publ.*, vol. 2015, no. CP679, 2015, doi: 10.1049/cp.2015.0392.
- [40] J. Keller and B. Kroposki, "Understanding Fault Characteristics of Inverter-Based Distributed Energy Resources," Golden, CO (United States), Jan. 2010. doi: 10.2172/971441.
- [41] S. Phuttapatimok, A. Sangswang, M. Seapan, D. Chenvidhya, and K. Kirtikara, "Evaluation of fault contribution in the presence of PV grid-connected systems," *Conf. Rec. IEEE Photovolt. Spec. Conf.*, 2008, doi: 10.1109/PVSC.2008.4922621.
- [42] S. Manson and E. McCullough, "Practical Microgrid Protection Solutions: Promises and Challenges," *IEEE Power Energy Mag.*, vol. 19, no. 3, pp. 58–69, May 2021, doi: 10.1109/MPE.2021.3057953.
- [43] Y. Pan, W. Ren, S. Ray, R. Walling, and M. Reichard, "Impact of inverter interfaced distributed generation on overcurrent protection in distribution systems," *PEAM 2011 - Proc. 2011 IEEE Power Eng. Autom. Conf.*, vol. 2, pp. 371–376, 2011, doi: 10.1109/PEAM.2011.6134963.
- [44] M. Popov *et al.*, "Enhancing distance protection performance in transmission systems with renewable energy utilization," *IEEE PES Innov. Smart Grid Technol. Conf. Eur.*, vol. 2020-Octob, pp. 181–185, 2020, doi: 10.1109/ISGT-Europe47291.2020.9248896.
- [45] A. Haddadi, I. Kocar, J. Mahseredjian, U. Karaagac, and E. Farantatos, "Negative

- sequence quantities-based protection under inverter-based resources - Challenges and impact of the German grid code," *Electr. Power Syst. Res.*, vol. 188, no. April, pp. 1–6, 2020, doi: 10.1016/j.epsr.2020.106573.
- [46] M. T. Villén, M. P. Comech, E. Martinez Carrasco, and A. A. Prada Hurtado, "Influence of Negative Sequence Injection Strategies on Faulted Phase Selector Performance," *Energies*, vol. 15, no. 16, p. 6018, Aug. 2022, doi: 10.3390/en15166018.
- [47] D. López *et al.*, "Negative sequence current injection by power electronics based generators and its impact on faulted phase selection algorithms of distance protection," *WPRC 2018*, no. August, pp. 1–18, 2018.
- [48] B. Mahamedi and J. E. Fletcher, "The Equivalent Models of Grid-Forming Inverters in the Sequence Domain for the Steady-State Analysis of Power Systems," *IEEE Trans. Power Syst.*, vol. 35, no. 4, pp. 2876–2887, 2020, doi: 10.1109/TPWRS.2020.2968114.
- [49] B. Mahamedi, J. G. Zhu, M. Eskandari, L. Li, and A. Mehrizi-Sani, "Analysis of fault response of inverter-interfaced distributed generators in sequence networks," *2018 IEEE Ind. Appl. Soc. Annu. Meet. IAS 2018*, pp. 1–9, 2018, doi: 10.1109/IAS.2018.8544547.
- [50] I. Nkhasi and A. K. Saha, "Real-time modelling and simulation of distribution system protection with and without renewable distribution generation," University of KwaZulu-Natal, 2017.
- [51] R. M. Muijal-Rosas, *Protección de sistemas eléctricos de potencia*. Iniciativa Digital Politécnica, 2014.
- [52] U. Shahzad, S. Kahrobaee, and S. Asgarpour, "Protection of Distributed Generation: Challenges and Solutions," *Energy Power Eng.*, vol. 09, no. 10, pp. 614–653, 2017, doi: 10.4236/epe.2017.910042.
- [53] M. A. Aftab, S. M. S. Hussain, I. Ali, and T. S. Ustun, "Dynamic protection of power systems with high penetration of renewables: A review of the traveling wave based fault location techniques," *Int. J. Electr. Power Energy Syst.*, vol. 114, no. July 2019, p. 105410, 2020, doi: 10.1016/j.ijepes.2019.105410.
- [54] Z. Chen, X. Pei, M. Yang, L. Peng, and P. Shi, "A Novel Protection Scheme for Inverter-Interfaced Microgrid (IIM) Operated in Islanded Mode," *IEEE Trans. Power Electron.*, vol. 33, no. 9, pp. 7684–7697, 2018, doi: 10.1109/TPEL.2017.2769559.
- [55] K. O. Oureilidis and C. S. Demoulias, "A Fault Clearing Method in Converter-Dominated Microgrids with Conventional Protection Means," *IEEE Trans. Power Electron.*, vol. 31, no. 6, pp. 4628–4640, 2016, doi: 10.1109/TPEL.2015.2476702.
- [56] M. Gilany, A. M. Al-Kandari, and J. Y. Madouh, "A new strategy for determining fault zones in distance relays," *IEEE Trans. Power Deliv.*, vol. 23, no. 4, pp. 1857–1863, 2008, doi: 10.1109/TPWRD.2008.2002871.
- [57] J. S. Farkhani, M. Zareein, A. Najafi, and R. Melicio, "The Power System and Microgrid Protection — A Review," *Appl. Sci.*, vol. 10, no. 22, pp. 1–30, 2020, [Online]. Available: doi:10.3390/app10228271.
- [58] E. Sortomme, S. S. Venkata, and J. Mitra, "Microgrid protection using communication-assisted digital relays," *IEEE Trans. Power Deliv.*, vol. 25, no. 4, pp. 2789–2796, 2010, doi: 10.1109/TPWRD.2009.2035810.

- [59] W. Huang, T. Nengling, X. Zheng, C. Fan, X. Yang, and B. J. Kirby, "An impedance protection scheme for feeders of active distribution networks," *IEEE Trans. Power Deliv.*, vol. 29, no. 4, pp. 1591–1602, 2014, doi: 10.1109/TPWRD.2014.2322866.
- [60] K. Yabe, "Power differential method for discrimination between fault and magnetizing inrush current in transformers," *IEEE Trans. Power Deliv.*, vol. 12, no. 3, pp. 1109–1115, 1997, doi: 10.1109/61.636909.
- [61] S. A. Hosseini, H. A. Abyaneh, S. H. H. Sadeghi, F. Razavi, and A. Nasiri, "An overview of microgrid protection methods and the factors involved," *Renew. Sustain. Energy Rev.*, vol. 64, pp. 174–186, 2016, doi: 10.1016/j.rser.2016.05.089.
- [62] M. Monadi, M. A. Zamani, J. I. Candela, A. Luna, and P. Rodriguez, "Protection of AC and DC distribution systems Embedding distributed energy resources: A comparative review and analysis," *Renew. Sustain. Energy Rev.*, vol. 51, pp. 1578–1593, 2015, doi: 10.1016/j.rser.2015.07.013.
- [63] M. Brucoli, T. C. Green, and J. D. F. McDonald, "Modelling and analysis of fault behaviour of inverter microgrids to aid future fault detection," *2007 IEEE Int. Conf. Syst. Syst. Eng. SOSE*, 2007, doi: 10.1109/SYSESE.2007.4304253.
- [64] M. A. Zamani, T. S. Sidhu, and A. Yazdani, "A protection strategy and microprocessor-based relay for low-voltage microgrids," *IEEE Trans. Power Deliv.*, vol. 26, no. 3, pp. 1873–1883, 2011, doi: 10.1109/TPWRD.2011.2120628.
- [65] C. H. Kim, H. Kim, Y. H. Ko, S. H. Byun, R. K. Aggarwal, and A. T. Johns, "A novel fault-detection technique of high-impedance arcing faults in transmission lines using the wavelet transform," *IEEE Trans. Power Deliv.*, vol. 17, no. 4, pp. 921–929, 2002, doi: 10.1109/TPWRD.2002.803780.
- [66] L. Angrisani, P. Daponte, M. D'Apuzzo, and A. Testa, "A measurement method based on the wavelet transform for power quality analysis," *IEEE Trans. Power Deliv.*, vol. 13, no. 4, pp. 990–998, 1998, doi: 10.1109/61.714415.
- [67] O. Poisson, P. Rioual, and M. Meunier, "Detection and measurement of power quality disturbances using wavelet transform," *IEEE Trans. Power Deliv.*, vol. 15, no. 3, pp. 1039–1044, Jul. 2000, doi: 10.1109/61.871372.
- [68] V. M. Reddy, S. S. Rao, and F. J. Mercede, "On the use of wavelets for the detection and analysis of power system transients," *IEEE Eng. Soc. Winter Meet.*, vol. 2, pp. 1293–1299, 1999, doi: 10.1109/pesw.1999.747403.
- [69] P. Pillaya Bhattacharjee, "Application of wavelets to model short-term power system disturbances," *IEEE Trans. Power Syst.*, vol. 11, no. 4, pp. 2031–2037, 1996, doi: 10.1109/59.544681.
- [70] R. Yu *et al.*, "Modeling and simulation analysis of single phase arc grounding fault based on MATLAB," *Proc. 2011 Int. Conf. Electron. Mech. Eng. Inf. Technol. EMEIT 2011*, vol. 9, no. 2, pp. 4607–4610, 2011, doi: 10.1109/EMEIT.2011.6024001.
- [71] F. E. Pérez, R. Aguilar, E. Orduna, J. Jäger, and G. Guidi, "High-speed non-unit transmission line protection using single-phase measurements and an adaptive wavelet: Zone detection and fault classification," *IET Gener. Transm. Distrib.*, vol. 6, no. 7, pp. 593–604, 2012, doi: 10.1049/iet-gtd.2011.0592.
- [72] F. A. Khan *et al.*, "Open-circuit fault detection in a multilevel inverter using sub-band wavelet energy," *Electronics*, vol. 11, no. 1, pp. 1–15, 2022, doi:

10.3390/electronics11010123.

- [73] MathWorks, "MATLAB/Simulink," 2022. <https://es.mathworks.com/products/simulink.html> (accessed Dec. 16, 2022).
- [74] PowerWorld Corporation, "PowerWorld," 2020. <https://www.powerworld.com/> (accessed Dec. 16, 2022).
- [75] Typhoon HIL Inc., "Typhoon HIL," 2022. <https://www.typhoon-hil.com/> (accessed Dec. 16, 2022).
- [76] J. A. Ledin, "Hardware-in-the-loop simulation," *Embed. Syst. Program.*, vol. 12, pp. 42–62, 1999.
- [77] P. M. Anderson and A. A. Fouad, "Power system control and stability, second edition," *Power Syst. Control Stability, Second Ed.*, pp. 1–658, 2002, doi: 10.1109/9780470545577.
- [78] P. Kundur, N. J. Balu, and M. G. Lauby, *Power System Stability and Control*. McGraw-Hill Education, 1994.
- [79] T. Qoria, F. Gruson, F. Colas, X. Kestelyn, and X. Guillaud, "Current limiting algorithms and transient stability analysis of grid-forming VSCs," *Electr. Power Syst. Res.*, vol. 189, no. April, 2020, doi: 10.1016/j.epsr.2020.106726.
- [80] L. Huang, H. Xin, Z. Wang, L. Zhang, K. Wu, and J. Hu, "Transient Stability Analysis and Control Design of Droop-Controlled Voltage Source Converters Considering Current Limitation," *IEEE Trans. Smart Grid*, vol. 10, no. 1, pp. 578–591, 2019, doi: 10.1109/TSG.2017.2749259.
- [81] J. L. Rodríguez Amenedo, S. Arnaltes Gómez, and J. Eloy-García Carrasco, *Generadores eléctricos*. Madrid: Ibergarceta, 2021.
- [82] A. Gkountaras, S. Dieckerhoff, and T. Sezi, "Evaluation of current limiting methods for grid forming inverters in medium voltage microgrids," *2015 IEEE Energy Convers. Congr. Expo. ECCE 2015*, pp. 1223–1230, 2015, doi: 10.1109/ECCE.2015.7309831.
- [83] H. Wu, X. Li, D. Stade, and H. Schau, "Arc fault model for low-voltage AC systems," *IEEE Trans. Power Deliv.*, vol. 20, no. 2 I, pp. 1204–1205, 2005, doi: 10.1109/TPWRD.2005.844231.
- [84] A. Parizad, H. R. Baghaee, A. Tavakoli, and S. Jamali, "Optimization of f Arc Models Parameter s Using Genetic Algorithm," in *2009 International Conference on Electric Power and Energy Conversion Systems, (EPECS)*, 2009, pp. 1–7.
- [85] D. Xiao, "Dielectric Strength of Atmosphere Air," in *Gas Discharge and Gas Insulation*, Springer, Berlin, Heidelberg, 2016, pp. 149–194.
- [86] A. Khan and N. Bengiamin, "Matlab/Simulink Simulation of Arc Faults," in *International Journal of Engineering Research & Innovation (IJERI)*, 2016, vol. 8, pp. 23–29.
- [87] Schweitzer Engineering Laboratories Inc., "SEL-751 Feeder Protection Relay," 2022. <https://selinc.com/products/751/> (accessed Dec. 16, 2022).
- [88] C. F. Horowitz, S. H., Phadke, A. G., & Henville, *Power system relaying*. 2022.
- [89] S. Paladhi, G. S. Member, A. K. Pradhan, and S. Member, "Adaptive Distance Protection for Lines Connecting Converter-Interfaced Renewable Plants," *IEEE J. Emerg. Sel. Top. Power Electron.*, vol. 9, no. 6, pp. 7088–7098, 2021, doi: 10.1109/JESTPE.2020.3000276.

- [90] A. P. S. Meliopoulos and Chien-Hsing Lee, "An alternative method for transient analysis via wavelets," *IEEE Trans. Power Deliv.*, vol. 15, no. 1, pp. 114–121, 2000, doi: 10.1109/61.847238.
- [91] S. Santoso, E. J. Powers, W. M. Grady, and P. Hofmann, "Power quality assessment via wavelet transform analysis," *IEEE Trans. Power Deliv.*, vol. 11, no. 2, pp. 924–930, 1996, doi: 10.1109/61.489353.
- [92] D. C. Robertson, O. I. Camps, J. S. Mayer, and W. B. Gish, "Wavelets and electromagnetic power system transients," *IEEE Trans. Power Deliv.*, vol. 11, no. 2, pp. 1050–1056, 1996, doi: 10.1109/61.489367.